

**HIGH RESOLUTION ELECTRONIC SPECTROSCOPY
OF LARGE POLYATOMIC MOLECULES:
STRUCTURES, INTERACTIONS AND ELECTRONIC DISTRIBUTIONS**

by

John T. Yi

B.S., La Roche College, 1992

Submitted to the Graduate Faculty of

Arts and Sciences in partial fulfillment

of the requirements for the degree of

Doctor of Philosophy

University of Pittsburgh

2005

UNIVERSITY OF PITTSBURGH
FACULTY OF ARTS AND SCIENCES

This dissertation was presented

by

John T. Yi

It was defended on

July 6, 2005

and approved by

Dr. Kenneth Jordan

Dr. Stephane Petoud

Dr. Linda Peteanu

Dr. David W. Pratt
Committee Chairperson

Copyright © by John T. Yi

HIGH RESOLUTION ELECTRONIC SPECTROSCOPY OF LARGE POLYATOMIC MOLECULES: STRUCTURES, INTERACTIONS AND ELECTRONIC DISTRIBUTIONS

John T. Yi, PhD

University of Pittsburgh, 2005

Abstract.

Rotationally resolved fluorescence excitation spectroscopy has been used to investigate both the structures and electronic characteristics of biologically relevant polyatomic molecules and the clusters in the environment of a supersonic jet expansion. The high resolution spectra have provided accurate and precise three-dimensional molecular structures for both ground (S_0) and excited (S_1) electronic states, and the corresponding electronic transition moment orientation. These studies gave detailed information about the preferred geometrical conformation of the molecules and have allowed insightful information of their interactions with water. Subsequently, the parameters extracted from the fit of these electronic spectra to characterize the electronic landscape for these biomolecules allow an unambiguous description of the conformational landscape. In addition, these experiments have allowed us to investigate the factors that influence the electronic organization upon excitation. All of this information is extended to the development of models to understand and characterize systems of chemical and biological essence.

FOREWORD

Every so often, seeing rotational resolved fluorescence excitation spectrum, I am mesmerized by this creation of nature. Very fortunate to see such immaculate art that I am enlightened by scientific research, this was my source of motivation to strive forward. And, all of this was made possible by my advisor Professor David Pratt. His knowledge and wisdom of science has been a great admiration to me. Also, his endless support and freedom have allowed me to search for the keys to science. I am greatly indebted to him.

I would also like to thank many members of the Pratt group, past and present. Especially, Dr. Jason Ribblett, who helped me understand the applications of the high resolution apparatus. Dr. Timothy Korter and Dr. David Borst, their presentations in the group meetings have taught me many issues pertaining to laser spectroscopy. Tri Nguyen and Leonardo Alvarez-Valtierra, my dear friends and colleagues, who shared many nights in the laboratory and I could always count on for their assistances. Also, I like to take this moment to thank the former group members Cheolwha Kang, Alexei Nikolaev and Jennifer Reese.

I would also like to thank Professor Terry Miller at Ohio State University for his support. My partner Jinjun Liu, thank you for assisting me in many ways in the laboratory.

I would like to thank my parents and brothers, Dennis Yi and Dr. Steven Yi, for their support throughout the years in school. My sister, Dr. Jennifer Yi, who showed me great will of strength which has been inspirational to me. Lastly but not least, I thank my dear wife and my son for their support and patience.

TABLE OF CONTENTS

1.	Introduction.....	1
1.1.	References.....	4
2.	High Resolution Electronic Spectra of Anisole and Anisole-Water in the Gas Phase. Hydrogen Bond Switching in the S ₁ State.....	5
2.1.	Abstract.....	5
2.2.	Introduction.....	6
2.3.	Experimental.....	6
2.4.	Results.....	6
2.5.	Discussion.....	15
2.6.	Summary.....	21
2.7.	Acknowledgments.....	21
2.8.	References.....	22
3.	Rotationally Resolved Electronic Spectra of 1,2–Dimethoxybenzene and the 1,2–Dimethoxybenzene-water Complex.....	24
3.1.	Abstract.....	24
3.2.	Introduction.....	25
3.3.	Experimental.....	27
3.4.	Results and Interpretation.....	28
3.5.	Discussion.....	42
	3.5.1. The bare molecule, DMB.....	43
	3.5.2. The water complex, DMB-H ₂ O.....	49
	3.5.3. Water motion in DMB/H ₂ O.....	54
3.6.	Conclusion.....	58
3.7.	Acknowledgments.....	58
3.8.	References.....	59
4.	Conformational Analysis by Laser Spectroscopy in the Gas Phase: p- Methoxyphenethylamine (a Neurotransmitter).....	62
4.1.	Abstract.....	62
4.2.	Introduction.....	63
4.3.	Experimental.....	64
4.4.	Results and Interpretation.....	65
4.5.	Discussion.....	70
4.6.	Conclusions.....	78
4.7.	Acknowledgments.....	78
4.8.	References.....	79

5.	Rotationally Resolved Electronic Spectroscopy of Tryptophol in the Gas Phase.....	81
5.1.	Abstract.....	81
5.2.	Introduction.....	82
5.3.	Experimental.....	83
5.4.	Results.....	84
5.5.	Discussion.....	91
5.6.	Summary and Conclusions.....	96
5.7.	Acknowledgments.....	96
5.8.	References.....	97
6.	Rotationally Resolved Electronic Spectra of Fluorene, Carbazole and Dibenzofuran: Evidence for Herzberg-Teller Vibrational Coupling with the S ₂ Electronic State.....	99
6.1.	Abstract.....	99
6.2.	Introduction.....	100
6.3.	Experimental.....	101
6.4.	Results.....	102
6.5.	Discussion.....	109
6.6.	Summary.....	118
6.7.	Acknowledgments.....	118
6.8.	References.....	119
	Appendix A.....	121
	Appendix B.....	124

LIST OF TABLES

Table 2-1.	Inertial parameters of anisole in its ground (S_0) and electronically excited (S_1) states.	10
Table 2-2.	Inertial parameters of anisole- H_2O in its ground (S_0) and electronically excited (S_1) states. ^a	14
Table 2-3.	Center of mass (COM) coordinates in Å of the water molecule in the principal axis frames of the bare anisole molecule and the anisole- H_2O complex.	17
Table 3-1.	Absolute and relative energies of several low frequency bands that appear in the $S_1 \leftarrow S_0$ fluorescence excitation spectrum of DMB.	30
Table 3-2.	Ground state rotational constants of Band A compared to the <i>ab initio</i> values of <i>trans</i> and <i>cis</i> -DMB (MP2/6-31G**).	35
Table 3-3.	Derived rotational constants from the fits of Band A through G in the fluorescence excitation spectrum of DMB (<i>cf.</i> Figure 3-1). ^a	35
Table 3-4.	Rotational and centrifugal distortion constants of the <i>A</i> and <i>B</i> subbands in the $S_1 \leftarrow S_0$ spectrum of DMB/ H_2O . ^a	40
Table 3-5.	Rotational and centrifugal distortion constants of the <i>A</i> and <i>B</i> subbands in the $S_1 \leftarrow S_0$ spectrum of DMB/ D_2O . ^a	42
Table 3-6.	Rotational parameters of DMB and the DMB- H_2O complex. The values for the complex are the average values of two subbands. ^a	50
Table 3-7.	Kraitchman coordinates (in Å) of the center-of-mass (COM) of water in both electronic states of DMB/ H_2O . (<i>a</i> , <i>b</i> , and <i>c</i> are the inertial axes of the complex.)	52
Table 3-8.	Rotational constants (in MHz) of H_2O , D_2O and their differences. The values shown are the average values for the two subbands in each electronic state.	53
Table 3-9.	Disubstituted Kraitchman analysis. The coordinates (in Å) are the locations of hydrogen atoms determined from a comparison of the rotational constants of DMB/ H_2O and D_2O . The H...H distance is calculated from these coordinates. (The actual H...H distance of water in 1.536 Å.) ²⁷	54
Table 3-10.	Internal rotation parameters of DMB/ H_2O	58
Table 4-1.	Inertial parameters of seven conformers of <i>p</i> -methoxyphenethylamine (MPEA) in their ground (S_0) and excited (S_1) electronic states.	67
Table 4-2.	Calculated (MP2/6-31G**) rotational constants and relative energies of nine conformers of MPEA in their ground (S_0) electronic states.	72
Table 4-3.	Assignments of specific bands in the electronic spectrum of MPEA to specific conformers (see Figs. 4-1 and 4-4).	77

Table 5-1. Inertial parameters of four conformers of tryptophol in their ground and excited electronic states.	91
Table 5-2. Calculated rotational constants, inertial defects, and relative energies of seven conformers of TRH in their ground electronic states at the MP2/6-31G** level. ^a	92
Table 6-1. Inertial parameters of the zero-point vibrational levels of the S_0 and S_1 electronic states of fluorene carbazole and dibenzofuran.	107
Table 6-2. Inertial parameters of some higher S_1 vibrational bands of fluorene, carbazole and dibenzofuran.	111
Table 6-3. Inertial defects (in amu \AA^2) of fluorene, carbazole and dibenzofuran in their S_0 and S_1 states.	112

LIST OF FIGURES

Figure 2-1.	Central portion of the rotationally resolved fluorescence excitation spectrum of the 0_0^0 origin band in the S_1 - S_0 electronic transition of anisole. Upper trace, experimental; lower trace, computed.....	8
Figure 2-2.	Expanded section (see Fig. 2-1) of the Q-branch in the rotationally resolved S_1 - S_0 fluorescence excitation spectrum of anisole is displayed in (a). The corresponding simulated spectrum, using a Voigt lineshape with 18 MHz Gaussian and 12 MHz Lorentzian components, is shown in (b). (c) and (d) show the contributions of a - and b -type components to this portion of the spectrum.	9
Figure 2-3.	Rotationally resolved fluorescence excitation spectrum of the origin band in the S_1 - S_0 transition of anisole- H_2O , shifted 119 cm^{-1} to the blue of the S_1 - S_0 origin band of anisole. The origin band of the complex is a superposition of two subbands that are separated by 0.024 cm^{-1} . The top trace is the experimental spectrum. The second and third traces are the calculated B and A subbands, respectively.	12
Figure 2-4.	Portion (see Fig. 2-3) of the high resolution spectrum of anisole- H_2O at full experimental resolution, extracted from the R branch of the stronger sub-band. The top trace (a) is the experimental spectrum. The corresponding simulated spectrum with a Voigt lineshape is shown in (b). The third (c) and fourth (d) traces show the separate calculated contributions of the two sub-bands in this region of the spectrum.	13
Figure 2-5.	Combined inversion and restricted internal rotation pathway for the water molecule in anisole- H_2O	19
Figure 3-1.	Vibrationally resolved fluorescence excitation spectrum of 1,2-dimethoxybenzene. The asterisk denotes a band that appears when H_2O is added to the sample; the insert shows how the spectrum of this band is changed when D_2O is added to the sample.	29
Figure 3-2.	Rotationally resolved fluorescence excitation spectrum of Band A of DMB.	31
Figure 3-3.	Two likely conformations of 1,2-dimethoxybenzene with their respective inertial axes.	32
Figure 3-4.	Portion of the R-branch taken from the spectrum of Band A of DMB at full resolution. Trace a is the experimental spectrum. Trace b is a simulated spectrum using a Voigt line shape function (18 MHz Gaussian and 40 MHz Lorentzian). Trace c is a stick figure representation of the spectrum.	34
Figure 3-5.	Rotationally resolved $S_1 \leftarrow S_0$ fluorescence excitation spectrum of 1,2-dimethoxybenzene / H_2O	36
Figure 3-6.	Autocorrelation spectrum of the 1,2-dimethoxybenzene / H_2O complex.	38

Figure 3-7.	At full resolution, a portion of the R-branch is shown from the spectrum of 1,2-dimethoxybenzene / H ₂ O. Trace a is the experimental spectrum, and traces c and d show the calculated rovibronic transitions in subbands <i>B</i> and <i>A</i> , respectively. Trace b is the simulated spectrum, using the Voigt lineshape function described in the text.....	39
Figure 3-8.	Rotationally resolved S ₁ ←S ₀ fluorescence excitation spectrum of 1,2-dimethoxybenzene / D ₂ O.....	41
Figure 3-9.	At full resolution, a portion of the R-branch is shown from the spectrum of 1,2-dimethoxybenzene / D ₂ O. The top trace is the experimental spectrum and the bottom traces c and d show the simulated rovibronic transitions in subbands <i>A</i> and <i>B</i> , respectively. Trace b is the simulated spectrum, using the Voigt lineshape function described in the text.	41
Figure 3-10.	<i>Ab initio</i> geometries of DMB in its S ₀ and S ₁ states. S ₁ state values are given in parentheses with bond lengths in Å (left) and angles in degrees (right).	46
Figure 3-11.	Potential energy surfaces of DMB/water in its two electronic states plotted as a function of the water torsional coordinate. The two minima arise from two equivalent orientations of the attached H ₂ O. Tunneling along this coordinate gives rise to symmetry distinguishable torsional subbands <i>A</i> and <i>B</i> . Allowed transitions between these two states are indicated by arrows with their corresponding intensity ratios.	56
Figure 4-1.	Vibrationally resolved fluorescence excitation spectrum of <i>p</i> -methoxyphenethylamine (MPEA) recorded in a supersonic jet. Bands labeled A through G are the S ₁ ← S ₀ electronic origins of seven different conformers of the isolated molecule. The band marked with an asterisk is a water complex of MPEA.	65
Figure 4-2.	Rotationally resolved fluorescence excitation spectrum of band A recorded in a molecular beam. The bottom panel shows a section of the R-branch together with two computer simulations with and without a deconvoluted lineshape.	66
Figure 4-3.	Comparisons of similar portions of the R-branch in Bands B through G, at full experimental demonstrating the unique character of each spectrum. The top trace is the experimental spectrum. Two computer simulations, with and without a deconvoluted lineshape, are shown below.	69
Figure 4-4.	Nine unique conformations of MPEA, based on <i>ab initio</i> calculations at the MP2/6-31G** level.	71
Figure 4-5.	Rotationally resolved fluorescence excitation spectrum of Band E recorded in a molecular beam. The bottom panel shows a section of the Q-branch at full resolution, and its deconvolution into <i>b</i> and <i>c</i> -type transitions.	75

Figure 5-1.	Vibrationally resolved S_1 - S_0 fluorescence excitation spectrum of tryptophol.	85
Figure 5-2.	Rotationally resolved S_1 - S_0 fluorescence excitation spectrum of tryptophol Band A. In the bottom panel, the top trace is a portion of the experimental spectrum and the succeeding traces are simulated spectra with and without a convoluted lineshape function.	86
Figure 5-3.	Rotationally resolved S_1 - S_0 fluorescence excitation spectrum of tryptophol Band B. In the bottom panel, the top trace is a portion of the experimental spectrum and the succeeding traces are simulated spectra with and without a convoluted lineshape function.	88
Figure 5-4.	Rotationally resolved S_1 - S_0 fluorescence excitation spectrum of tryptophol Band C obtained in an argon carrier gas. In the bottom panel, the top trace is a portion of the experimental spectrum and the succeeding traces are simulated spectra with and without a convoluted lineshape function.	89
Figure 5-5.	Rotationally resolved S_1 - S_0 fluorescence spectrum of tryptophol Band C obtained in a helium carrier gas. The bottom panel shows a portion of the experimental spectrum and two simulated spectra, the Band C spectrum (a) and the additional simulated spectrum (b), shifted by $+ 0.55 \text{ cm}^{-1}$, that is required to fit all of the intensity in the observed spectrum.	90
Figure 5-6.	The nine conformers of TRH as calculated at the MP2/6-31G** level. See text for a description of the nomenclature used.	93
Figure 6-1.	Fluorescence excitation spectra of the $S_1 \leftarrow S_0$ electric transitions of fluorene, carbazole and dibenzofuran in a supersonic jet. The origins are indicated as 0_0^0 and the first vibronic bands of each molecule are also shown. Bands marked with asterisks are due to argon complexes.	103
Figure 6-2.	Rotationally resolved fluorescence excitation spectrum of the electronic origin in the $S_1 \leftarrow S_0$ transition of fluorene (top). A portion of the experimental spectrum at full resolution and the corresponding simulated spectrum with and without a convoluted line-shape function are also shown (bottom).	104
Figure 6-3.	Rotationally resolved fluorescence excitation spectrum of the electronic origin in the $S_1 \leftarrow S_0$ transition of carbazole (top). A portion of the experimental spectrum at full resolution and the corresponding simulated spectrum with and without a convoluted line-shape function are also shown (bottom).	105
Figure 6-4.	Rotationally resolved fluorescence excitation spectrum of the electronic origin in the $S_1 \leftarrow S_0$ transition of dibenzofuran (top). A portion of the experimental spectrum at full resolution and the corresponding simulated spectrum with and without a convoluted line-shape function are also shown (bottom).	106

Figure 6-5. Rotationally resolved fluorescence excitation $S_1 \leftarrow S_0$ spectra of the a_1 -symmetry vibronic bands of FLU, CAR and DBF in a molecular beam. For every single spectrum, a portion at full experimental resolution is also shown, together with the corresponding fits. Note that every spectrum is unique.	108
Figure 6-6. Rotationally resolved fluorescence excitation $S_1 \leftarrow S_0$ spectra of the b_2 -symmetry vibronic bands of CAR and DBF in a molecular beam. For each spectrum, a portion at full experimental resolution is also shown, together with their respective simulations.	110
Figure 6-7. MP2 6-31G** molecular orbitals of fluorene, cabazole and dibenzofuran.	114

LIST OF SCHEMES

Scheme 2-1.....	15
Scheme 3-1: Symmetry axes of DMB.....	25
Scheme 3-2: The structure of anisole with its inertial frame.....	43
Scheme 3-3: Kekulé structures of <i>trans</i> -DMB.....	44
Scheme 3-4: Orientation of the methyl hydrogens in <i>cis</i> -MVE.....	44
Scheme 3-5: Structural changes in mono-substituted benzenes on S ₁ excitation.....	45
Scheme 3-6: Structural changes in <i>trans</i> -DMB on S ₁ excitation.....	46
Scheme 3-7: CIS/6-31G* calculated one-electron molecular orbitals of DMB.....	47
Scheme 3-8: Low frequency vibrations of DMB in the ground state.....	48
Scheme 3-9: The TM orientation of DMB and its water complex are indicated by an arrow.....	49
Scheme 3-10: Circles indicate the four equivalent positions of the COM of the attached water molecule in the <i>ab</i> and <i>bc</i> planes of DMB/H ₂ O.....	51

1. Introduction.

Molecular structures and inter/intra molecular interactions have a direct influence on the type of structural framework that large biomolecules can adopt. These have profound influence on many of their key functions; adhesion, growth and communication, to name a few.¹ Understanding of fundamental processes and the dynamics, such as seen in the helical structure of DNA and in the folding process of proteins at molecular level, is our main goal. One ideal technique to achieve these objectives is high resolution spectroscopy in the gas phase, which allows us to study and examine in detail the three-dimensional structure of individual molecular parts by isolating them from the biological bulk and have a controlled environment.

Ultraviolet spectroscopy study provides detailed information about biomolecules. First, under a supersonic jet, collision free environment, we have isolated and controlled single molecular identities to be explored. Then, the inertial parameters obtained from the detailed analysis provide insightful structural information of the molecules in both S_0 and S_1 electronic states. One additional type of information that provides the electronic distribution of a molecule is the orientation of the S_0 - S_1 electronic transition moment (TM) upon excitation.

The parts of these experiments touch general implications of molecular spectroscopy, but important oriented aspects are presented here. Part I involves structural integrities such as detailed analyses of structural displacements in both ground and excited electronic states: preferred molecular orientation, distinguishing conformational rotamers and structural changes upon excitation. Next, Part II, of a great extent, describes inter and intra molecular interactions, where it was evident to observe a unique behavior of the water moiety weakly bound to a bare molecule and self preservation of the side chain to the main frame of the structure. Lastly, Part

III discusses electronic distribution in symmetric molecules; the factors that influence the electronic organization upon excitation.

In Chapter 1, a simple methoxy substituted benzene, anisole, provides an example of an “in-plane” geometry of the methoxy group “in-plane” with respect to benzene. In Chapter 2, addition of a second methoxy group in *ortho* position results in a molecule (1,2-dimethoxybenzene) that maintains its planar structure with *trans*-disposed methoxy groups in its ground and excited electronic states. Detailed information of molecular structures is extended to identity of the conformational isomers in biologically relevant molecules such as *p*-methoxyphenethylamine (Chapter 3) and tryptophol (Chapter 4). The flexible side chain has many degrees of rotation about its ethylamine (or ethyl alcohol) bonds which offers many possible conformers. However, these two side-chain molecules exhibit different and limited number of electronic origins of conformational isomers in the gas phase, seven conformers for *p*-methoxyphenethylamine and four conformers for tryptophol were found in our experiments. The parameters extracted from the fit of these electronic spectra were sufficient to characterize the different conformers of these biomolecules, allowing an unambiguous description of their conformational landscape.

Also described in Chapter 1 and 2 are water complexes of anisole and 1,2-dimethoxybenzene, in which a single water molecular is joined by two hydrogen bonds to the aromatic frame. The preferred binding sites and orientation of the attached water molecule have been determined in both cases. Additionally, a motion of the water molecule is revealed by the appearance of torsional sub-bands in the spectra. Barriers to these motions in both electronic states have been determined from analyses of the spectra.

Also, in Chapters 3 and 4, we show that the existence of the different possible conformers heavily relies upon intra molecular hydrogen bond in the gas phase. We have explored two remarkable examples; ethylamino- and ethylhydroxy- substituted molecules, which contain two hydrogens interacting with one lone pair orbital and one hydrogen interacting with two lone electron pair orbitals, respectively. However, in the ethylamino- substituted molecules *p*-methoxyphenethylamine and tryptamine² more conformers were observed than in the ethylhydroxy substituted molecules *p*-hydroxyphenylethanol³ and tryptophol. In both cases, the more favored structures have folded (*gauche*) structures in which a lone pair or a hydrogen atom interacts with the aromatic π -cloud. Such inter/ intra- molecular interactions have a direct influence on the type of structural framework that larger biomolecules can adopt; for example, in the helical structure of DNA, and also in the α -helix or β -sheet secondary structures seen in large proteins.⁴

The final Chapter is devoted to a study of the electronic distribution of highly symmetric molecules, such as fluorene, carbazole and dibenzofuran. They share the same molecular frame with a different central atom (C9), but their transition moment orientation vectors turn out to be very different. Furthermore, another fascinating observation was detected when we analyzed some higher vibronic bands of these molecular systems. The symmetry-forbidden transitions were observed and their transition moment orientations were orthogonal with respect to their origin bands. The latter observation suggested that a possible coupling with the S_2 electronic state was taking place in some higher vibronic bands. This phenomenon is known as the Herzberg-Teller coupling.

Furthermore in Chapter 5, we exploit the consequences of different substituted atoms on molecular electronic orbital conjugations with the dibenzo framework yielding different

excitation energies. This is an evidence of different involvements of the atomic orbitals of the central atom. In addition, the isolated species of substituted ethyl molecules (Chapters 3 and 4) have different relative excitation energies which are further deduced from the involvement of various intra-molecular interaction strengths of the side chain with the framework.

1.1. References.

1. J. M. Hicks and T. Petralli-Mallow, *Appl. Phys. B*, **68**, 589 (1999).
2. T. V. Nguyen, T. M. Korter and D. W. Pratt, *Mol. Phys.*, **103**, 1603 (2005).
3. M. R. Hockridge, S. M. Knight, E. G. Robertson, J. P. Simons, J. McCombie and M. Walker, *Phys. Chem. Chem. Phys.* **1**, 407 (1999).
4. R. H. Garrett and C. M. Grisham, “*Biochemistry*”, Saunders College Publishing, New York, (1995).

2. High Resolution Electronic Spectra of Anisole and Anisole-Water in the Gas Phase. Hydrogen Bond Switching in the S_1 State.

Jason W. Ribblett,¹ Wayne E. Sinclair,² David R. Borst,³ John T. Yi, and David W. Pratt⁴

¹Department of Chemistry, Ball State University, Muncie IN 47306.

²Bristol-Myers Squibb Pharmaceuticals, Moreton U.K.

³Intel Corporation, MS RA2-283, Hillsboro, OR 97124.

⁴Department of Chemistry, University of Pittsburgh, Pittsburgh, Pennsylvania 15260 USA

2.1. Abstract.

Rotationally resolved $S_1 \leftarrow S_0$ electronic spectra of anisole and its hydrogen bonded complex containing one water molecule have been obtained. The results provide evidence for an “in-plane” complex in which the water molecule is attached *via* two hydrogen bonds to the anisole molecule, a donor O-H---O(CH₃) bond, and an acceptor H-O---H(ring) bond. Analysis of the sub-bands that appear in the spectrum of the complex suggests that hydrogen bond “switching” occurs when the complex absorbs light. The former O-H---O(CH₃) bond is stronger in the ground (S_0) state, whereas the latter H-O---H(ring) bond is stronger in the excited (S_1) state. Dynamical consequences of this phenomenon are discussed.

J. Phys. Chem., in press

2.2. Introduction.

Three recent reports have described rotationally resolved spectra of anisole and its hydrogen bonded water complex, anisole-H₂O.¹⁻³ This complex is interesting because it appears to exhibit a structure in which the water molecule acts as an acid, donating one of its protons to the oxygen atom of the methoxy group. Previously, we have given preliminary descriptions of our own spectra of these two systems.^{4,5} In this report, we present a more thorough account of these findings with special emphasis on the hydrogen bond dynamics in anisole-H₂O that are revealed by a careful study of its high resolution electronic spectrum. The results suggest that the attached water molecule is “amphoteric”, behaving as an acid when anisole is in its ground electronic (S₀) state but as a base when anisole is in its excited electronic (S₁) state.

2.3. Experimental.

Anisole was supplied by Aldrich (99% purity) and used as received. High resolution spectra were obtained using the CW molecular beam laser spectrometer described elsewhere.⁶ Typically, the sample was heated to 370 K, seeded into ~ 300 torr of Ar, and expanded through a 240 μ nozzle. The sample was then skimmed once at 2 cm downstream and probed by the laser 12 cm downstream of the nozzle. Some experiments were performed in a high resolution port, 100 cm downstream. Complexes were formed by adding water to the expansion. More complete details are given elsewhere.^{7,8}

2.4. Results.

Figure 2-1 shows the rotationally resolved fluorescence excitation spectrum of the origin band of the S₁ ← S₀ transition of anisole at 36384.07 cm⁻¹. In agreement with previous work,¹

this spectrum was found to be a mainly *b*-type band which is consistent with assignment of the S_1 state of anisole as a 1L_b state, as in the case of most singly substituted benzenes. A small amount of *a*-type character was detected in the spectrum owing to the inertial contribution of the “off-axis” methoxy group. The final fit shown in Figure 2-2 utilized 2.7% *a*-type character, corresponding to a tilt of the transition moment vector of $\pm 9^\circ$ with respect to the *b* axis. This is equal in magnitude to the contribution predicted by *ab initio* calculations.⁷ No *c*-type transitions were found in the spectrum.

400 lines were ultimately employed in the least squares fit of the 0_0^0 band of anisole, resulting in an OMC standard deviation of 2.0 MHz for the spectrum recorded in the high resolution port. The calculated Gaussian and Lorentzian contributions to the observed Voigt lineshape profiles of single rovibronic lines are 3 ± 1 and 12 ± 2 MHz, respectively. The two reported lifetimes of S_1 anisole are 30 nsec⁹ and 22 nsec¹⁰ which would give Lorentzian contributions of 5 and 7 MHz, respectively. Apparently, the true lifetime of S_1 anisole at the band origin is less than 20 nsec.

Table 2-1 lists the rigid rotor constants that were derived from fits of the data in Figures 2-1 and 2-2 together with other relevant data for comparison. Our values of the ground state rotational constants are somewhat more precise than those of Eisenhardt, *et al.*¹ but significantly less precise than the microwave values.¹¹ Nonetheless, all three sets of values agree within the stated errors. Theory (MP2/6-31G**)¹² also reproduces the experimental results very well. Structurally, the most significant conclusion about anisole in its S_0 state is that all heavy atoms lie in the aromatic plane. Only the methyl group hydrogen atoms lie out of this plane. The inertial defect of anisole in its S_0 state ($-3.4 \text{ amu } \text{\AA}^2$) is virtually identical to that of 1-methylnaphthalene ($-3.3 \text{ amu } \text{\AA}^2$).¹³

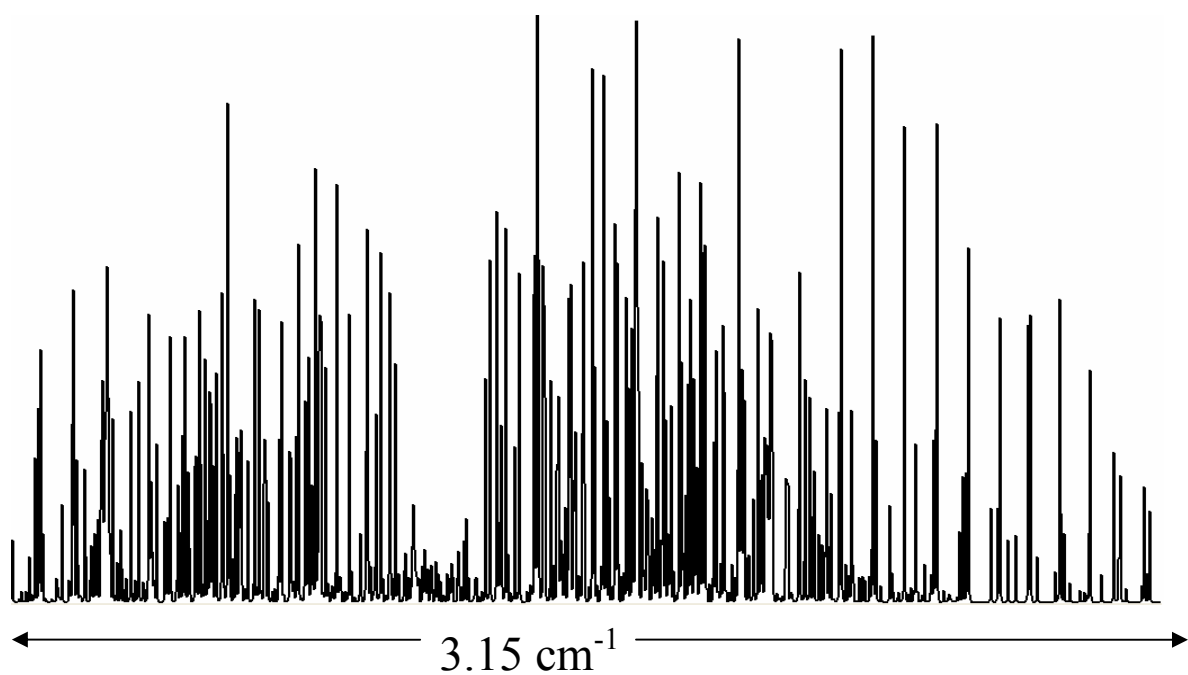
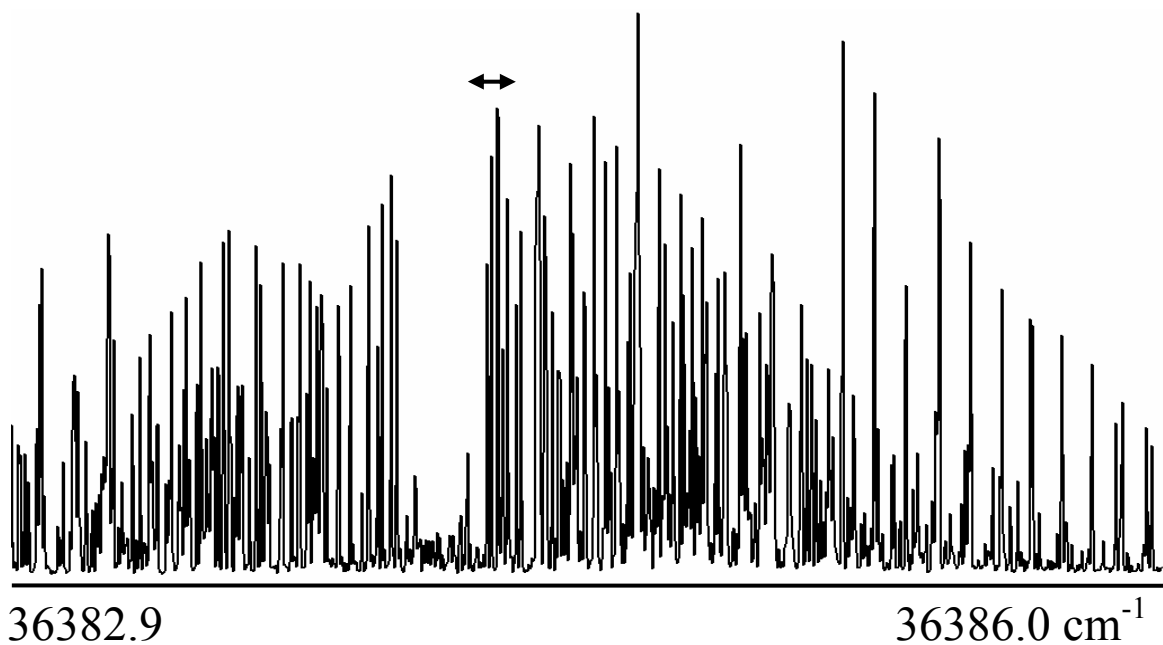


Figure 2-1. Central portion of the rotationally resolved fluorescence excitation spectrum of the 0_0^0 origin band in the S_1 - S_0 electronic transition of anisole. Upper trace, experimental; lower trace, computed.

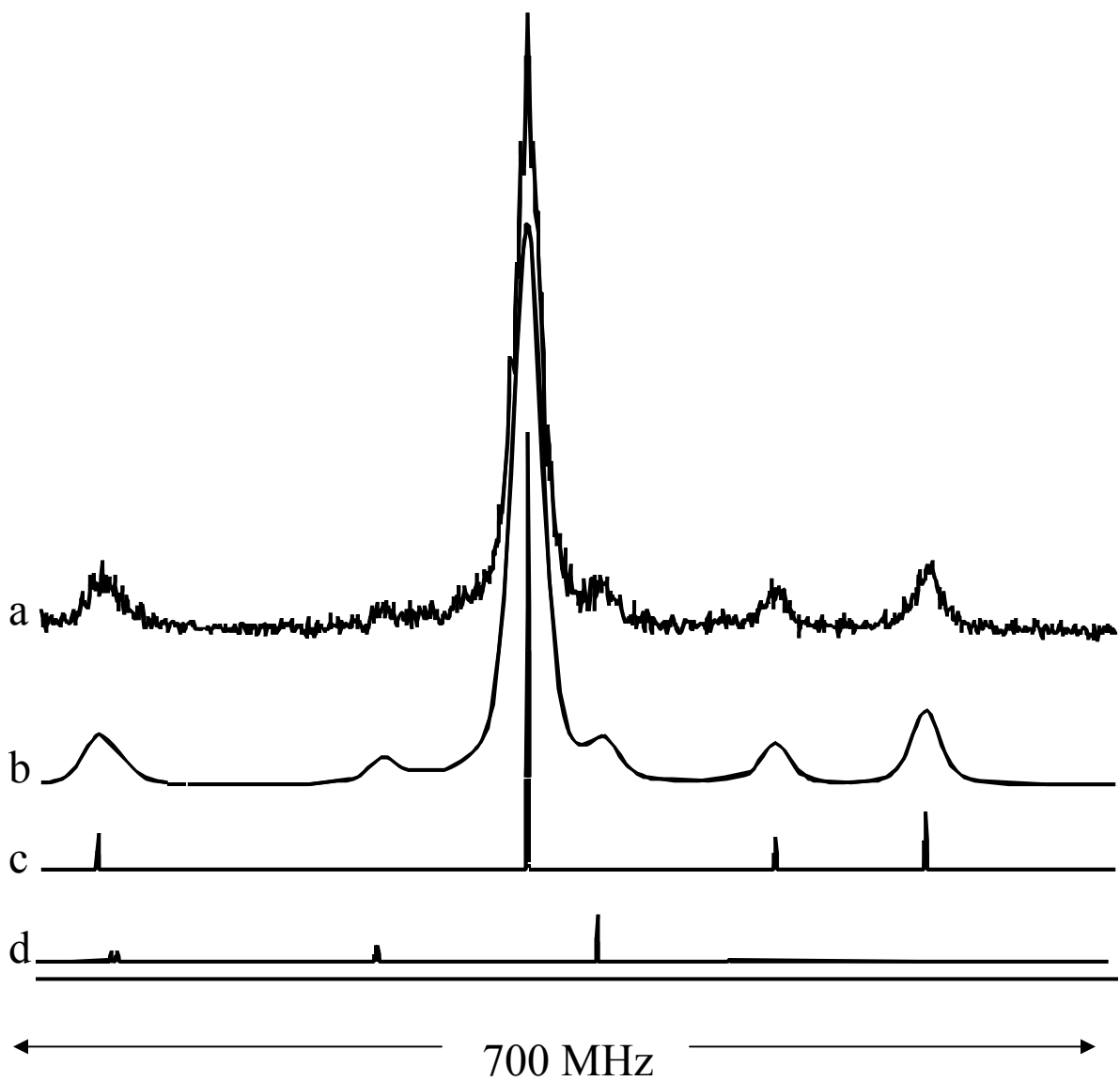


Figure 2-2. Expanded section (see Fig. 2-1) of the Q-branch in the rotationally resolved S_1 - S_0 fluorescence excitation spectrum of anisole is displayed in (a). The corresponding simulated spectrum, using a Voigt lineshape with 18 MHz Gaussian and 12 MHz Lorentzian components, is shown in (b). (c) and (d) show the contributions of *a*- and *b*-type components to this portion of the spectrum.

Table 2-1. Inertial parameters of anisole in its ground (S_0) and electronically excited (S_1) states.

	This Work	Eisenhardt, et al.^a	Microwave^b	MP2/6-31G**
A''(MHz)	5028.8 (1)	5028.87 (1)	5028.867 (11)	5021.3
B''(MHz)	1569.3 (1)	1569.375 (3)	1569.375 (3)	1570.4
C''(MHz)	1205.8 (1)	1205.837 (3)	1205.836 (3)	1205.4
κ	-0.810	-0.810	-0.810	-0.8087
$\Delta I(\text{amu } \text{Å}^2)$	-3.415	-3.41	-3.410	-3.200
$\Delta A'$ (MHz)	-233.21 (4)	-232.85 (1)		
$\Delta B'$ (MHz)	-13.53 (1)	-13.57 (1)		
$\Delta C'$ (MHz)	-21.25 (1)	-21.21 (1)		
κ	-0.794	-0.794		
$\Delta I(\text{amu } \text{Å}^2)$	-3.584	-3.596		
OMC (MHz)	2	10		
Assigned lines	400	440		
Band origin (cm^{-1})	36384.07	36384		
% <i>b</i> -type	97	96		
Temp (K)	3.6	1.9		

^aRef. 1 ^bRef.11.

The inertial defect of anisole in its S_1 state ($-3.6 \text{ amu } \text{Å}^2$) is slightly larger in magnitude than that of the ground state. This provides evidence for increased vibrational amplitude along out-of-plane coordinates. And, as in the case of most other singly substituted benzenes, the S_1 state of anisole has a significantly larger aromatic ring, compared to the ground state. The ΔA , ΔB , and ΔC values of anisole ($\Delta A = A' - A''$, *etc.*) are very similar to those of phenol.¹⁴ No evidence was found for any methyl or methoxy group torsional activity in the high resolution spectrum of the bare molecule. This is consistent with the results of state-of-the art density functional theory calculations¹⁵ which clearly show that anisole is “planar” with a $\sim 12 \text{ kJ/mole}$ barrier to internal rotation of the methoxy group in the S_0 state.

Figure 2-3 shows the rotationally resolved $S_1 \leftarrow S_0$ fluorescence excitation spectrum of anisole- H_2O . Again in agreement with previous work,² this spectrum is found to be mainly a *b*-

type band, consistent with assignment of the S_1 state of the complex as a 1L_b state. However, a more careful examination of this spectrum reveals several interesting features not apparent at lower resolution. First, an in-plane binding site of the attached H_2O is suggested by the observed band polarization. A binding site above or below the plane of the ring would result in a mainly c -type band as in the case of aniline- H_2O .¹⁶ Second, the spectrum consists of two overlapping sub-bands separated by $\sim 0.024\text{ cm}^{-1}$. These two sub-bands were detected by Becucci, *et al.*² and called “vibrational satellites”. We have found that the two sub-bands have different relative intensities that are independent of temperature. The observed intensity ratio is $\sim 3:1$. This provides evidence that two protons are being exchanged by some large amplitude motion. (An exchange of three or more protons would result in two or more sub-bands with different relative intensities.) A likely explanation for this behavior is that the attached water molecule is undergoing a hindered internal motion that exchanges its two protons. The two sub-bands are then “torsional” sub-bands that connect the nuclear-spin distinguishable A and B sub-torsional levels in the two electronic states. These result from tunneling along a two-fold symmetric torsional coordinate in the two states. Similar behavior has been observed in several other systems such as indole- H_2O ,¹⁷ benzonitrile- H_2O ¹⁸ and *p*-difluorobenzene- H_2O .¹⁹ And third, a satisfactory fit of the two sub-bands could only be obtained by incorporating Watson distortion terms into the rotational Hamiltonians of the two electronic states.²⁰

Figure 2-4 shows an example of this fit. Individual rovibronic lines have widths of ~ 20 MHz. A Voigt lineshape analysis suggests comparable Lorentzian and Gaussian contributions of ~ 18 MHz. The Gaussian contribution is larger in this spectrum because it was recorded in the low resolution port.

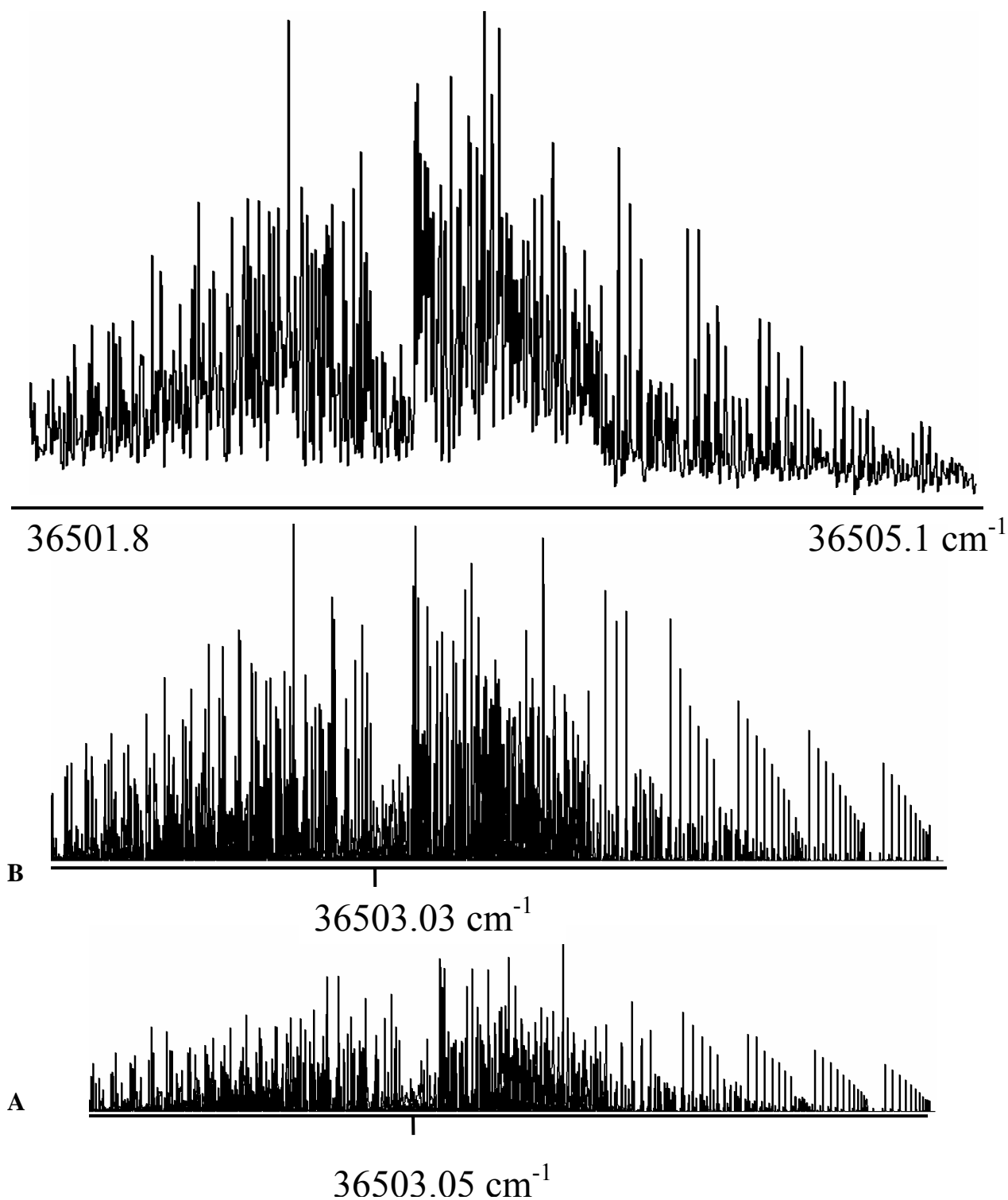


Figure 2-3. Rotationally resolved fluorescence excitation spectrum of the origin band in the S_1 - S_0 transition of anisole- H_2O , shifted 119 cm^{-1} to the blue of the S_1 - S_0 origin band of anisole. The origin band of the complex is a superposition of two subbands that are separated by 0.024 cm^{-1} . The top trace is the experimental spectrum. The second and third traces are the calculated B and A subbands, respectively.

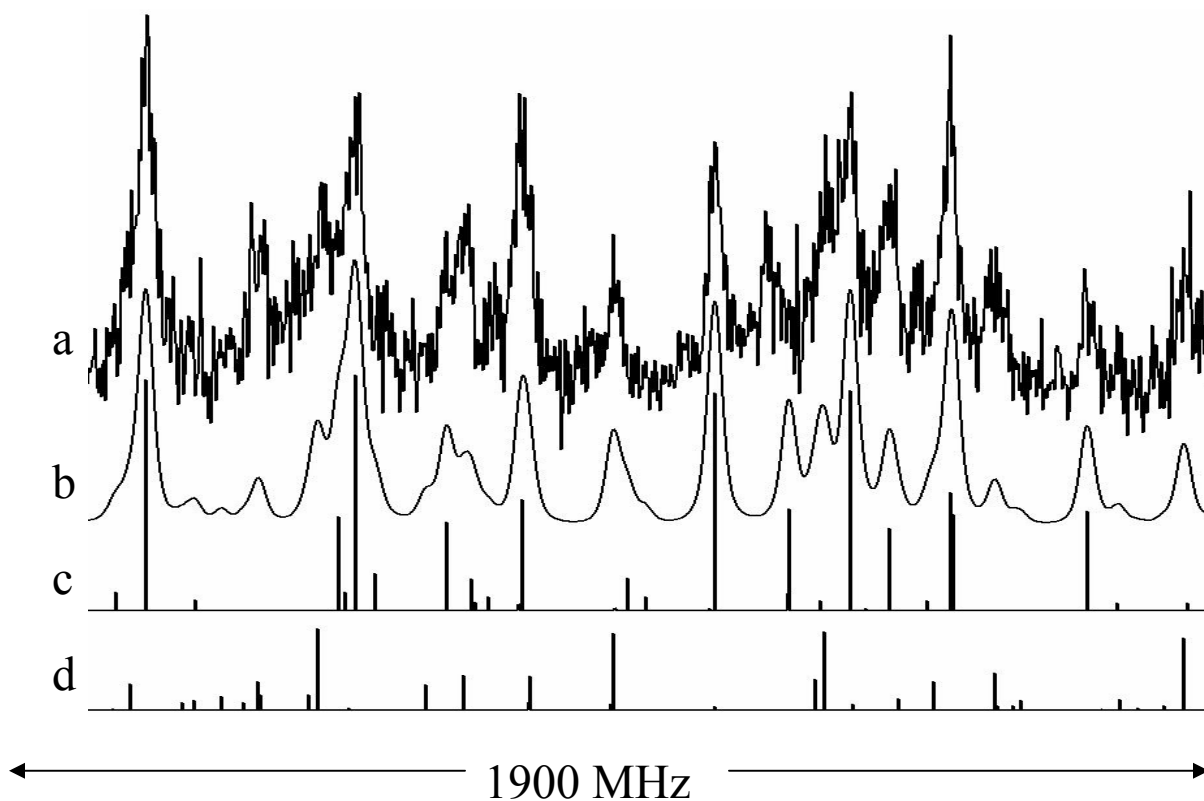


Figure 2-4. Portion (see Fig. 2-3) of the high resolution spectrum of anisole-H₂O at full experimental resolution, extracted from the R branch of the stronger sub-band. The top trace (a) is the experimental spectrum. The corresponding simulated spectrum with a Voigt lineshape is shown in (b). The third (c) and fourth (d) traces show the separate calculated contributions of the two sub-bands in this region of the spectrum.

Table 2-2 lists the rotational constants that were derived from fits of the two sub-bands in the spectrum of anisole-H₂O. The two sub-band origins are at 36503.03 and 36503.05 cm⁻¹ and are separated by 732.65 MHz. The rotational constants of the two sub-bands are very different from those of the bare molecule (Table 2-1), reflecting the additional mass and displacement of the attached water molecule. Despite this fact, the inertial defect of the complex is found to be very similar to that of the bare molecule, increasing in magnitude by only 1.8 amu Å². For comparison, aniline-H₂O has a greatly enhanced inertial defect ($\Delta I = 141.4 \text{ amu } \text{Å}^2$)¹⁶ compared to the bare molecule ($\Delta I = 0.406 \text{ amu } \text{Å}^2$).²¹

Table 2-2. Inertial parameters of anisole-H₂O in its ground (S₀) and electronically excited (S₁) states.^a

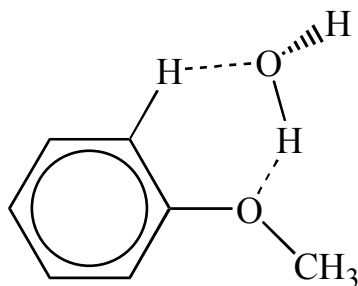
State	Parameter	Strong (B) This work	Strong (B) Ref 2	Strong (B) Ref 3	Weak (A) This work	Weak (A) Ref 2	Weak (A) Ref 3
S ₀	A''	2944.5 (2)	2941.38 (1)	2943.578 (2)	2945.4 (3)	2941.32 (2)	2943.058 (2)
	B''	900.3 (1)	899.65 (1)	900.0276 (8)	900.7 (2)	899.68 (1)	900.1885 (9)
	C''	694.4 (1)	693.93 (1)	694.1155 (8)	694.4 (2)	694.08 (1)	694.1488 (9)
	D _J ''	0.004 (4)		0.00422 (2)	0.008 (2)		0.00425 (2)
	D _{JK} ''	-0.052 (2)		-0.0538 (1)	-0.028 (5)		-0.0540 (1)
	D _K ''	0.218 (3)		0.2183 (2)	0.208 (5)		0.2190 (2)
	d _j ''	-0.0015 (2)		-0.001751 (2)	-0.0032 (8)		-0.001760 (2)
	d _k ''	-0.0001 (8)		-0.000106 (1)	0.0024 (3)		-0.000108 (1)
	κ''	-0.817	-0.817	-0.817	-0.817	-0.817	-0.817
	ΔI''	-5.198	-5.2835	5.0870	-4.909	-5.4256	-5.0519
	S ₁	A'	3090.2 (1)	3089.27 (1)		3091.4 (2)	3089.51 (1)
B'		848.0 (1)	847.54 (1)		848.4 (2)	847.57 (1)	
C'		671.4 (1)	671.24 (1)		671.0 (2)	671.30 (1)	
D _J '		0.0003 (4)			0.001 (1)		
D _{JK} '		-0.003 (2)			0.018 (4)		
D _K '		0.016 (2)			0.006 (4)		
d _j '		-0.0001(2)			-0.0026 (6)		
d _k '		-0.0001(1)			-0.0026 (3)		
κ'		-0.854	-0.854		-0.853	-0.854	
ΔI'		-6.830	-6.9698		-6.044	-7.0032	
Band origin		36503.03	36503		36503.05	36503	
Assignments	176	328	42	83	219	42	
OMC	3.56	10	0.005	3.72	10	0.005	

^a Band origins in cm⁻¹, inertial defects in amu Å², all other parameters in MHz.

Finally, we note that the rotational constants of the two sub-bands are not the same. In the ground state, the A'' values differ by 1.0 MHz, well outside experimental error (± 0.5 MHz). The two B'' values are equal, within error. But there also is a small difference in the two C'' values of 0.5 MHz (compared to the estimated error of ± 0.3 MHz). The two ground state levels have inertial defects that differ by $0.4 \text{ amu } \text{\AA}^2$. These differences have been confirmed in a recent study of the ground state of anisole- H_2O using microwave techniques (*cf.* Table 2-2).³ In the excited state, the two A' values differ by 1.2 MHz, the two B' values differ by 0.8 MHz, and the two C' values differ by 0.9 MHz, with all differences being greater than the errors. There also are differences in their inertial defects, $\sim 0.3 \text{ amu } \text{\AA}^2$ in the S_0 state and $\sim 0.8 \text{ amu } \text{\AA}^2$ in the S_1 state. The fact that the rotational constants of the two sub-bands are not the same is intimately related to the internal rotation dynamics of the attached water molecule in both electronic states, as the following discussion will show.

2.5. Discussion.

As noted, the observed rotational constants, inertial defects, and transition moment orientations of anisole- H_2O in its electronic ground state place the water molecule approximately in the aromatic plane, closest to the oxygen atom of the methoxy group. The likely structure is thus the σ -hydrogen bonded structure shown below in Scheme 2-1:



Scheme 2-1

Here, the oxygen atom lone pair electrons on the OCH₃ group accept at least one proton from the attached water molecule. Water thus behaves primarily as an acid in anisole-H₂O rather than as a base. Additionally, there is a “basic” interaction involving the water molecule; its oxygen atom donates a lone pair of electrons to an *ortho* hydrogen atom, forming a weaker H-O---H hydrogen bond with the aromatic ring. Strong support for such a structure is found in the results of the molecular mechanics calculations described by Becucci, *et al.*²

Refinements in our understanding of the structure and dynamics of the complex may be made in the following way. First, we compare the rotational constants of anisole-H₂O in its ground state with those of the bare molecule using Kraitchman’s equations.²² (Here, we used the average constants of a hypothetical rigid rotor complex of anisole-H₂O, corrected for the higher order effects of centrifugal distortion.) Treating the water molecule as a single particle with mass 18 yields the COM coordinates listed in Table 2-3. These data confirm the proposed structure shown in Scheme 2-1, above. They also show that the COM of the water molecule is displaced vertically from the plane defined by the aromatic ring, either because the equilibrium structure is distorted along that coordinate, or because of a large amplitude vibrational motion in this direction (see Scheme 2-1). The displacement ($|z_c| = 0.43 \text{ \AA}$) is not large but it is significant. Finally, the data show that this displacement increases by at least 0.04 \AA on excitation of anisole-H₂O to its S₁ state. At the same time, the distance of the hypothetical particle of mass 18 from the COM increases by $\sim 0.13 \text{ \AA}$ in the excited state, compared to the ground state. Whatever the nature of the intermolecular hydrogen bonds, they get weaker when the photon is absorbed.

Table 2-3. Center of mass (COM) coordinates in Å of the water molecule in the principal axis frames of the bare anisole molecule and the anisole-H₂O complex.

State	Coordinate	Bare Molecule Frame (Å)	Complex Frame (Å)
S ₀	a	3.243 (1)	3.661 (1)
	b	3.055 (4)	1.142 (1)
	c	0.43 (2)	0.124 (8)
	r	4.477 (1)	3.837 (1)
S ₁	a	3.5897 (6)	3.814 (1)
	b	2.849 (4)	1.013 (1)
	c	0.47 (2)	0.141 (8)
	r	4.607 (1)	3.949 (1)

That the intermolecular hydrogen bonds in the S₁ state of anisole-H₂O are weaker than those in the S₀ state also is clear from the observation that the origin band of the complex is blue shifted (by $\sim 119 \text{ cm}^{-1}$) relative to that of the bare molecule. This is typical of water donor hydrogen bonds.^{23,24} The oxygen lone pair electrons of the methoxy group are less available for hydrogen bonding in the S₁ state owing to their increased conjugation with the aromatic ring. In contrast, hydrogen bonds in which the water molecule accepts a proton from an attached group are typically stronger in the S₁ state, leading to red shifts of their spectra relative to the bare molecule. Indole-H₂O, with an NH \cdots OH₂ hydrogen bond in which water acts as a base, is a prototypical example of this behavior.¹⁷

More surprising is the observation, concerning the two sub-bands that lie within the S₁-S₀ origin band of the complex, that the weaker A sub-band is blue shifted with respect to the stronger B sub-band, by $\sim 0.024 \text{ cm}^{-1}$. This shows that the barrier controlling the motion of the

attached water molecule is *higher* in the S_1 state than in the S_0 state. A higher barrier implies that the motion of the water molecule cannot be a simple torsional motion about one of the two hydrogen bond axes. As we have seen, both sub-bands are blue shifted relative to the origin band of the bare molecule, showing that, on balance, the hydrogen bonding in the S_1 state is weaker than that in the ground S_0 state. A weakening of these bonds should lead to a decrease in the magnitude of the barrier, if the motion were a simple torsional motion about one of the hydrogen bond axes. Thus, the “torsional” dynamics of the attached water molecule in anisole- H_2O must be more complicated than first imagined.

Detailed information about these dynamics is contained in the measured rotational constants of the two sub-bands of anisole- H_2O , in both electronic states. Recall that, in the ground state, the two A values differ by 1.0 MHz, and that there is also a small difference in the two C values. These differences have their origins in a vibrational motion of the attached water molecule. In the case of a two-fold barrier, the contributions to A, B, and C are second-order in nature, and their relative magnitudes depend upon the axes about which the motion is occurring, among other factors.¹³ So, since the two A values are different in the ground state, with some smaller differences in C, we can conclude that whatever the nature of the motion, it occurs mainly about the *a* principal axis of the complex. In contrast, the A, B, *and* C values in the two sub-bands are all different in the S_1 excited state, so the motion of the attached water molecule must be very different in this state, compared to the ground state.

The fact that the two sub-bands have a 3:1 intensity ratio means that the motion that is responsible for them must exchange the two water hydrogens, at least in the ground state. In the language of NMR, they must be “equivalent”. As we¹⁹ (and others²⁵) have discussed elsewhere,

one mechanism that accomplishes this is the “two-step” process shown in Figure 2-5. Step one in this scheme is an inversion, in which the oxygen lone pairs on water are switched in hydrogen bond B, moving hydrogen H₂ from “above” the plane to “below”. Step two in this scheme is an internal rotation, in which the two hydrogen atoms of the water molecule are switched, hydrogen H₂ replacing hydrogen H₁ in hydrogen bond A. The two steps taken in concert exchange the roles of hydrogens H₁ and H₂, accomplishing the desired objective.

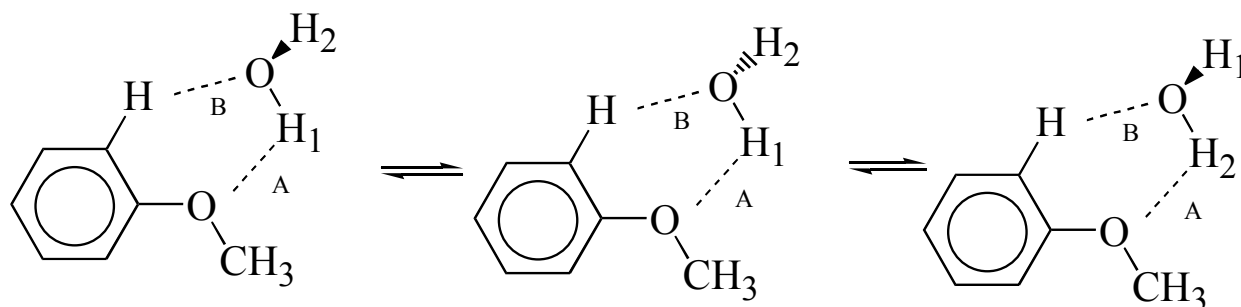


Figure 2-5. Combined inversion and restricted internal rotation pathway for the water molecule in anisole-H₂O.

The mechanism described above is probably best viewed as a single step process, along a “diagonal” reaction coordinate, with a single activation energy. But for some purposes, it is more convenient to imagine the process as a two-step process with separate activation energies for each step. Step one, inversion at oxygen, requires breaking hydrogen bond B, whereas step two, internal rotation, requires breaking hydrogen bond A. We suppose that, of the two bonds, hydrogen bond A is the stronger bond in the ground state, in which water acts as an acid and anisole acts as a base. Therefore, step two must be more important in this state. But as we have

seen, the energy of the O-H---O(CH₃) bond is observed to decrease on excitation of anisole-H₂O to its S₁ state, whereas the barrier impeding the motion of the attached water molecule is observed to increase. Therefore, step one must be more important in the S₁ state, breaking hydrogen bond B. We conclude, then, that hydrogen bond “switching” has occurred; hydrogen bond A is the stronger bond in the S₀ (ground) state, but hydrogen bond B is the stronger bond in the S₁ (excited) state. The water molecule acts as a base in this state, accepting a proton from the attached anisole molecule.

Quantitative estimates of the two barrier heights may be obtained in the following way. We assume that the water molecule undergoes an internal rotation about an axis making an angle of 55° with its *b* axis, with an internal rotor constant of 339 MHz,¹⁷ in the ground state. This axis is approximately parallel to the *a* axis of the complex. Then, from the difference in the two rotational constants ($\Delta A_{\text{eff}}'' = A_a'' - A_b'' = 1.0 \text{ MHz}$), we calculate a barrier of $V_2'' = 224 \text{ cm}^{-1}$ in the ground state. Next, we assume that the water molecule undergoes an inversion motion about an axis making an angle of -55° with its *b* axis, with a similar internal rotor constant, in the excited state. In this case, all three rotational constants are different since the motion of the water molecule is about an axis that makes non-zero projections along *a*, *b*, and *c*, making it difficult to model the observed behavior. So, we chose to vary the excited state barrier until we fit the observed difference in tunneling splittings in the two states (~ 733 MHz), obtaining the value $V_2' = 237 \text{ cm}^{-1}$. The determined values of V_2 are the effective barrier heights for the combined inversion-torsion motion described above. Thus, V_2 increases in the S₁ state because the H-O---H (ring) bond is stronger in this state.

More detailed information about the motion of the attached water molecule in the two electronic states of anisole-H₂O will require a careful analysis of the data on different isotopomers recently reported for the ground state by Giuliano and Caminati³, and comparable data for the excited state.

2.6. Summary.

We have observed and assigned the high resolution electronic spectra of anisole and its single water complex, anisole-H₂O. The data provide evidence for an “in-plane” complex in which the water molecule is attached to the anisole molecule *via* two hydrogen bonds, an O-H---O(CH₃) donor bond and an H-O---H(ring) acceptor bond. Excitation of the chromophore with light changes its electron distribution. These changes are reflected in observed differences in the strengths of the two hydrogen bonds and in the nature of the water motion in the two electronic states. This motion involves both internal rotation and inversion coordinates, but the barrier to the former is larger in the ground state, whereas the barrier to the latter is larger in the excited state. As a result, the water molecule in anisole-H₂O behaves like an acid when anisole is in its ground state, but it behaves like a base when anisole is in its excited state.

2.7. Acknowledgments.

We thank Cheolhwa Kang, Tim Korter, and Tri Nguyen for helpful conversations. Mat Mattox assisted with the fits of the spectra. This work has been supported by NSF (CHE-0315584).

2.8. References.

1. C. G. Eisenhardt, G. Pietraperzia and M. Becucci, *Phys. Chem. Chem. Phys.* **3**, 1407 (2001).
2. M. Becucci, G. Pietraperzia, M. Pasquini, G. Piani, A. Zoppi, R. Chelli, E. Castellucci and W. Demtröder *J. Chem. Phys.* **120**, 5601 (2004).
3. B. M. Giuliano and W. Caminati, *Angew. Chem. Int. Ed.* **44**, 603 (2005).
4. J. W. Ribblett and D. W. Pratt, “*The $S_1 \leftarrow S_0$ Fluorescence Excitation Spectra of Anisole and Styrene Using High Resolution Techniques*”, 52nd International Symposium on Molecular Spectroscopy, Columbus, Ohio, June 16-20, 1997.
5. J. W. Ribblett, D. R. Borst, and D. W. Pratt, “*The High Resolution $S_1 \leftarrow S_0$ Spectrum of the Anisole/Water Complex: Water as an Acid*”, 55th International Symposium on Molecular Spectroscopy, Columbus, Ohio, June 12-16, 2000.
6. W. A. Majewski, J. F. Pfanstiel, D. F. Plusquellic and D. W. Pratt, in *Laser Techniques in Chemistry*, T. R. Rizzo and A. B. Myers, Eds. (J. Wiley & Sons, New York, 1995), p. 101.
7. J. W. Ribblett, Ph.D. Thesis, University of Pittsburgh, 1999.
8. D. R. Borst, Ph.D. Thesis, University of Pittsburgh, 2001.
9. G. Köhler and N. Getoff, *J. Mol. Struct.* **115**, 331 (1984).
10. A. Zehnacker, F. Lahmani, E. Breheret, J. P. Desvergne, H. Bouas-Laurent, A. Germain, V. Brenner and P. Millie, *Chem. Phys.* **208**, 243 (1996).
11. M. Oda, A. Toda, S. Mori and I. Yamaguchi, *J. Mol. Struct.* **144**, 47 (1986). See also O. Desyatnyk, L. Psczolkowski, S. Thorwirth, T.M. Krygowski, and Z. Kisiel, *Phys. Chem. Chem Phys.* **7**, 1 (2005).
12. M. J. Frisch, G. W. Trucks, H. B. Schlegel, P. M. W. Gill, B. G. Johnson, M. A. Robb, J. R. Cheeseman, T. Keith, G. A. Petersson, J. A. Montgomery, K. Raghavachari, M. A. Al-Laham, V. G. Zakrevewski, J. V. Ortiz, J. B. Foresman, J. Cioslowski, B. Stefanov, A. Nanayakkara, M. Challacombe, C. Y. Peng, P. Y. Ayala, W. Chen, M. W. Wong, J. L. Andres, E. S. Replogle, R. Gomperts, R. L. Martin, D. J. Fox, J. S. Binkley, D. J. Defrees,

- J. Baker, J. P. Stewart, M. Head-Gordon, C. Gonzalez, J. A. Pople, Gaussian 98, Revision A9, Gaussian, Inc., Pittsburgh, PA, 1998.
13. X. -Q. Tan, W. A. Majewski, D. F. Plusquellic and D. W. Pratt, *J. Chem. Phys.* **94**, 7721 (1991).
 14. G. Berden, W. L. Meerts, M. Schmitt and K. Kleinermanns, *J. Chem. Phys.* **104**, 972 (1996)
 15. S. Tsuzuki, H. Houjou, Y. Nagawa and K. Hiratani, *J. Phys. Chem. A* **104**, 1332 (2000).
 16. U. Spoerel and W. Stahl, *J. Mol. Spectr.* **190**, 278 (1998).
 17. T. M. Korter, D. W. Pratt and J. Küpper, *J. Phys. Chem. A* **102**, 7211 (1998).
 18. M. Schäfer, D. R. Borst, D. W. Pratt, and K. Brendel, *Mol. Phys.* **100**, 3553 (2002).
 19. C.-H. Kang, D. W. Pratt, and M. Schäfer, *J. Phys. Chem. A* **109**, 767 (2005).
 20. W. Gordy and R.L. Cook, *Microwave Molecular Spectra*, J. Wiley & Sons, New York, 1970.
 21. W. E. Sinclair and D. W. Pratt, *J. Chem. Phys.* **105**, 7942 (1996).
 22. J. Kraitchman, *Am. J. Phys.* **21**, 17 (1953).
 23. J. A. Dickinson, M. R. Hockridge, E. G. Robertson, and J. P. Simons, *J. Phys. Chem. A* **103**, 6938 (1999).
 24. A. V. Federov and J.R. Cable, *J. Phys. Chem. A* **104**, 4943 (2003).
 25. M. Schütz, T. Bürgi, S. Leutwyler, and T. Fischer, *J. Chem. Phys.* **98**, 3763 (1993).

3. Rotationally Resolved Electronic Spectra of 1,2-Dimethoxybenzene and the 1,2-Dimethoxybenzene-water Complex

John T. Yi, Jason W. Ribblett,¹ and David W. Pratt²

¹Department of Chemistry, Ball State University, Muncie IN 47306,

²Department of Chemistry, University of Pittsburgh,
Pittsburgh PA 15260 USA.

3.1. Abstract.

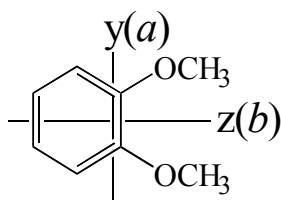
Rotationally resolved $S_1 \leftarrow S_0$ electronic spectra of 1,2-dimethoxybenzene (DMB) and its water complex have been observed and assigned. The derived values of the rotational constants show that the bare molecule has a planar heavy-atom structure with *trans*-disposed methoxy groups in its ground and excited electronic states. The 0_0^0 transition of DMB is polarized along the *b*-axis bisecting the methoxy groups demonstrating that its S_1 state is an 1L_b state. Higher energy bands of DMB are also polarized along the *b*-axis and have been tentatively assigned to different vibrational modes of the 1L_b state. The water complex origin appears 127 cm^{-1} to the blue of the bare molecule origin. Analyses of the high resolution spectra of DMB/ H_2O and DMB/ D_2O suggest that the water molecule is attached *via* two O-H \cdots O hydrogen bonds to the methoxy groups in both electronic states. A tunneling motion of the attached water molecule is revealed by a splitting of these spectra into two subbands. Potential barriers to this motion have been determined.

J. Phys. Chem., in press

3.2. Introduction.

Investigations of molecular conformers and their complexes continue to provide vital information about *intra* and *intermolecular* forces. In this report, we focus on 1,2-dimethoxybenzene (DMB) and its hydrogen bonded complex with a single water molecule.

The conformational preferences of dimethoxy-substituted benzenes have been the subject of several studies.¹⁻⁷ Hill, *et al.*² used near ultraviolet spectroscopy to determine the polarization directions of the 1L_b and 1L_a transitions of a series of homo and hetero disubstituted benzene derivatives. In DMB, they found the polarization direction of the 1L_b transition at 278 nm to be along the *z*-symmetry axis and the polarization direction of the 1L_a transition at 227 nm to be along the *y*-axis, as shown in Scheme 3-1. Based on time-of-flight mass spectroscopy (TOFMS)



Scheme 3-1: Symmetry axes of DMB.

experiments combined with dispersed emission results, Bernstein and co-workers proposed that DMB in the gas phase is probably planar in nature.⁵ The lower excited state frequency bands were also analyzed utilizing isotopic substitution; these were assigned to torsional motions of the methoxy groups.

There have been no previous reports of a DMB/water complex. However, other hydrogen bonded aromatic molecule/water complexes, particularly benzene and substituted benzene water

complexes, have been extensively studied. Currently,⁸⁻¹⁰ it is believed that in benzene/water, the water forms hydrogen bonds with the π -electrons in an “a-top” binding site. In contrast, substituted benzene/water complexes display equilibrium structures in which the water lies in the plane of the aromatic ring.¹¹⁻¹⁸ Benzonitrile,^{11,12} anisole,¹³ and mono- and difluorobenzene¹⁴⁻¹⁶ water complexes exhibit double hydrogen bonds. One hydrogen atom of the water molecule (the hydrogen donor) is bound to the substituent atom ($\text{H}\cdots\text{X}$), whereas the oxygen atom of the water (the hydrogen acceptor) is bound to a hydrogen atom ($\text{H}\cdots\text{OH}_2$) of the bare molecule. In phenol¹⁷ and indole¹⁸ clusters, the water (hydrogen acceptor) is bound to the electrophilic hydrogen atom of the bare molecule ($\text{H}\cdots\text{OH}_2$). A molecular plane bisects the plane of the singly bonded water so that its hydrogens are out-of-plane.

In all such complexes, the attached water also undergoes a large amplitude motion with respect to the parent molecule. In benzene/water, Gutowsky, *et al.*⁸ showed that the plane of the water is 34° off the C_2 axis and rotates about the C_6 axis of benzene. Also, using resonant ion-dip infrared spectroscopy with resonant two-photon (R2PI) spectroscopy, Pribble, *et al.*⁹ recorded the infrared spectra of the O-H stretch of benzene- H_2O and showed that a large tumbling motion of water about the six-fold axis of benzene occurs. Previous substituted benzene/water cluster studies have reported the observation of a variety of different types of motion of the attached water molecules. Studies of small molecule- H_2O complexes, such as $\text{H}_2\text{O}-\text{H}_2\text{O}$ and $\text{CO}-\text{H}_2\text{O}$, also have revealed a variety of tunneling motions.^{19,20}

In this work, we report the results of fluorescence excitation studies that shed light on the geometry and dynamical properties of DMB and its water complex in their S_0 and S_1 electronic

states. First, the preferred structure of DMB will be determined in its ground and excited electronic states from fits of its rotationally resolved fluorescence excitation spectrum. This spectrum also gives information about the distribution of electrons in the ground state, and how this changes when the photon is absorbed. Second, tentative assignments of several low frequency bands that appear in this spectrum will be made based on their rotational constants and vibrational frequency calculations. Third, the preferred structure of the water complex of DMB will be determined from analysis of the corresponding excitation spectra of DMB-H₂O and DMB-D₂O. The results show a new type of water (hydrogen donor) interaction involving the lone pair electrons of the oxygen atoms in DMB. Finally, information about the internal rotation dynamics of the attached water molecule will be obtained from an analysis of the perturbations that appear in these spectra.

3.3. Experimental.

1,2-Dimethoxybenzene (veratrole) was purchased from Aldrich and purified by fractional distillation with CaH₂ under vacuum conditions. In the vibrationally resolved electronic experiment, the sample was seeded into 40 psi of He gas (premixed with H₂O or D₂O for the complex) and expanded into a vacuum chamber (10⁻⁵ torr) through a 1 mm diameter pulsed nozzle (General Valve Series 9), operating at 10 Hz. One centimeter downstream of the valve, the sample was excited with the second harmonic of a Quanta Ray Nd³⁺: YAG (Model DCR-1A) pumped dye laser (Model PDL-1). The dye (Fluorescein 548) laser output was frequency doubled with an external β-barium borate (BBO) crystal providing a spectral resolution of 0.6 cm⁻¹ in the ultraviolet. From the point of intersection between the nozzle and laser, the molecules were excited and the fluorescence was collected with a photomultiplier tube. Finally,

the collected data were processed by a boxcar integrator (Stanford Research Systems) and recorded with a DataAcq data acquisition system.

Rotationally resolved electronic experiments on DMB were performed using a CW laser spectrometer, described elsewhere.²¹ Briefly, the sample was seeded into He gas (premixed with H₂O or D₂O for the complex), expanded through a 240 μm quartz nozzle, and probed 15 cm downstream of the nozzle by an Ar⁺ pumped CW tunable dye laser. The CW laser operated with Rhodamine 110 dye; 100-200 μW of UV radiation was obtained by intracavity frequency doubling using a BBO 560 crystal. The fluorescence excitation spectrum, the iodine absorption spectrum, the relative frequency markers, and the laser output power were simultaneously collected and processed by a j95a data acquisition system.²¹ Transition frequencies were calibrated by comparison with the I₂ absorption spectrum and frequency markers from a stabilized etalon with a free spectral range of 299.7520 ±0.0005 MHz.

3.4. Results and Interpretation.

The low resolution S₁←S₀ fluorescence excitation spectrum of DMB in a supersonic jet is shown in Figure 3-1. It exhibits several bands. Band A, at 35751 cm⁻¹ (~280 nm), has been identified as the electronic origin, or 0₀⁰ band of DMB.^{6,22} This band is red shifted from the benzene origin due to conjugation of the benzene π-orbitals and methoxy non-bonding orbitals; the corresponding band of benzene is at 38091 cm⁻¹ (~260 nm).²³ Bands B-G, at relatively small displacements from the DMB origin, are unique to DMB. The bands at still higher displacements have analogs in benzene. For example, the band at 36254 cm⁻¹ (0₀⁰ + 503 cm⁻¹) in Figure 3-1 is the analog of the 6₀¹ band in benzene.²³

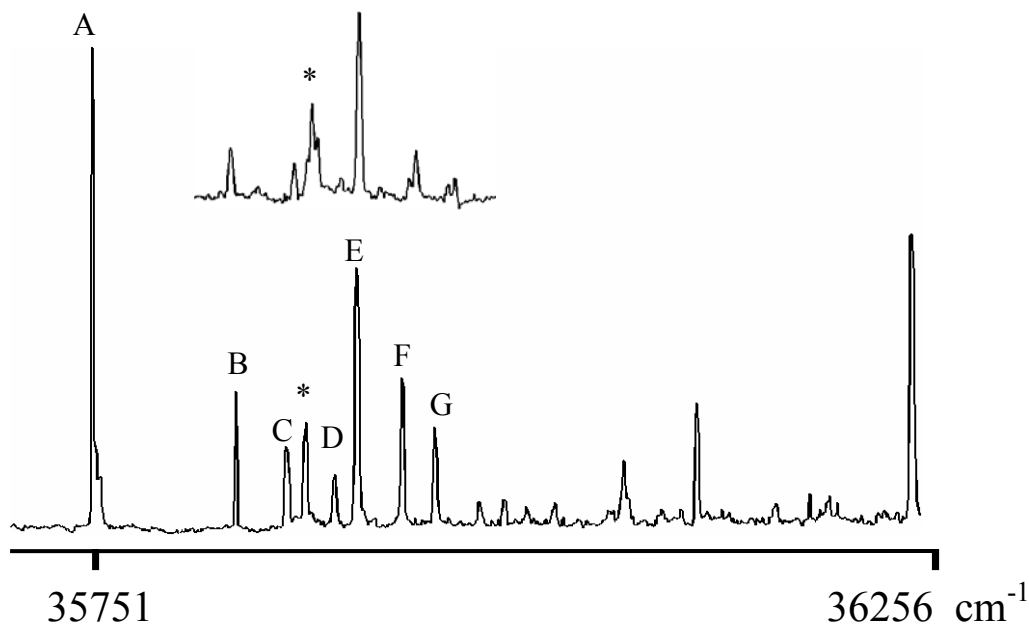


Figure 3-1. Vibrationally resolved fluorescence excitation spectrum of 1,2-dimethoxybenzene. The asterisk denotes a band that appears when H₂O is added to the sample; the insert shows how the spectrum of this band is changed when D₂O is added to the sample.

The bands of primary interest to us in Figure 3-1 are the origin band, Band A, and Bands B-G, which have no analogs in the spectrum of benzene. Table 3-1 lists the frequencies of these bands. Apparently, Bands B, C, and D form a progression beginning at $0_0^0 + 84 \text{ cm}^{-1}$, and Bands E, F, and G form a similar progression beginning at $0_0^0 + 151 \text{ cm}^{-1}$. If these are progressions, their nature (*i.e.*, the vibrational motions that are responsible for them) are unknown. It is also possible that these bands are the bands of different conformers of DMB whose origins are shifted in frequency by different amounts.

Table 3-1. Absolute and relative energies of several low frequency bands that appear in the $S_1 \leftarrow S_0$ fluorescence excitation spectrum of DMB.

Bands	Energy (cm^{-1})	Relative energy (cm^{-1})	ΔI (amu \AA)	Assignments ^a
A	35751	0	-7.68	a_1
B	35835	84	-10.23	$2a_1^\dagger$ or $2b_1^\dagger$
C	35868	117	-9.46	$a_2^\dagger a_2^\ddagger$
D	35893	142	-9.06	$2b_1^\ddagger$
E	35902	151	-8.95	$2a_2^\ddagger$
F	35931	180	-8.87	$a_2^\dagger a_2^\ddagger$
G	35952	201	-7.50	a_1

^a See Scheme 3-8 for individual vibrational modes

Also of interest is the band marked with an asterisk in Figure 3-1, at $0_0^0 + 127 \text{ cm}^{-1}$. This band grows in intensity relative to the other vibronic bands when water is added to the expansion, suggesting that it belongs to a DMB/ H_2O complex, a DMB molecule to which one or more water molecules are attached. Replacing the H_2O with D_2O leads to further changes in the structure of this band as shown in the insert to Figure 3-1. The band is fragmented, which may be attributed to isotopic exchange.

An unambiguous determination of the structure of DMB responsible for Band A was made possible by a study of the spectrum at high resolution. Figure 3-2 shows the rotationally resolved $S_1 \leftarrow S_0$ fluorescence excitation electronic spectrum of Band A recorded in a molecular beam. It spans approximately 4 cm^{-1} and displays two well-defined branches. The lower frequency region of the spectrum is the P-branch ($\Delta J = -1$ transitions) and the higher frequency

region is the R-branch ($\Delta J = +1$ transitions). These branches are separated by a “Zero Gap”, where the center (or origin) of the band is located. The lack of central Q branch ($\Delta J = 0$) transitions in this gap indicates that the spectrum is a classic *b*-type spectrum.

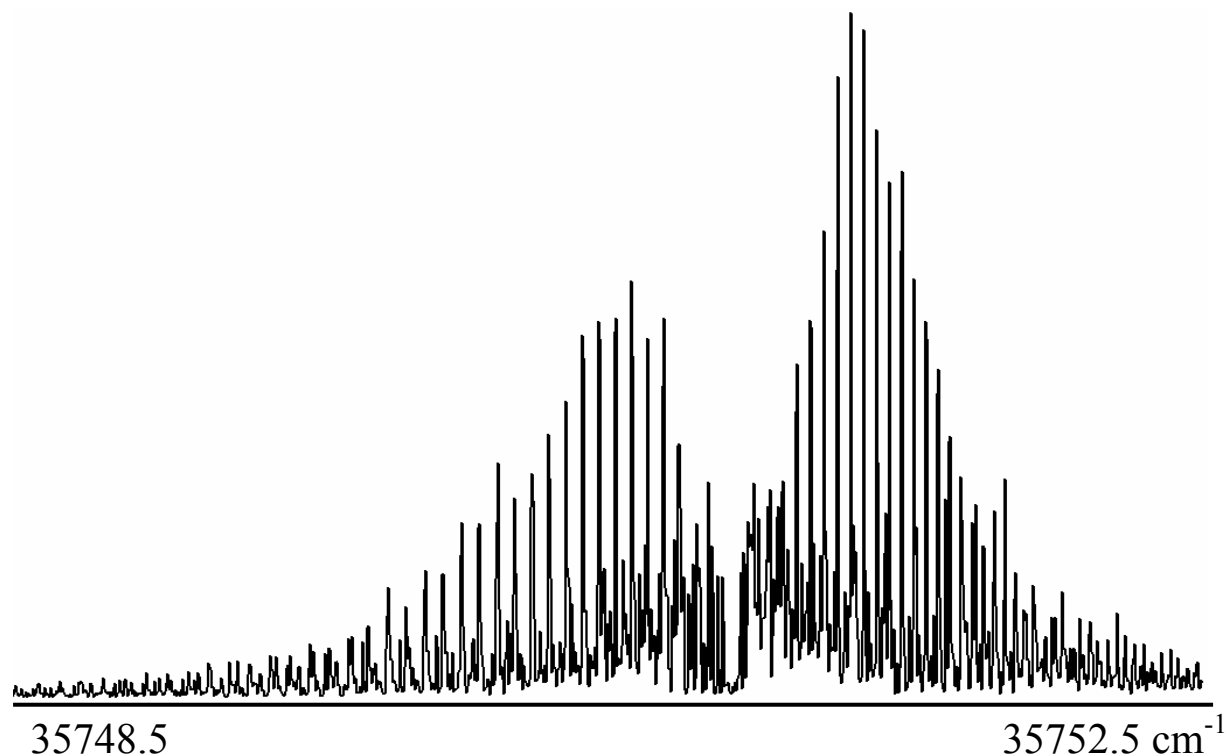


Figure 3-2. Rotationally resolved fluorescence excitation spectrum of Band A of DMB.

Rotational analysis of this spectrum was performed with the *jb95* program²⁴, which utilizes the rigid rotor Hamiltonian:

$$H_r = A P_a^2 + B P_b^2 + C P_c^2$$

Here, P_a^2 , P_b^2 and P_c^2 are the components of the angular momentum about the *a*, *b*, and *c* inertial axes; A, B, and C are the respective rotational constants, $A = \frac{\hbar}{4\pi I_a}$, etc.; and I_a , I_b , and I_c

are the principal moments of inertia about these axes. The fitting process began with the simulation of a spectrum using an assumed structure of DMB in both electronic states and a band type. From the appearance of the spectrum, *b*-type selection rules ($\Delta J = 0, \pm 1$, $\Delta K_a = \pm 1$, and $\Delta K_c = \pm 1$) were assumed. The structures of the ground state were taken from *ab initio* calculations, using Møller-Plesset 2nd order perturbation theory (MP2) with a 6-31G** basis set.²⁵ The two lowest energy structures (*trans* and *cis*) are displayed in Figure 3-3. They difference in energy is $\sim 900\text{ cm}^{-1}$ with the *trans*-isomer lying at lower energy. Clearly, the two structures have different rotational constants, providing a basis for their distinction.

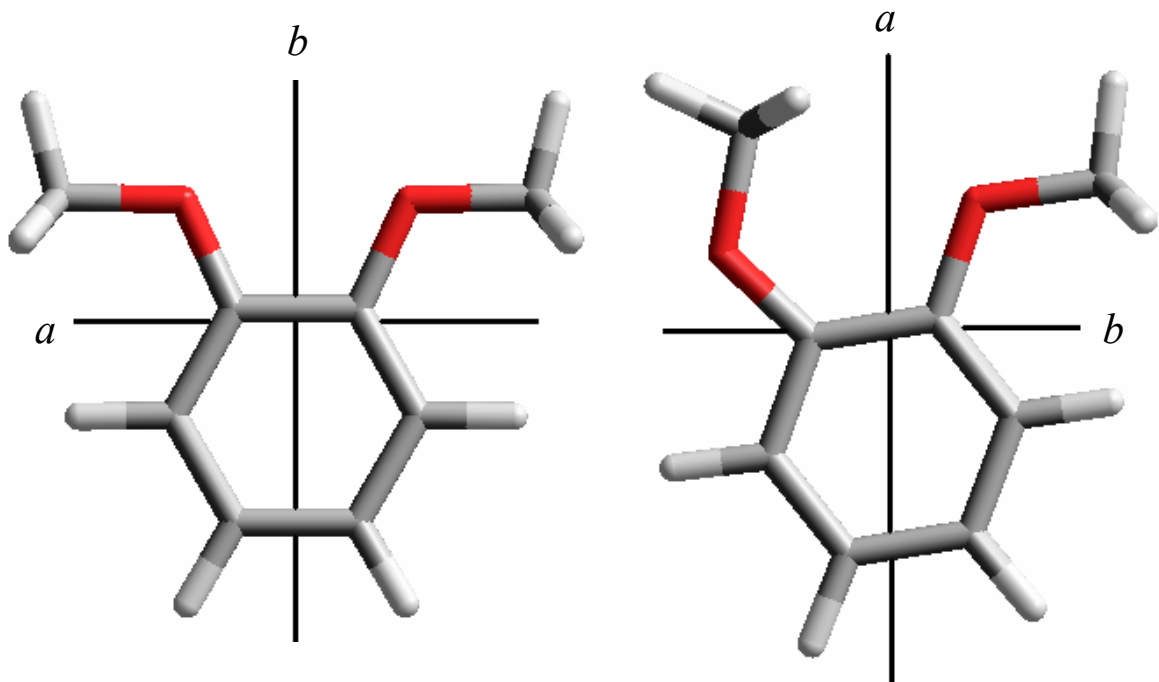


Figure 3-3. Two likely conformations of 1,2-dimethoxybenzene with their respective inertial axes.

Single transitions were selected from the simulation which corresponded to the experimental spectrum and used for initial assignments. Further improvements were made by assigning $K = 0$ and 1 transitions because their intensities were expected to be strong. These assignments were iteratively optimized by a least squares analysis routine. At a maximum J of 40 with the rotational temperature of 2.9 K, approximately 300 rovibronic transitions were assigned resulting in an OMC (observed minus calculated frequency) of 3.3 MHz. Finally, single transitions in the spectrum were fit to a line shape (Voigt profile) with Doppler-broadened Gaussian and lifetime-broadened Lorentzian components. The spectrum of a heavily congested portion of the R branch at full resolution is shown in Figure 3-4 to illustrate the quality of the fit. Individual lines have full width at half maximum (FWHM) linewidths of $\sim 45 (\pm 5)$ MHz; the lineshape analysis yields a Gaussian linewidth of 18 MHz and a Lorentzian linewidth of 40 MHz, corresponding to a lifetime of 4 ns.

The results of the rotational analysis are listed in Table 3-2 together with the calculated rotational constants. The results show unambiguously that the isomer responsible for Band A is *trans*-DMB.

Once the identity of the carrier of Band A was established, the recorded spectra of Bands B through G also were analyzed. All of these bands exhibit the same *b*-type bands as Band A. Further, the ground state rotational constants of all of these bands are the same as those for Band A, as shown in Table 3-3. This clearly indicates that these bands originate from the same zero point vibrational level (ZPL) in the electronic ground state, and that the isomer which is responsible for these bands is also *trans*-DMB. However, the excited state rotational parameters

are all different, showing that these bands terminate in levels of the S_1 state having different vibrational characters.

Additional properties of the excited state are noted in Table 3-3. The differences in rotational constants ($\Delta A=A'-A''$), ΔB , and ΔC are all negative. Since rotational constants are inversely proportional to the moments of inertia ($I_a = \sum m_i (b_i+c_i)$, *etc.*), which in turn are sensitive to the displacements of atomic masses, the observed decreases in the constants are a direct result of expansion of the molecule with respect to each of the principal axes in the excited state. In addition, the magnitude of the inertial defect (ΔI) (defined as $\Delta I=I_c-I_b-I_a$) is a measure of

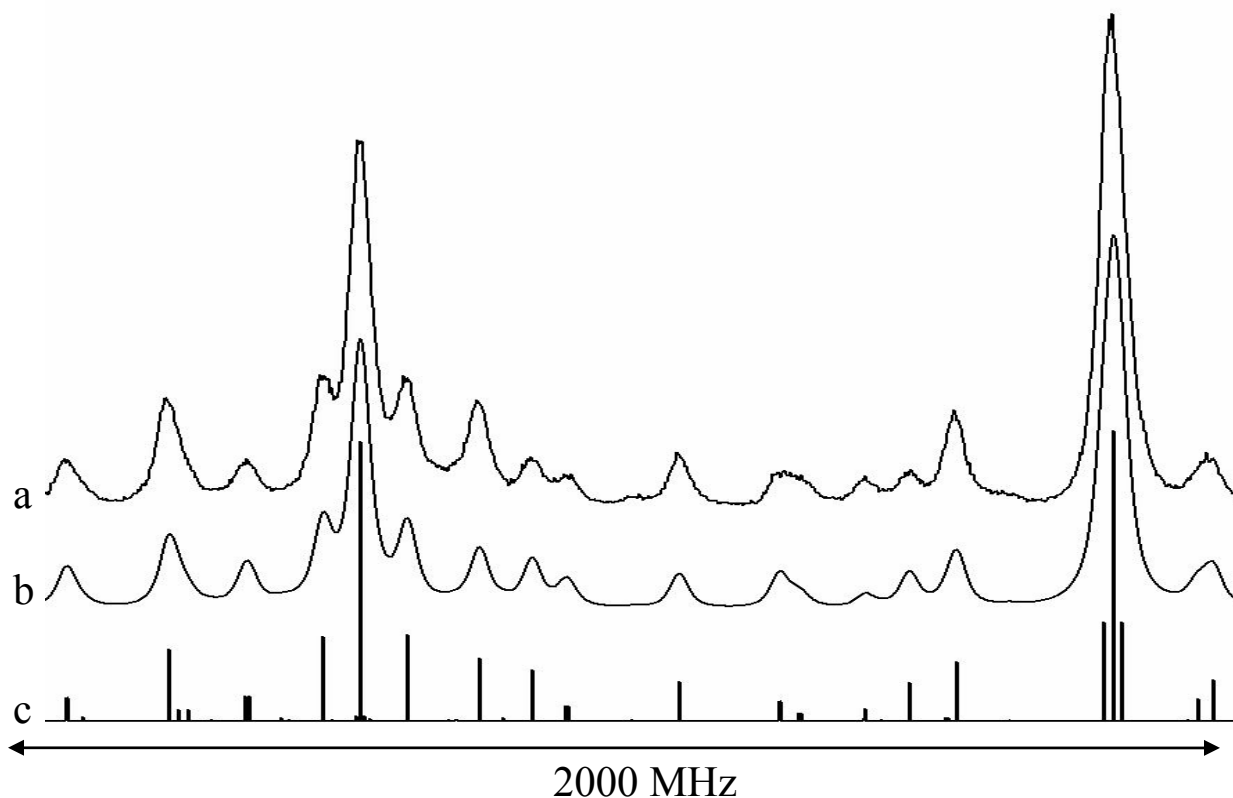


Figure 3-4. Portion of the R-branch taken from the spectrum of Band A of DMB at full resolution. Trace a is the experimental spectrum. Trace b is a simulated spectrum using a Voigt line shape function (18 MHz Gaussian and 40 MHz Lorentzian). Trace c is a stick figure representation of the spectrum.

Table 3-2. Ground state rotational constants of Band A compared to the *ab initio* values of *trans* and *cis*-DMB (MP2/6-31G**).

Parameter	Band A	<i>Trans</i> -DMB	<i>Cis</i> - DMB
A''	1663.1(1) MHz	1663.1 MHz	1752.0 MHz
B''	1349.8(2) MHz	1349.6 MHz	1367.9 MHz
C''	752.6(1) MHz	752.1 MHz	775.7 MHz
$\Delta I''$	-6.80 amu Å ²	-6.39 amu Å ²	-6.37 amu Å ²

the molecule's planarity. A rigidly planar molecule has an inertial defect of zero. As atoms deviate from the plane, the inertial defect becomes more negative. In-plane and out-of-plane vibrational motions drive the inertial defect towards more positive and negative values, respectively. The source of the inertial defect in ground state *trans*-DMB (-6.80 amu Å²) are the out-of-plane hydrogens of the two methyl groups. In the excited state, the inertial defect

Table 3-3. Derived rotational constants from the fits of Band A through G in the fluorescence excitation spectrum of DMB (*cf.* Figure 3-1).^a

S ₀	Bands						
	A	B	C	D	E	F	G
A''	1663.1(1)	1662.9 (1)	1663.0(1)	1663.1(1)	1662.9(1)	1662.9 (1)	1663.2(1)
B''	1349.8(1)	1349.7 (2)	1349.9(2)	1349.9(2)	1349.7(1)	1349.7 (2)	1350.0(2)
C''	752.6(1)	752.6 (1)	752.6(1)	752.6(1)	752.6(1)	752.6 (1)	752.6(1)
$\Delta I''$	-6.80	-6.80	-6.77	-6.77	-6.90	-6.80	-6.73
S ₁							
A'	1641.6(1)	1642.8 (1)	1641.3(1)	1634.7(1)	1640.2(1)	1639.0 (1)	1640.9(1)
B'	1329.1(1)	1330.3 (1)	1331.5(2)	1333.8(2)	1330.9(1)	1330.6 (2)	1330.3(2)
C'	742.7(1)	746.2 (1)	745.4(1)	744.3(1)	744.4(1)	744.0 (1)	742.8(1)
$\Delta I'$	-7.68	-10.23	-9.46	-9.06	-8.95	-8.87	-7.50

^aRotational constants in MHz, inertial defect in amu Å²

increases in magnitude by 0.88 amu \AA^2 . Thus, DMB distorts along some out-of-plane coordinate and becomes less planar in the S_1 state.

The DMB/ H_2O complex band, at $0_0^0 + 127 \text{ cm}^{-1}$, also was recorded in the molecular beam. Its rotationally resolved $S_1 \leftarrow S_0$ fluorescence excitation spectrum is shown in Figure 3-5. The appearance of this spectrum is very different from that of the bare molecule. Now the

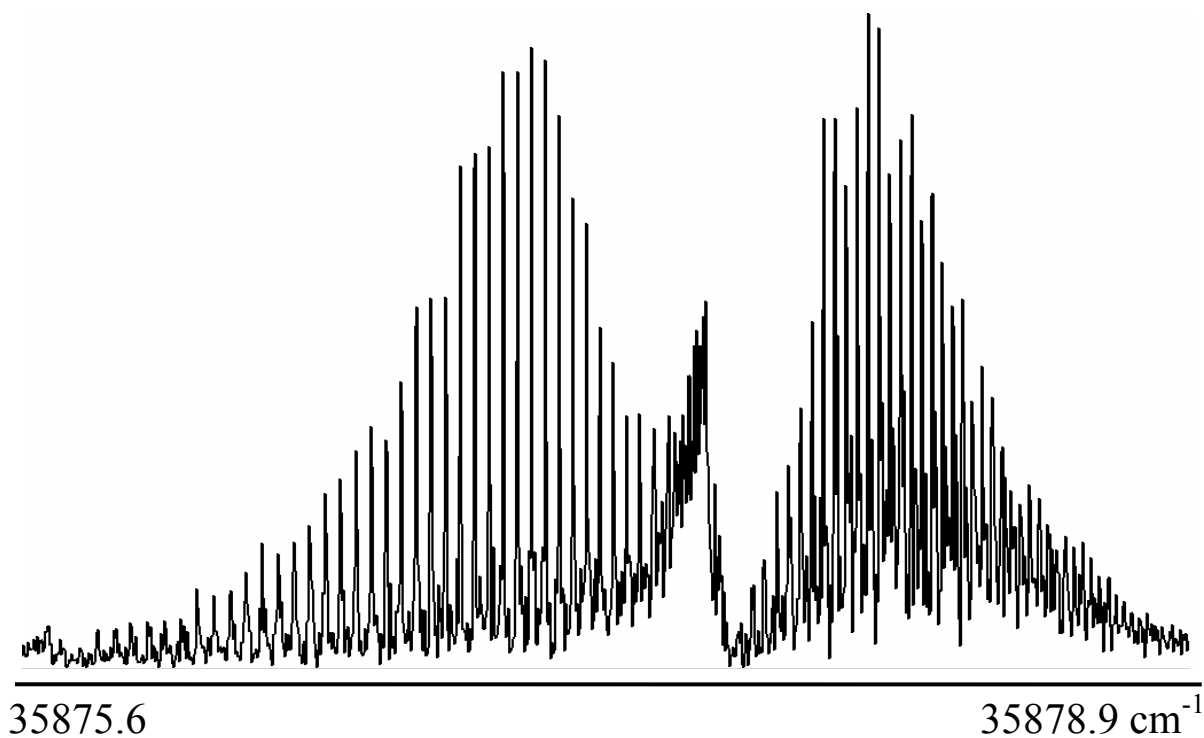


Figure 3-5. Rotationally resolved $S_1 \leftarrow S_0$ fluorescence excitation spectrum of 1,2-dimethoxybenzene / H_2O .

spectrum displays a strong central Q-branch ($\Delta J=0$ transitions), suggesting an *a*-type band. Rotational analysis of this band was performed with the *jb95* program²⁴, that utilizes the non-rigid rotor Hamiltonian

$$H = H_r + H_d$$

$$H_d = \Delta_J P^4 - \Delta_{JK} P^2 P_a^2 - \Delta_K P_a^4 - 2\delta_J P^2 (P_b - P_c) - 2\delta_K [P_a^2 (P_b^2 - P_c^2) + (P_b^2 - P_c^2) P_a^2] \quad (2)$$

Here, H_r is the rigid rotor Hamiltonian defined in Eq. (1), and H_d is the distortion Hamiltonian, introduced by Watson²⁶ and discussed in more detail in Gordy and Cook.²⁷ Δ_J , Δ_{JK} , Δ_K , δ_J , and δ_K are the quartic distortion coefficients, and the total angular momentum (P^2) is equal to the sum of P_a^2 , P_b^2 and P_c^2 .

Not knowing the structure of DMB-H₂O, the bare molecule rotational constants and *a*-type selection rules ($\Delta J = 0, \pm 1$, $\Delta K_a = \pm 0$, and $\Delta K_c = \pm 1$) were used to generate an initial simulated spectrum. This was then refined, using a strategy similar to that discussed earlier, by comparison with the experimental results. Initially, a rigid rotor Hamiltonian was assumed; however, the assignments resulted in a large OMC (~15 MHz). When the Watson distortion terms were then incorporated into the fit, an assignment of 560 lines yielded an OMC of 3.3 MHz. Despite the quality of this fit, the experimental spectrum still had observed transitions that were missing from the simulated spectrum. An autocorrelation analysis²⁸ was then used to assess to whether or not multiple bands might be present. This analysis demonstrated that there are a few possible repetitive separations in the spectrum; 1.2, 2.6, and 3.7 GHz; see Figure 3-6. Among these, the peak at 1.2 GHz is the most intense.

Given this result, a second simulated spectrum was generated, using the rotational constants from the main band. The initial position of origin of the second band was placed at 1.2 GHz to the blue of the first. Manipulating the origin to determine a crude frequency position,

simulated rovibronic transitions were then assigned. Again distortion terms were implemented in the final assignment of 355 lines resulting in an OMC of 4.0 MHz. The fit of the spectrum was compared with Voigt profiles convoluting the two sub-bands; a careful measurement of the relative intensities of the two sub-bands gave a 3:1 ratio, within $\pm 5\%$.

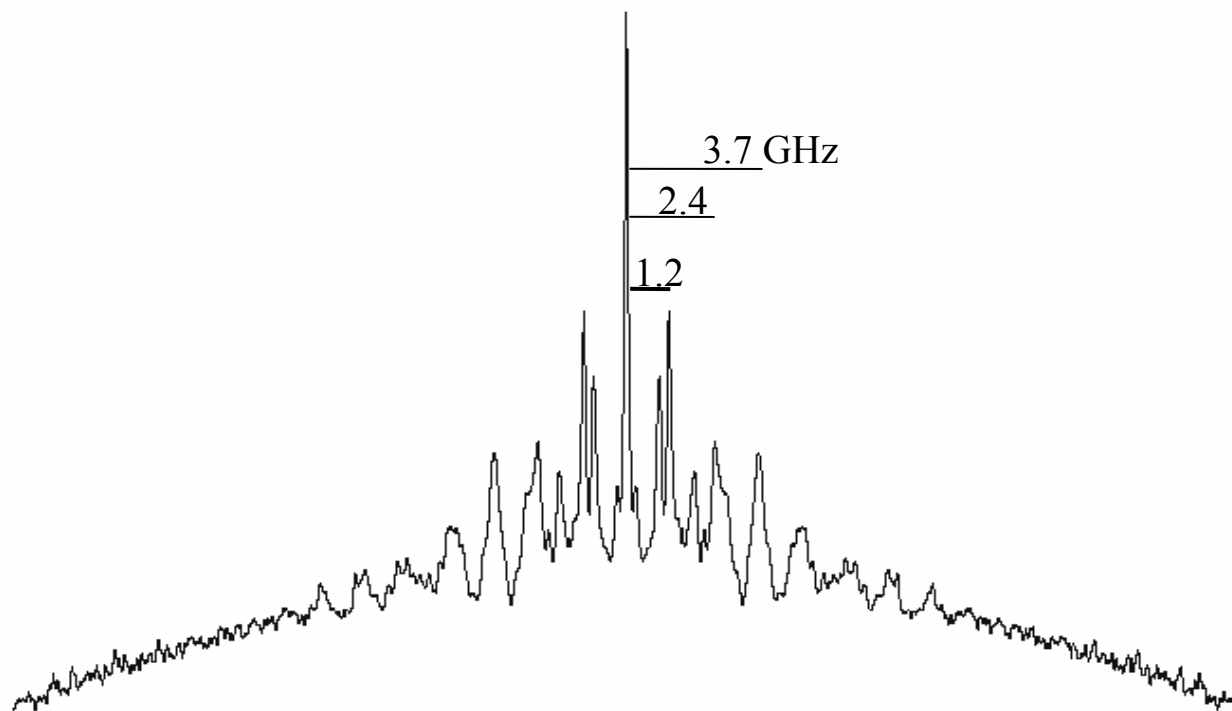


Figure 3-6. Autocorrelation spectrum of the 1,2-dimethoxybenzene / H₂O complex.

A portion of the R branch in the spectrum of DMB/H₂O is shown at full resolution in Figure 3-7. The top trace (Figure 3-7a) is the fluorescence excitation spectrum with individual lines FWHM linewidths of 40 ± 5 MHz. Figures 3-7c and 3-7d show the contributions to this spectrum from the two sub-bands. Finally, Figure 3-7b shows the quality of the fit with the Voigt profile composed of a Gaussian linewidth of 18 MHz and a Lorentzian linewidth of 40 MHz, convoluting the two sub-bands. The complete inertial parameters for both electronic states

are listed in Table 3-4. Note that these parameters are very different from those of the bare molecule (Table 3-3).

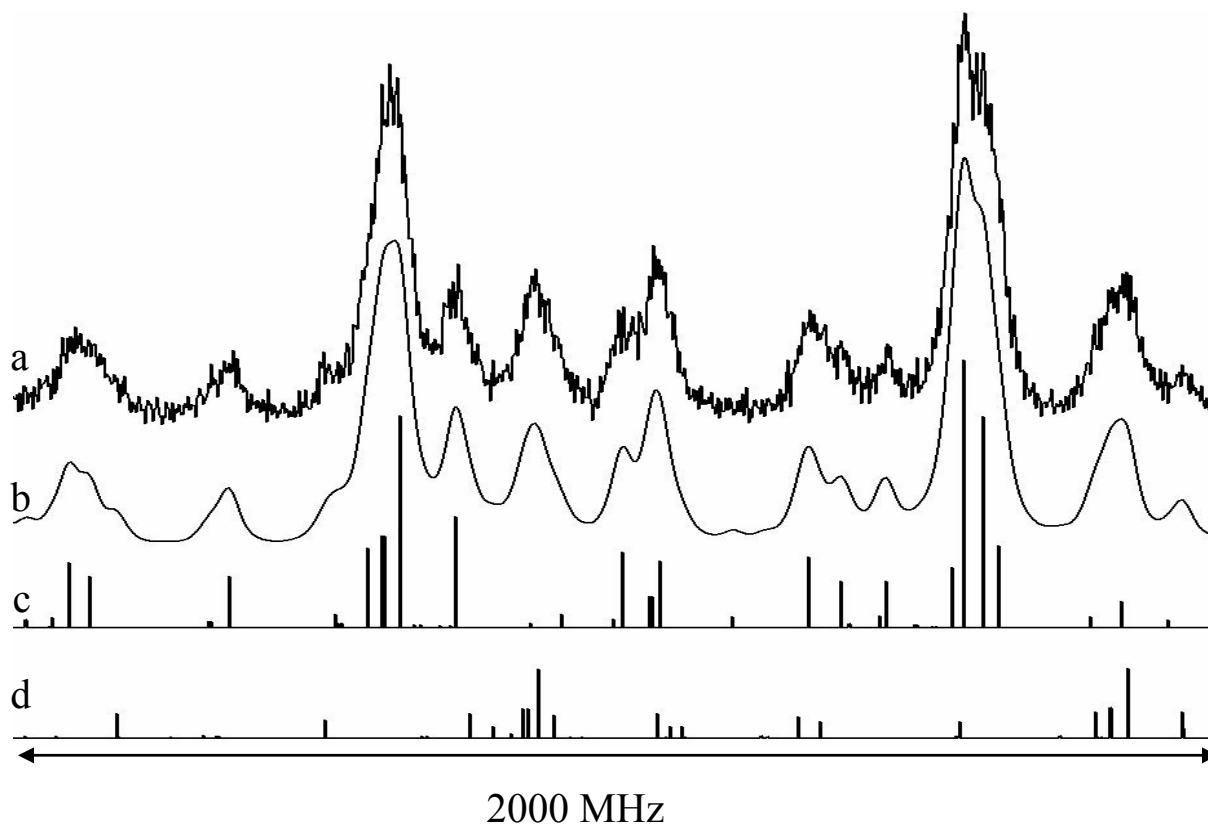


Figure 3-7. At full resolution, a portion of the R-branch is shown from the spectrum of 1,2-dimethoxybenzene / H₂O. Trace a is the experimental spectrum, and traces c and d show the calculated rovibronic transitions in subbands B and A, respectively. Trace b is the simulated spectrum, using the Voigt lineshape function described in the text.

Figure 3-8 shows the rotationally resolved S₁←S₀ fluorescence excitation spectrum of the D₂O complex band. This spectrum displays an *a*-type band very similar to that of H₂O complex, slightly red shifted by 0.6 cm⁻¹ relative to that of DMB-H₂O. The spectrum in Figure 3-8 was fit by starting with the same constants as the water complex for the initial simulations, and then

iterated as described before. At full resolution, a portion of the fitted R-branch is shown in Figure 3-9. Two simulated spectra were also required to fit the experimental spectrum. Their intensity ratio is 1:2 within $\pm 5\%$. The weaker intensity band (*B* sub-band) is red shifted by only 45 MHz relative to stronger band (*A* sub-band). Voigt profiles composed of a Gaussian linewidth of 18 MHz and Lorentzian linewidth of 40 MHz were require to fit both sub-bands. The final results of the fit are listed in the Table 3-5.

Table 3-4. Rotational and centrifugal distortion constants of the *A* and *B* subbands in the $S_1 \leftarrow S_0$ spectrum of DMB/H₂O.^a

<i>S</i> ₀ state	<i>A</i> subband	<i>B</i> subband
A''	1356.0(3)	1357.6 (2)
B''	880.7(1)	880.6 (1)
C''	538.1(1)	538.0 (1)
Δ_J''	-0.00027(9)	0.000109 (3)
Δ_{JK}''	0.0128 (6)	0.00845 (2)
Δ_K''	-0.061 (4)	-0.0070 (1)
δ_j''	0.00009(4)	0.000030 (2)
δ_k''	-0.0041 (5)	0.00422 (2)
<i>S</i> ₁ state	<i>A</i> subband	<i>B</i> subband
A'	1335.4(3)	1337.0 (2)
B'	874.1(1)	874.0 (1)
C'	533.5(1)	533.4 (1)
Δ_J'	-0.0001 (1)	0.000052 (3)
Δ_{JK}'	0.0081 (6)	0.00438 (2)
Δ_K'	-0.056 (4)	-0.0028 (1)
δ_j'	0.00015(5)	0.000030 (2)
δ_k'	-0.0049 (5)	0.00204 (2)

^aAll constants in MHz. The separation of the two subband is 1197.10 MHz (0.04 cm⁻¹)

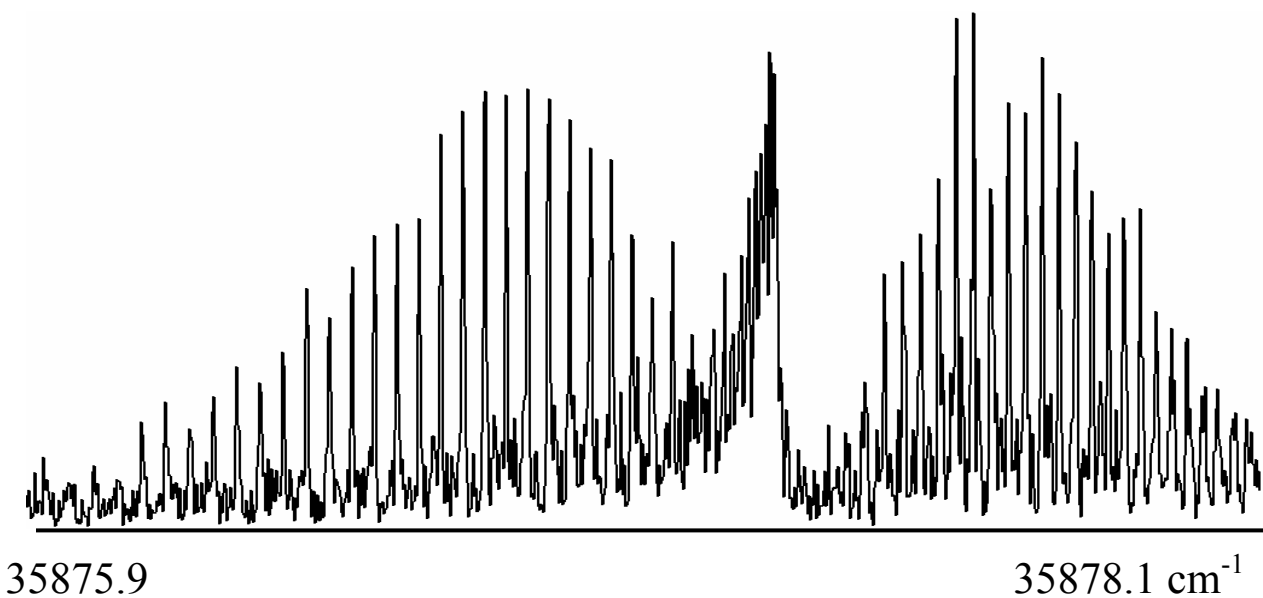


Figure 3-8. Rotationally resolved $S_1 \leftarrow S_0$ fluorescence excitation spectrum of 1,2-dimethoxybenzene / D_2O .

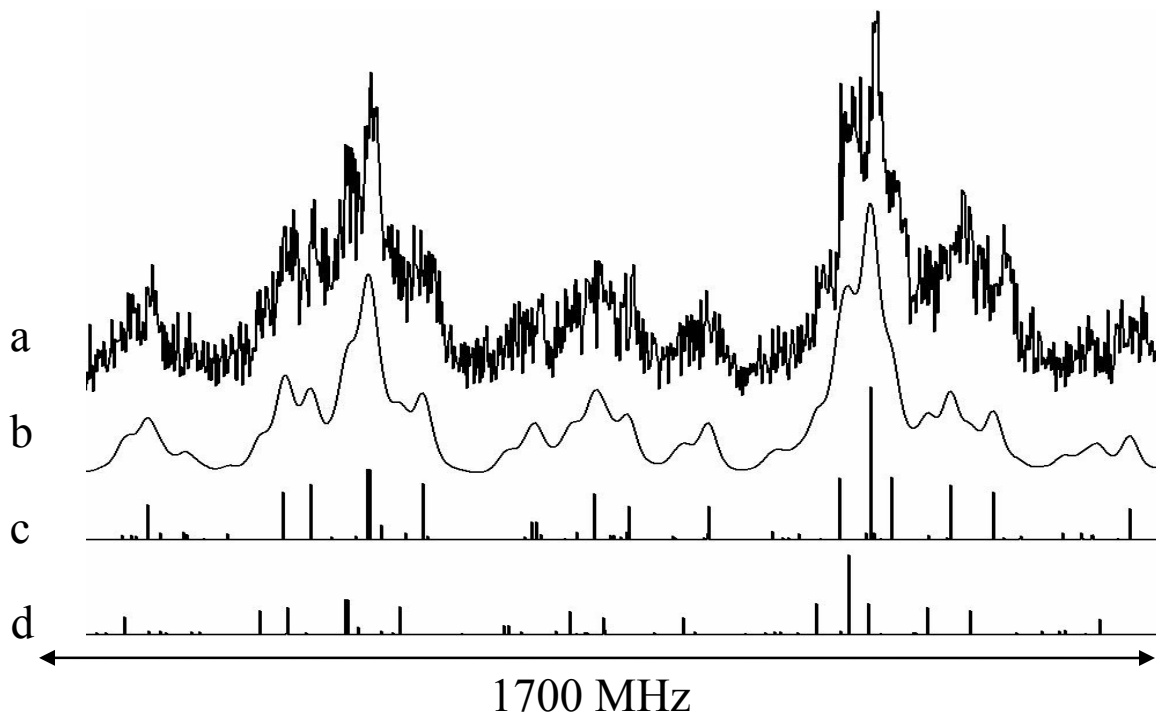


Figure 3-9. At full resolution, a portion of the R-branch is shown from the spectrum of 1,2-dimethoxybenzene / D_2O . The top trace is the experimental spectrum and the bottom traces c and d show the simulated rovibronic transitions in subbands *A* and *B*, respectively. Trace b is the simulated spectrum, using the Voigt lineshape function described in the text.

Table 3-5. Rotational and centrifugal distortion constants of the *A* and *B* subbands in the $S_1 \leftarrow S_0$ spectrum of DMB/D₂O.^a

S_0 state	<i>A</i> subband	<i>B</i> subband
A''	1356.1(4)	1356.0(6)
B''	846.6(1)	846.6(1)
C''	525.2(1)	525.4(1)
Δ_J''	0.0008 (1)	0.0003 (2)
Δ_{JK}''	0.0027 (7)	0.008 (1)
Δ_K''	0.008 (6)	0.002 (8)
δ_j''	0.00022 (6)	0.00024 (8)
δ_k''	0.0054 (9)	0.007 (2)
S_1 state	<i>A</i> subband	<i>B</i> subband
A'	1335.0(4)	1334.9(6)
B'	840.3(1)	840.4(1)
C'	521.4(1)	521.2(1)
Δ_J'	0.0008 (1)	0.0005 (2)
Δ_{JK}'	-0.0015 (8)	0.004 (1)
Δ_K'	0.012 (6)	0.006 (8)
δ_j'	0.00026 (6)	0.00035 (8)
δ_k'	0.0037 (9)	0.006 (2)

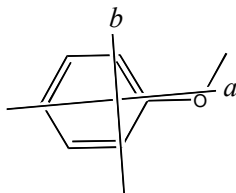
^aAll constants in MHz. The separation of the two subband is 45.4 MHz (0.0015 cm⁻¹)

3.5. Discussion.

We have determined the rotational constants of the ground and excited electronic states of DMB, of DMB-H₂O and the orientation of the $S_1 \leftarrow S_0$ electronic transition moments in both species. We begin with a discussion of the structure of the isolated molecule, in its ground state.

3.5.1. The bare molecule, DMB.

Anisole (Scheme 3-2), the parent molecule, has the ground state rotational constants $A=5028.867$, $B=1568.375$ and $C=1205.836$ MHz as determined by microwave spectroscopy.²⁹



Scheme 3-2: The structure of anisole with its inertial frame.

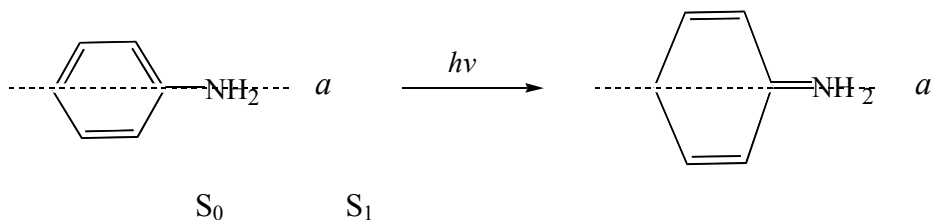
As shown in Table 3-2, the ground state rotational constants of DMB are drastically different, $A=1663.1$, $B=1349.8$ and $C=752.6$ MHz. The substantially larger A rotational constant of anisole is due to its smaller moment of inertia; this is a direct result of the relatively small displacements of atoms perpendicular to the a -axis. Mono-substituted benzenes typically have larger A than B and C constants.³⁰ In contrast, the displacement of the atoms from the a and b axes is more evenly distributed in DMB, and the rotational constants are more nearly equal.

Inertial defects also may be used to provide information about structure. Thus, anisole in its ground state has an inertial defect of $-3.410 \text{ amu } \text{\AA}^2$,²⁹ whereas DMB in its ground state has an inertial defect of $-6.820 \text{ amu } \text{\AA}^2$. Since this value is twice as large as that for anisole, we can conclude that the atoms responsible for the non-zero values are the out-of-plane hydrogens of the methoxy substituent(s). The heavy atom structure of both molecules is planar.

An important contributor to the planar geometry of DMB is the conjugation between the methoxy lone pairs and the benzene π -orbitals. Rumi and Zerbi³¹ have demonstrated that the

The calculated barrier to internal rotation of the methyl group in *cis*-MVE is 1339.5 cm⁻¹ (3.83 kcal/mol).³⁰ A barrier on the order of 1000 cm⁻¹ will produce a tunneling splitting on the order of 10 MHz in an electronic spectrum, making it difficult to observe.

Excitation of DMB to its S₁ state produces large changes in its rotational constants; $\Delta A = (A' - A'') = -21.5$ (1.3%), $\Delta B = -20.7$ (1.5%) and $\Delta C = -9.9$ MHz (1.3%). All values are negative, suggesting an expansion of the molecular frame. An increase in molecular size is a natural consequence of excitation by light, since antibonding orbitals are populated and bonding orbitals are depopulated. However, the ΔA , ΔB , and ΔC values in DMB are all of the same magnitude, whereas typical mono-substituted benzenes exhibit much larger ΔA values compared to ΔB and ΔC . For example, aniline has $\Delta A = -331.2$, $\Delta B = 39.6$, and $\Delta C = -17.8$ MHz, revealing significant bond lengthening in directions perpendicular to the *a*-axis.³⁴ The quinoidal model first proposed by Cvitas³⁵ and shown in Scheme 3-5 seems to account for these changes.



Scheme 3-5: Structural changes in mono-substituted benzenes on S₁ excitation.

Clearly, DMB is different; the primary C₂ symmetry axis is now along the *b* inertial axis rather than *a*. This explains the different in its ΔA , ΔB and ΔC values. We have explored the possible structural changes using *ab initio* methods, MP2 with a 6-31G** basis set for the S₀ state and CIS with a 6-31+G* basis set for the S₁ state. The calculations reproduce well the A, B,

and C values of the S_0 state, and the ΔA , ΔB , and ΔC values for the S_1 state; hence, they should be reliable indicators of the geometries of the two states. Figure 3-10 shows the results obtained. The major changes in bond lengths on electronic excitation are in C_1-O_1 and C_6-O_2 ; these decrease from 1.368 to 1.328 Å. The $C_1-O_1-C_7$ and $C_6-O_2-C_8$ bond angles increase from 116.1 to

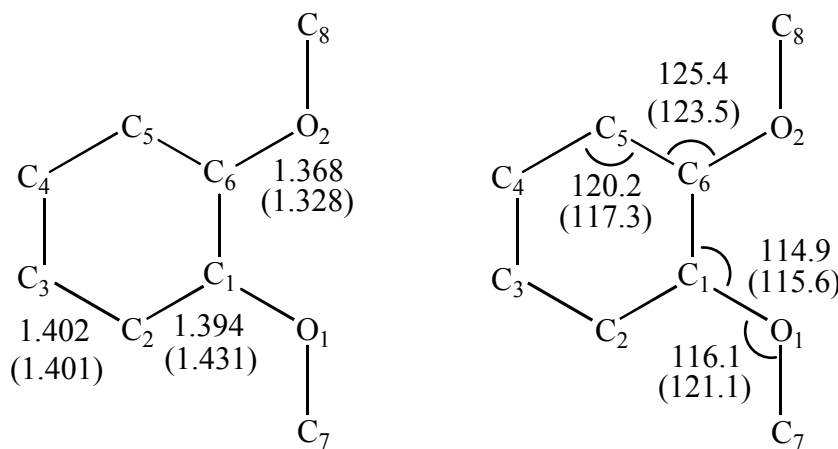
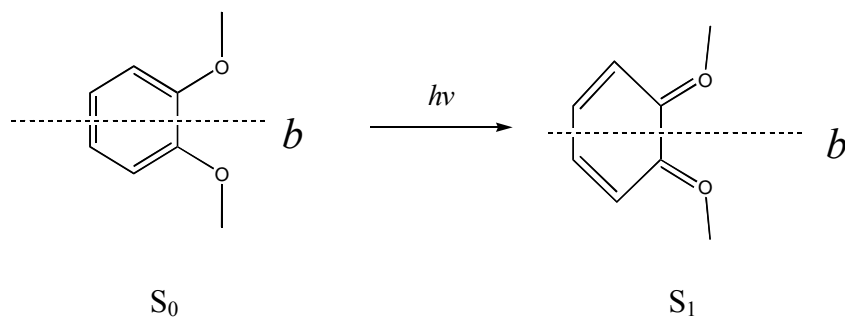


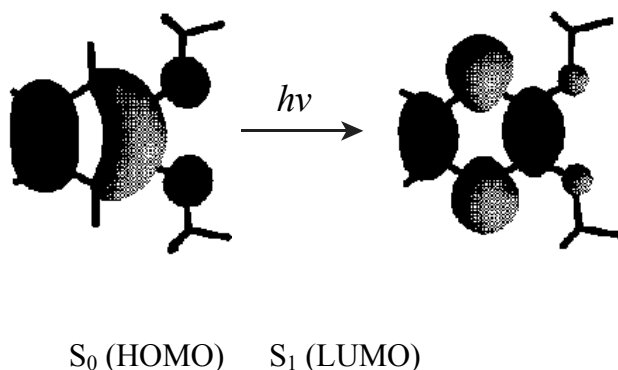
Figure 3-10. *Ab initio* geometries of DMB in its S_0 and S_1 states. S_1 state values are given in parentheses with bond lengths in Å (left) and angles in degrees (right).

121.1°. In the ring, the C_1-C_2 and C_5-C_6 bond lengths increase from 1.394 to 1.431 Å. The observed changes in structure are consistent with those shown schematically in Scheme 3-6, below.



Scheme 3-6: Structural changes in *trans*-DMB on S_1 excitation.

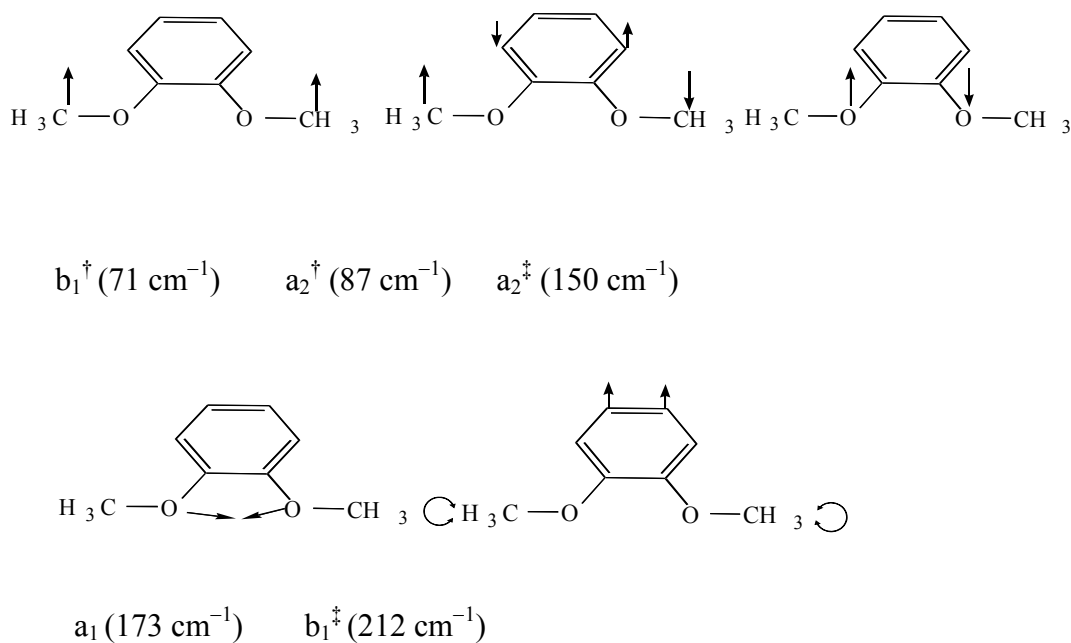
The calculations also provide some insight into the changes in electronic distribution that occur on excitation of the S_1 state. Shown in Scheme 3-7 are two of the relevant orbitals, HOMO



Scheme 3-7: CIS/6-31G* calculated one-electron molecular orbitals of DMB.

(highest occupied molecular orbital) and LUMO (lowest unoccupied molecular orbital) that participate in the $S_1 \leftarrow S_0$ electronic transition. Clearly, absorption of a photon introduces antibonding character into the C_1 - C_2 and C_5 - C_6 bonds and increases the electron density at C_2 and C_5 . Also, the electron density decreases at all remaining heavy atoms, especially the O_1 and O_2 atoms. These changes, in turn, produces changes in the equilibrium geometries of the two states; those shown in Scheme 3-6 are consistent with those shown in Scheme 3-7. We also see from Scheme 3-7 that the light induced oscillations of electron density occur mainly along b , explaining why the 0_0^0 band of *trans*-DMB is b -axis polarized. The observed TM orientation in DMB is consistent with the observed S_1 - S_0 TM orientations of a large variety of other substituted benzenes.³⁶

The structural changes shown in Scheme 3-6 also explain the substantial vibrational activity that appears in the low resolution S₁-S₀ spectrum of DMB (Figure 3-1). To further evaluate the nature of these vibrations, normal mode calculations were performed on S₀ DMB using the 6-31G* basis set. *Trans*-DMB has 54 normal modes; the five lowest fundamental vibrational frequencies are 71, 87, 150, 173 and 212 cm⁻¹ (These values were scaled by the multiplicative factor of 0.89). A careful examination of the atomic displacements in each mode shows two dimethoxy in-phase, out-of-plane bending modes at 71 (b₁[†]) and 212 (b₁[‡]) cm⁻¹, two out-of-phase modes at 87 (a₂[†]) and 150 (a₂[‡]) cm⁻¹, and an in-plane symmetric bending mode (a₁) at 173 cm⁻¹, as shown in Scheme 3-8.



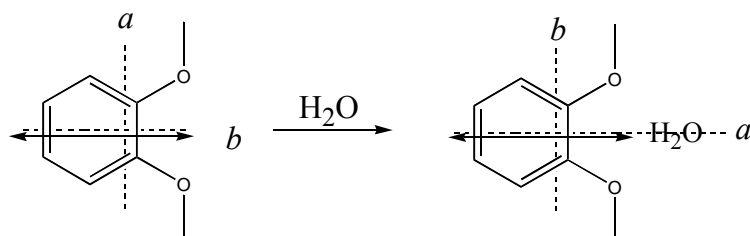
Scheme 3-8: Low frequency vibrations of DMB in the ground state.

Thus, we tentatively assign band B (at + 84.2 cm⁻¹) as the first overtone of an out-of-plane bending mode (b₁[†] or a₂[†]) since it exhibits the largest (in magnitude) inertial defect (-10.23 amu

\AA^2). Band G (at $+201.8\text{ cm}^{-1}$) can be assigned to the in-plane bending mode (a_1 symmetry) since it exhibits the smallest inertial defect (-7.50 amu \AA^2). Other bands have been assigned as overtones and combinations of these modes as shown in Table 3-1.

3.5.2. The water complex, DMB-H₂O.

The $S_1 \leftarrow S_0$ electronic transition moment of DMB is oriented along the b -axis in the plane of the molecule as shown in Scheme 3-9. The corresponding transition in DMB/water has its transition moment parallel to a . Given the relatively weak nature of the intermolecular bond(s) between the two species, attachment of the water molecule is not likely to change the nature of the S_1 - S_0 electronic transition. Therefore, the most likely H₂O bonding site is along b , nestled between the two methoxy groups (see Scheme 3-9). Owing to its increased mass, the attachment of the weakly bound water exchanges the two inertial axes, a and b , resulting in an a -type origin band in DMB-H₂O.



Scheme 3-9: The TM orientation of DMB and its water complex are indicated by an arrow.

Further evidence for this binding site comes from the observed rotational constants. If the water moiety lies on the b -principal axis of the bare molecule, then that particular rotational constant will remain unchanged upon complexation. The rotational constants of DMB and the

water complex are compared in Table 3-6. Those of the bare molecule are larger than those of the complex, of course; the reduction is due to the addition of the water molecule. But the average A rotational constant of the two subbands of the complex is close to the B rotational constant of the bare molecule. This shows that the water molecule lies on the *b*-axis of the bare molecule. Also notice that the differences in the excited state rotational constants, ΔB of the bare

Table 3-6. Rotational parameters of DMB and the DMB-H₂O complex. The values for the complex are the average values of two subbands.^a

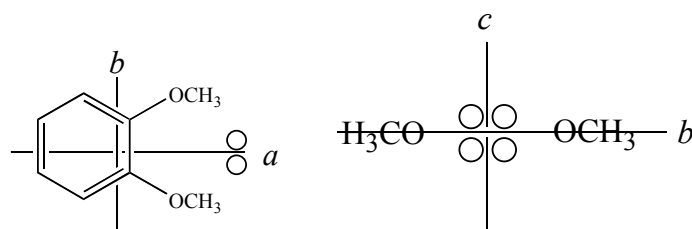
	DMB		DMB/H ₂ O
A''	1663.1	A'' _H	1356.8
B''	1349.8	B'' _H	880.7
C''	752.6	C'' _H	538.1
$\Delta I''$	-6.80	$\Delta I''_{H}$	-7.1
A'	1641.6	A' _H	1336.2
B'	1329.1	B' _H	874.1
C'	742.7	C' _H	533.5
$\Delta I'$	-7.68	$\Delta I'_{H}$	-9.119
ΔA	-21.5	ΔA_{H}	-20.6
ΔB	-20.8	ΔB_{H}	-6.6
ΔC	-9.9	ΔC_{H}	-4.6

^a Rotational constants in MHz, inertial defects in amu Å².

molecule and ΔA of the complex, are identical, confirming this conclusion. Further, the relatively small inertial defects of the complex suggest that the water lies in the plane of DMB.

The small differences in the inertial defects can be accounted for by out-of-plane hydrogen atoms of the water molecule.

More quantitatively, we have determined the COM coordinates of the attached water molecule using the Kraitchman method.²⁷ The results are listed in Table 3-7 and shown approximately in Scheme 3-10. According to this analysis, the water molecule lies well outside



Scheme 3-10: Circles indicate the four equivalent positions of the COM of the attached water molecule in the ab and bc planes of DMB/H₂O.

the two methoxy groups at a distance of 4.05 Å along the a axis in the ground state. This distance decreases slightly on excitation of DMB to its S_1 state, but this decrease in a is likely caused by expansion of the bare molecule, not a tighter binding of the attached H₂O. (The DMB/H₂O origin band is blue shifted by 127 cm⁻¹ with respect to that of the bare molecule, indicating a weaker intermolecular interaction in the S_1 state.) The coordinate $|b|$ is substantially different from zero in both states. Apparently, the water molecule is localized on one side of the ac plane or the other. In contrast, the coordinate $|c|$ is significantly smaller, suggesting a large amplitude motion perpendicular to the ab plane.

Table 3-7. Kraitchman coordinates (in Å) of the center-of-mass (COM) of water in both electronic states of DMB/H₂O. (*a*, *b*, and *c* are the inertial axes of the complex.)

coordinate	S ₀	S ₁
<i>a</i>	4.053(5)	4.029(5)
<i>b</i>	0.61(2)	0.68(2)
<i>c</i>	0.14(7)	0.29(3)
<i>r</i>	4.100(1)	4.098(1)

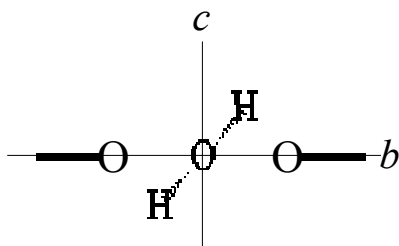
Information about the orientation of the attached water molecule and the position of its hydrogen atoms comes from a similar comparison of the rotational constants of DMB/H₂O and DMB/D₂O. This comparison is shown in Table 3-8. Examining these results, we see that deuterium substitution produces a large change in B and C, but only a small change in A. The large change in B is a direct consequence of the larger displacement of the water molecule from the *b* axis (*cf.*, Table 3-7) and is a “trivial” result. But the fact that deuterium substitution produces a much larger change in C than in A is a non-trivial result. This result demonstrates that the water hydrogens are tilted out of the *ab* plane and make a much larger projection on *c* than *a*. Each methoxy group oxygen has two lone pairs of electrons, pointing above and below the *ab* plane. Thus, the hydrogens of the attached water molecule are most probably hydrogen bonded to two of these lone pairs, one above the *ab* plane and the other below.

Table 3-8. Rotational constants (in MHz) of H₂O, D₂O and their differences. The values shown are the average values for the two subbands in each electronic state.

		H ₂ O		D ₂ O		H ₂ O-D ₂ O
S ₀	A'' _H	1356.8	A'' _D	1356.0	A'' _{H-D}	-0.8
	B'' _H	880.7	B'' _D	846.6	B'' _{H-D}	-34.1
	C'' _H	538.1	C'' _D	525.5	C'' _{H-D}	-12.6
S ₁	A' _H	1336.2	A' _D	1335.0	A' _{H-D}	-1.2
	B' _H	874.1	B' _D	840.4	B' _{H-D}	-33.7
	C' _H	533.5	C' _D	521.3	C' _{H-D}	-12.2

Table 3-9 lists the hydrogen atom coordinates that were derived from a comparison of the rotational constants of the two complexes. In accord with our expectation, the plane of the water molecule is tilted with respect to the *b* and *c* axis, so that one hydrogen lies above the *ab* plane and one lies below. The hydrogen atoms are “inside” the water oxygen (*cf.*, Table 3-7), making donor hydrogen bonds with one of the two methoxy oxygen lone pairs, one above and one below. The H-H distance in the water molecule that is projected onto the *bc* plane of the complex is 1.13 Å in the S₀ state (1.46 Å in the S₁ state), compared to an actual separation of 1.536 Å.²⁷

Table 3-9. Disubstituted Kraitchman analysis. The coordinates (in Å) are the locations of hydrogen atoms determined from a comparison of the rotational constants of DMB/H₂O and /D₂O. The H...H distance is calculated from these coordinates. (The actual H...H distance of water in 1.536 Å.)²⁷



	S ₀		S ₁
a	3.378	a	3.365
b	0.335	b	0.426
c	0.453	c	0.591
H...H	1.127	H...H	1.456

3.5.3. Water motion in DMB/H₂O.

The two subbands in the fluorescence excitation spectrum of DMB/H₂O arise from a hindered internal motion of water. The motion of water perturbs and splits the degenerate torsional level ($\nu = 0$) into nondegenerate sub-torsional levels ($\sigma = 0$ and 1) in the two-fold potential energy surface, resulting in different energy level separations in the ground and excited electronic states. This is shown schematically in Figure 3-11. Allowed transitions $A \leftrightarrow A$ and $B \leftrightarrow B$ (according to the selection rule) are responsible for the A subband and B subband, respectively. In DMB/H₂O, the two subbands are split by 1197 MHz (0.04 cm^{-1}). The A subband is blue shifted relative to the B subband. This indicates that the sub-torsional level splitting in the S_1 state is smaller than that in the S_0 state. Thus, the excited state barrier (V_2') is larger

than the ground state barrier (V_2''). The two subbands have different relative intensities, 3:1. This intensity difference has its origin in nuclear spin statistical weights. Thus, the motion of the attached H₂O interconverts the two protons, making them equivalent.

The intensity difference of the two subbands (3:1) comes from nuclear spin statistical weights. Ordinary water has a pair of identical hydrogen nuclei ($I = \frac{1}{2}$). The total wavefunction of the molecule (Ψ_T) is comprised of electronic (Ψ_E), vibrational (Ψ_V), rotational (Ψ_R), and nuclear spin (Ψ_{ns}) wavefunctions. Ψ_T must be antisymmetric with respect to exchange of the two nuclei since they are fermions. Ψ_e is symmetric and Ψ_v is either symmetric (A sub-torsional level) or antisymmetric (B sub-torsional level). The rotational wavefunction (Ψ_R) is either symmetric (ee or oo) or antisymmetric (eo or oe). Since there are three symmetric spin functions and one antisymmetric, rotational levels belonging to the A sub-torsional level have a statistical weight of one and rotational levels belonging to the B sub-torsional level have a statistical weight of three. In DMB/D₂O, the nuclear spin wavefunction for sub-torsional band A is symmetric and that for sub-torsional band B is antisymmetric, leading to a 2:1 intensity ratio.

Motion of the water molecule also changes the effective rotational constants of the complex.³⁷ The difference between the rotational constants of the sub-torsional levels are $\Delta A''_{v\sigma} = A''_{01} - A''_{00}$. The values of these in DMB-water are $\Delta A''_{v\sigma} = 1.7 \pm 0.9$ and $\Delta A'_{v\sigma} = 1.6 \pm 0.9$ MHz. The $\Delta B_{v\sigma}$ and $\Delta C_{v\sigma}$ values are significantly smaller, less than 0.2 MHz, suggesting that the axis about which the water moves is nearly parallel to the a -axis of the complex. A quantitative approach to this problem is represented by the effective rotational Hamiltonian,²⁷

$$H_{v\sigma}^{eff} = A_{v\sigma} P_a^2 + B_{v\sigma} P_b^2 + C_{v\sigma} P_c^2 \quad (3)$$

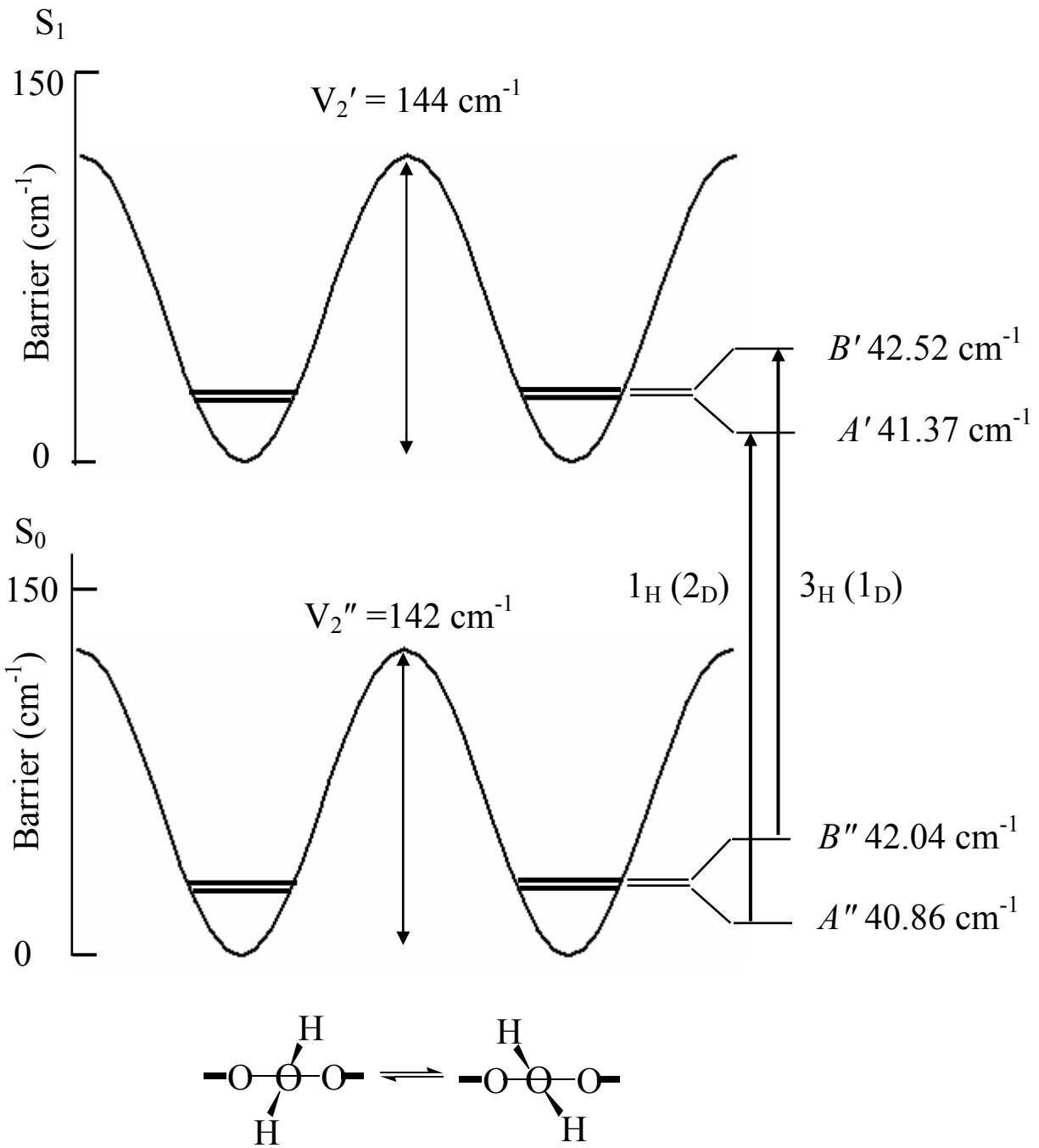


Figure 3-11. Potential energy surfaces of DMB/water in its two electronic states plotted as a function of the water torsional coordinate. The two minima arise from two equivalent orientations of the attached H₂O. Tunneling along this coordinate gives rise to symmetry distinguishable torsional subbands *A* and *B*. Allowed transitions between these two states are indicated by arrows with their corresponding intensity ratios.

where $A_{v\sigma}$, *etc.* are effective rotational constants given by

$$A_{v\sigma} = A + F W_{v\sigma}^{(2)} \rho_a^2, \quad \textit{etc.} \quad (4)$$

Here, A is the rigid rotor rotational constant, F is the reduced rotational constant for internal rotation ($= \hbar^2 / 2rI_a$), $W_{v\sigma}^{(2)}$ is a second-order perturbation constant,³⁸ and ρ_a is a weighted direction cosine of the angle between the axis of the internal rotor and the a principal axis of the complex, $\rho_a = \lambda_a (I_a/I_a)$. I_a is the moment of inertia of the attached top, and r is a reduction factor

$$r = 1 - \sum \frac{\lambda_g^2 I_a}{I_g}, \quad g = a, b, c. \quad (5)$$

Projecting the symmetry axis of the water molecule onto the a -axis of the complex, the reduced rotational constant (F) is calculated to be 436.7 GHz in both states. Then, to determine the barrier height, the difference ΔA was set equal to $FW_{v\sigma}^{(2)}\rho_a^2$, and the second-order correction terms $W_{v\sigma}^2$ were calculated, from which (using Herschbach's tables³⁸) the reduced barriers and two-fold barrier heights V_2 were determined. The results of these calculations are shown in Table 3-10. We find $V_2'' = 142 \pm 50$ and $V_2' = 144 \pm 55 \text{ cm}^{-1}$, nearly the same values in both electronic states. The calculated sub-torsional band splittings yield a tunneling of splitting $0.03 \pm 0.90 \text{ cm}^{-1}$ which agrees with the experimental value of 0.04 cm^{-1} . The MP2/6-31G** value of the torsional barrier is $\sim 450 \text{ cm}^{-1}$.

Table 3-10. Internal rotation parameters of DMB/H₂O

	S ₀	S ₁
ΔA	1.7±0.9	1.6±0.9
λ_a/α (deg)	1 / 0	1 / 0
F (GHz)	436.71	436.71
$W_{v\sigma}^{(2)}$	0.408	0.389
s	9.75	9.88
V_2 (cm ⁻¹)	142±50	144±50
Subtorsional split (cm ⁻¹)	1.18±0.63	1.15±65

3.6. Conclusion.

Rotationally resolved fluorescence excitation spectra of 1,2-dimethoxybenzene (DMB) and its single water complex DMB/H₂O have been observed and assigned. This analysis shows that the methoxy groups of DMB lie in the plane of the aromatic ring in a *trans*-disposed fashion, with the methyl groups being staggered relative to the benzene ring. This configuration provides a unique binding site for a single water molecule in DMB/H₂O. The water molecule is linked *via* two donor hydrogen bonds to the oxygen lone pairs of the methoxy groups. Torsional subbands appear in the spectrum of DMB/H₂O showing that the attached water molecule moves within the complex from one set of lone pairs to the other. The potential barriers to this motion have been measured, $V_2'' = 142 \pm 50$ and $V_2' = 144 \pm 55$ cm⁻¹ in the two electronic states.

3.7. Acknowledgments.

This work has been supported by NSF (CHE-0315584) to whom we are grateful.

3.8. References.

1. L. M. Dibello, H. M. McDevitt and D. M. Roberti, *J. Phys. Chem.* **72** (1968) 1405.
2. W. G. Hill, S. F. Mason and R.D. Peacock, *J. Chem. Soc. Perkin II* (1977) 1262.
3. G. M. Anderson, P. A. Kollman, L. N. Domelsmith and K. N. Houk, *J. Am. Chem. Soc.* **101** (1979) 2344.
4. H. Konschin, H. Tylli and B. Westermark, *J. Mol. Struct.* **102** (1983) 279.
5. S. Yamamoto, K. Okuyama, N. Mikami and M. Ito, *Chem. Phys. Let.* **125** (1986) 1; P. J. Breen, E. R. Bernstein, H. V. Secor and J. I. Seeman, *J. Am. Chem. Soc.* **111** (1989) 1958.
6. T. Basche, C. Brauchle and J. Voitlander, *Chem. Phys. Letters* **144** (1988) 226.
7. M. Gerzain, G. W. Buchanan, A. B. Driega, G. A. Facey, G. Enright and R. A. Kirby, *J. Chem. Soc. Perkin II* (1996) 2687.
8. H. S. Gutowsky, T. Emilsson and E. Arunan, *J. Chem. Phys.* **99** (1993) 4883.
9. R. N. Pribble, A.W. Garrett, K. Haber and T. S. Zwier, *J. Chem. Phys.* **103** (1995) 531.
10. S. Y. Fredericks, K. D. Jordan and T. S. Zwier, *J. Phys. Chem.* **100** (1996) 7810.
11. S. Melandri, D. Consalvo, W. Caminati and P. G. Favero, *J. Chem. Phys.* **111** (1999) 3874.
12. M. Schäfer, D.R. Borst, D.W. Pratt and K. Brendel, *Mol. Phys.* **100** (2002) 3553.
13. M. Becucci, G. Pietraperzia, M. Pasquini, G. Piani, A. Zoppi, R. Chelli, and E. Castellucci, *J. Chem. Phys.* **120** (2004) 5601; B. Giuliano and W. Caminati, *Angew. Chem. Int. Ed.* **44**, 603 (2005); J. Ribblett, W. Sinclair, D. Borst, J. Yi, and D. Pratt, *submitted*.
14. P. Tarakeshwar, K. S. Kim and B. Brutschy, *J. Chem. Phys.* **110** (1999) 8501.
15. H. D. Barth, K. Buchhold, S. Djafari, B. Reimann, U. Lommatzsch and B. Brutschy, *Chem. Phys.* **239** (1998) 49.
16. C.-H. Kang, D. W. Pratt and M. Schäfer, *J. Phys. Chem. A* **109** (2005) 767.
17. G. Berden, W. L. Meerts, M. Schmitt and K. Kleinermanns, *J. Chem. Phys.* **104** (1996) 972.

18. T. M. Korter, D. W. Pratt and J. Küpper, *J. Phys. Chem. A* **102** (1998) 7211.
19. L. B. Braly, J. D. Cruzan, K. Liu, R. S. Fellers and R. J. Saykally, *J. Chem. Phys.* **112** (2000) 10293; U. Spoerel and W. Stahl, *J. Mol. Spectr.* **190** (1998) 278.
20. M. D. Brookes and A. R. W. McKellar, *J. Chem. Phys.* **109** (1998) 5823.
21. W. A. Majewski, J. F. Pfanstiel, D. F. Plusquellic and D. W. Pratt, in *Laser Techniques in Chemistry*, T. R. Rizzo and A. B. Myers, Eds., J. Wiley & Sons, New York, 1995, p. 101.
22. D. Marjit, P. K. Bishui and S. B. Banerjee, *Indian J. Phys.* **46** (1971) 49.
23. D. Harris and M. D. Bertolucci, *Symmetry and Spectroscopy: An Introduction to Vibrational and Electronic Spectroscopy*. Dover Publications, Inc., New York, 1978.
24. Described in D. F. Plusquellic, R. D. Suenram, B. Matá, J. O. Jensen, and A. C. Samuels, *J. Chem. Phys.* **115** (2001) 3057.
25. M. J. Frisch, G. W. Trucks, H. B. Schlegel, G. E. Scuseria, M. A. Robb, J. R. Cheeseman, V. G. Zakrzewski, J. A. Montgomery, Jr., R. E. Stratmann, J. C. Burant, S. Dapprich, J. M. Millam, A. D. Daniels, K. N. Kudin, M. C. Strain, O. Farkas, J. Tomasi, V. Barone, M. Cossi, R. Cammi, B. Mennucci, C. Pomelli, C. Adamo, S. Clifford, J. Ochterski, G. A. Petersson, P. Y. Ayala, Q. Cui, K. Morokuma, D. K. Malick, A. D. Rabuck, K. Raghavachari, J. B. Foresman, J. Cioslowski, J. V. Ortiz, A. G. Baboul, B. B. Stefanov, G. Liu, A. Liashenko, P. Piskorz, I. Komaromi, R. Gomperts, R. L. Martin, D. J. Fox, T. Keith, M. A. Al-Laham, C. Y. Peng, A. Nanayakkara, M. Challacombe, P. M. W. Gill, B. Johnson, W. Chen, M. W. Wong, J. L. Andres, C. Gonzalez, M. Head-Gordon, E. S. Replogle and J. A. Pople, Gaussian, Inc., Gaussian 98, Revision A.9, Pittsburgh PA, 1998.
26. J. K. G. Watson, in *Vibrational Spectra and Structure*, J. R. Durig, Ed., Elsevier Amsterdam, Vol. 6. (1977) p. 1.
27. W. Gordy and R.L. Cook, *Microwave Molecular Spectra*, J. Wiley & Sons, New York, 1970.
28. R. M. Helm, H. P. Vogel and H. J. Neusser, *Chem. Phys. Letters* **270** (1997) 285.
29. M. Onda, A. Toda, S. Mori and I. Yamaguchi, *J. Mol. Struct.* **144** (1986) 47.
30. D. M. Upadhyay, M. K. Shukla and P. C. Mishra, *J. Mol. Struct.* **531** (2000) 249.

31. M. Rumi and G. Zerbi, *J. Mol. Struct.* **509** (1999) 11.
32. T. M. Krygowski, E. Pietka, R. Anulewicz, M. K. Cyransk and J. Nowacki, *Tetrahedron* **54** (1998) 12289.
33. P. Cahill, L. P. Gold and N. L. Owen, *J. Chem. Phys.* **48** (1967) 1620.
34. W. E. Sinclair and D. W. Pratt, *J. Chem. Phys.* **105** (1996) 7942.
35. T. Cvitas, J. M. Hollas and G. H. Kirby, *Mol. Phys.* **19** (1970) 305.
36. See, for example, T. M Selby, J. R. Clarkson, D. Mitchell, J. A. J. Fitzpatrick, H. D. Lee, D. W. Pratt and T. S. Zwier, *J. Phys. Chem. A* **109** (2005) 4484.
37. X.-Q. Tan, W. A. Majewski, D. F. Plusquellic, and D. W. Pratt, *J. Chem. Phys.* **94** (1991) 7721.
38. D. R. Herschbach, *J. Chem. Phys.* **31** (1959) 91.
39. T. M. Krygowski, E. Pietka, R. Anulewicz, M. K. Cyransk and J. Nowacki, *Tetrahedron* **54** (1998) 12289.
40. P. Cahill, L. P. Gold and N. L. Owen, *J. Chem. Phys.* **48** (1967) 1620.
41. W. E. Sinclair and D. W. Pratt, *J. Chem. Phys.* **105** (1996) 7942.
42. T. Cvitas, J. M. Hollas and G. H. Kirby, *Mol. Phys.* **19** (1970) 305.
43. T. M selby, J. R. Clarkson, D. Mitchell, J. A. J. Fitzpatrick, H. D. Lee, D. W. Pratt and T. S. Zwier, *J. Phys. Chem. A*, in press.
44. X. -Q. Tan W. A. Majewski, D. F. Plusquellic, and D. W. Pratt, *J. Chem. Phys.* **94** (1991) 7721.
45. D. R. Herschbach, *J. Chem. Phys.* **31** (1959) 91.

4. Conformational Analysis by Laser Spectroscopy in the Gas Phase: *p*-Methoxyphenethylamine (a Neurotransmitter).

John T. Yi, Evan G. Robertson¹ and David W. Pratt²

¹School of Chemistry, Monash University, Victoria 3800 Australia.

²Department of Chemistry, University of Pittsburgh,
Pittsburgh, Pennsylvania 15260 USA.

4.1. Abstract.

Rotationally resolved fluorescence excitation spectra of seven different S₁-S₀ origin bands of *p*-methoxyphenethylamine have been obtained in the collision-free environment of a molecular beam. Analyses of these spectra permit unambiguous assignments of specific bands to specific conformers, based on differences in their inertial defects, rotational constants, and electronic transition moment orientations, thereby resolving a controversy in the recent literature.

Published in *Phys. Chem. Chem. Phys.*, **4** (2002) 5244.

4.2. Introduction.

A conundrum has developed in the recent literature regarding the proper attribution of seven different origin bands that appear in the S_1 - S_0 electronic spectrum of *p*-methoxyphenethylamine (MPEA) in a supersonic jet.¹⁻⁴ Castaño and co-workers^{2,4} have assigned these bands to *gauche* or *anti* conformers on the assumption that pairs of *gauche* conformers which differ only in the orientation of the methoxy group on the ring have their band origins split by a constant amount. But Simons and co-workers³ have argued that attributions based on this criterion are incorrect, noting that in related systems, the splitting varies considerably from one group to the next. Robertson, *et al.*³ also observe that the assignments of Unamuno, *et al.*^{2,4} conflict with the well established assignments of the origin bands in β -phenylethylamine (PEA) itself.^{1, 5-7}

PEA, MPEA, and related molecules belong to a family of neurotransmitters that control the flow of ions across the plasma membranes of postsynaptic cells.⁸ Their flexible structures, consisting of substituted aromatic molecules with alkylamine tails, may be essential to their biological activity. For example, some conformers may be capable of binding to an ion channel and opening it, whereas others may not. Therefore, to further delineate the mechanism of action of such species, it is important that any ambiguities concerning the properties of their energy landscapes be resolved. In this report, we use the technique of high resolution electronic spectroscopy in the gas phase to unambiguously assign the seven different S_1 - S_0 origin bands in the spectrum of MPEA to specific conformers of the isolated molecule.

4.3. Experimental.

MPEA was purchased from Aldrich and used as received. In the low resolution experiment, the sample was seeded into 45 psi of He gas and expanded into a vacuum chamber (10^{-5} torr) through a 1 mm diameter orifice pulsed valve (General Valve Series 9), operating at 10 Hz. One centimeter downstream of the valve, the sample was excited with the second harmonic of a Quanta Ray Nd³⁺: YAG (Model DCR-1A) pumped dye laser (Model PDL-1). The dye (Fluorescein 548) laser output was frequency doubled with an external KDP crystal into the ultraviolet. From the point of intersection between the supersonic jet and laser, the molecules were excited and the fluorescence was collected with a photomultiplier tube (PMT). Finally, the collected data were processed by a boxcar integrator (Stanford Research Systems) and digitally recorded with a data acquisition system.

The rotationally resolved electronic experiments were performed using the CW laser spectrometer described elsewhere.⁹ Briefly, the sample was seeded into He gas, expanded through a 280 μ m quartz nozzle, and probed 15 cm downstream of the nozzle by an Ar⁺ pumped CW tunable dye laser. The CW laser was operated with Rhodamine 110 dye. 100-200 μ W of UV radiation was produced by intracavity frequency doubling with a β -barium borate (BBO) crystal. Absolute transition frequencies were calibrated by comparing with the I₂ absorption spectrum. Relative frequency calibration was performed using a stabilized etalon with a free spectral range of 299.7520 ± 0.0005 MHz at the fundamental of the dye. The fluorescence excitation spectrum, the iodine absorption spectrum, the relative frequency markers, and the laser output power were simultaneously collected and processed by a data acquisition system.

4.4. Results and Interpretation.

Figure 4-1 shows the low resolution S_1 - S_0 fluorescence excitation spectrum of MPEA. Band A, the lowest energy band, is located at $\sim 35500\text{ cm}^{-1}$ ($\sim 281\text{ nm}$). Six other origin bands, labelled B-G, are separated by 41, 55, 96, 125, 140, and 149 cm^{-1} from Band A. (An eighth band, at 184 cm^{-1} from Band A, is a water complex of MPEA).¹⁰ Our goal is to achieve an unambiguous assignment of Bands A-G using high resolution techniques.

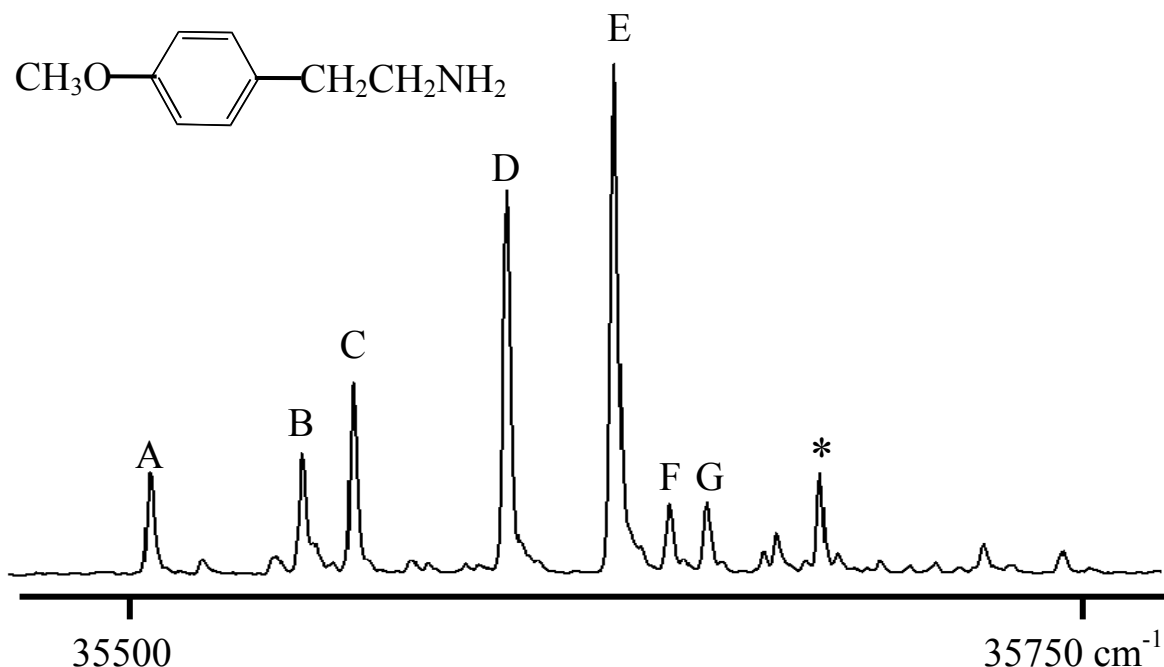


Figure 4-1. Vibrationally resolved fluorescence excitation spectrum of *p*-methoxyphenethylamine (MPEA) recorded in a supersonic jet. Bands labeled A through G are the $S_1 \leftarrow S_0$ electronic origins of seven different conformers of the isolated molecule. The band marked with an asterisk is a water complex of MPEA.

Figure 4-2 shows the high resolution fluorescence excitation spectrum of Band A. The spectrum spans about 4 cm^{-1} and exhibits well-defined P and R branches, indicating that the spectrum is dominated by *b*-type transitions. Approximately 3500 lines were observed in the spectrum, several of which could be assigned to single transitions having linewidths of $\sim 70\text{ MHz}$.

(FWHM). The frequency positions of these lines were least-squares fit to rigid rotor Hamiltonians for both states using the Windows-based program jb95.¹¹ More than 50 rovibronic transitions were assigned resulting in an OMC (observed minus calculated) standard deviation of less than 5 MHz. Table 4-1 lists the inertial parameters derived from this fit.

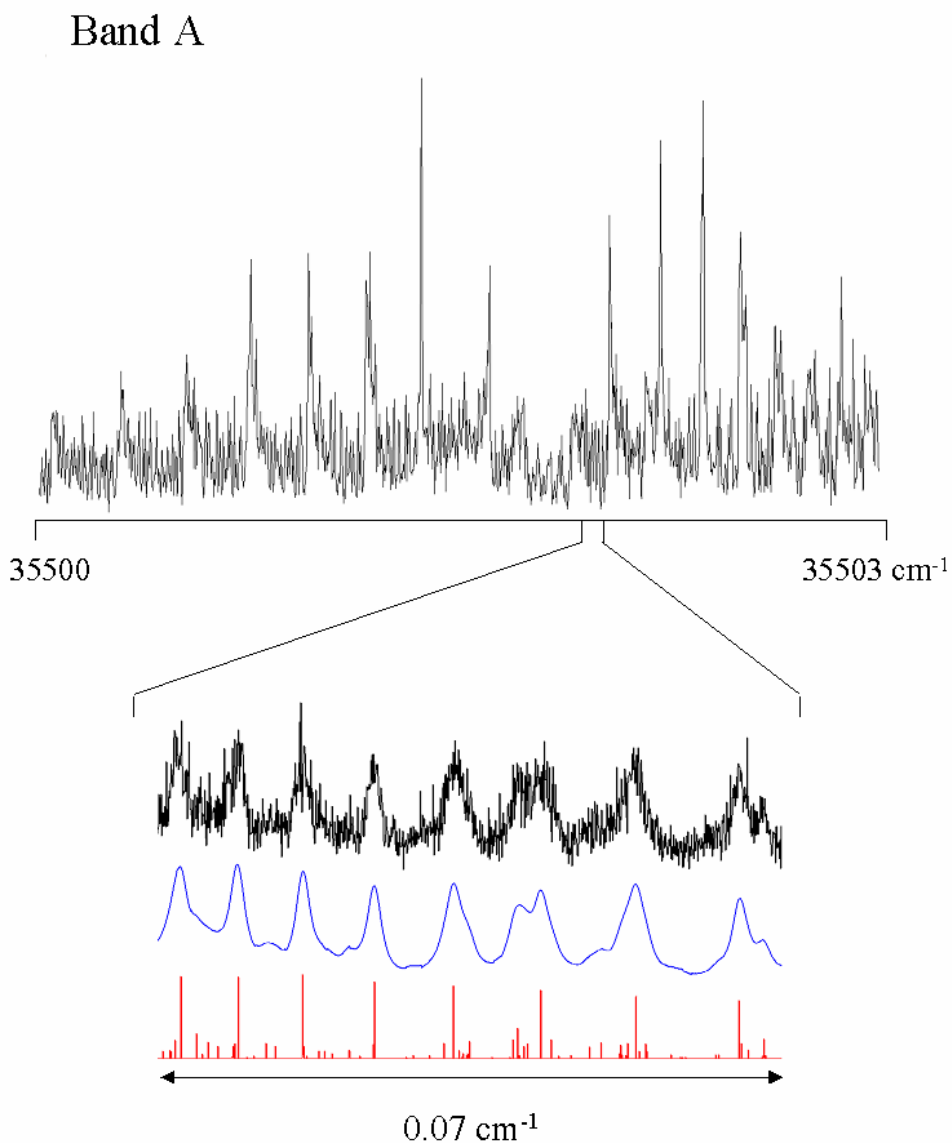


Figure 4-2. Rotationally resolved fluorescence excitation spectrum of band A recorded in a molecular beam. The bottom panel shows a section of the R-branch together with two computer simulations with and without a deconvoluted lineshape.

Table 4-1. Inertial parameters of seven conformers of *p*-methoxyphenethylamine (MPEA) in their ground (S_0) and excited (S_1) electronic states.

Band	A	B	C	D	E	F	G
S_0							
A" (MHz)	2789.7(2)	3624.4(3)	2740.2(1)	2832.6(2)	2750.6(1)	3662.4(9)	3670.8(4)
B" (MHz)	535.5(1)	457.8(1)	542.1(1)	538.3(1)	547.2(1)	458.0(1)	457.8(1)
C" (MHz)	509.6(1)	428.6(1)	507.6(1)	509.1(1)	508.5(1)	428.6(1)	428.6(1)
κ''	-0.977	-0.982	-0.969	-0.975	-0.966	-0.982	-0.982
$\Delta I''$ (amu \AA^2)	-133.31	-64.25	-120.93	-124.57	-113.49	-62.43	-62.62
S_1							
ΔA (MHz)	-115.2(3)	-202.1(5)	-86.7(1)	-108.2(3)	-92.1(1)	-217.7(5)	-170.0(8)
ΔB (MHz)	1.1(1)	3.1(1)	-0.8(1)	0.2(1)	0.3(1)	3.6(1)	1.6(1)
ΔC (MHz)	0.9(1)	1.0(1)	0.4(1)	-0.4(1)	-1.0(1)	0.3(1)	0.0(1)
κ'	-0.976	-0.979	-0.969	-0.973	-0.963	-0.978	-0.98
$\Delta I'$ (amu \AA^2)	-141.04	-67.73	-128.97	-130.55	-117.42	-63.47	-65.64
Origin (cm $^{-1}$)	35501.2	35541.8	35555.9	35597	35625.9	35641.5	35650.6
%Inten							
$a(\pm 3)/b(\pm 4)/c(\pm 3)$	4/89/7	3/94/3	3/79/18	7/84/9	4/79/17	3/94/3	3/94/3
OMC (MHz)	4.28	3.09	2.83	4.41	4.82	3.77	3.65

Subsequently, the spectrum of Band A was subjected to an intensity analysis. This analysis showed that weak *a*-type and *c*-type transitions also are present, from which a hybrid band ratio $a:b:c = 4:89:7$ was determined. The relative intensities of the transitions within each sub-spectrum could be fit to a rotational temperature of 8 ± 3 K, without invoking spin statistics. Finally, individual rovibronic lines were fit to Voigt lineshape profiles, yielding Doppler-

broadened (Gaussian) and lifetime-broadened (Lorentzian) components of 18 and 50 MHz, respectively. The latter corresponds to a fluorescence lifetime of 3 ns.

A comparison of a heavily congested portion of the R branch in the experimental spectrum of Band A to its computer simulation, with and without a superimposed lineshape function, is shown at the bottom of Figure 4-2, to illustrate the quality of the fit.

Analogous procedures were used to analyze the high resolution spectra of Bands B-G. Each of these spectra is similar in overall appearance to the others, and to Band A (Fig. 4-2). But, at high resolution, each band exhibits a unique spectrum, as shown in Figure 4-3. Shown there are corresponding portions of the high resolution spectra of all six bands, and their computer simulations. Each band exhibits a similar single rovibronic Voigt lineshape function (18 MHz Gaussian and 50 MHz Lorentzian). But the pattern of lines in each spectrum is unique, making possible its assignment to a unique conformer of MPEA. The data upon which these attributions will rest were all derived from least-square fits of these spectra and are also listed in Table 4-1.

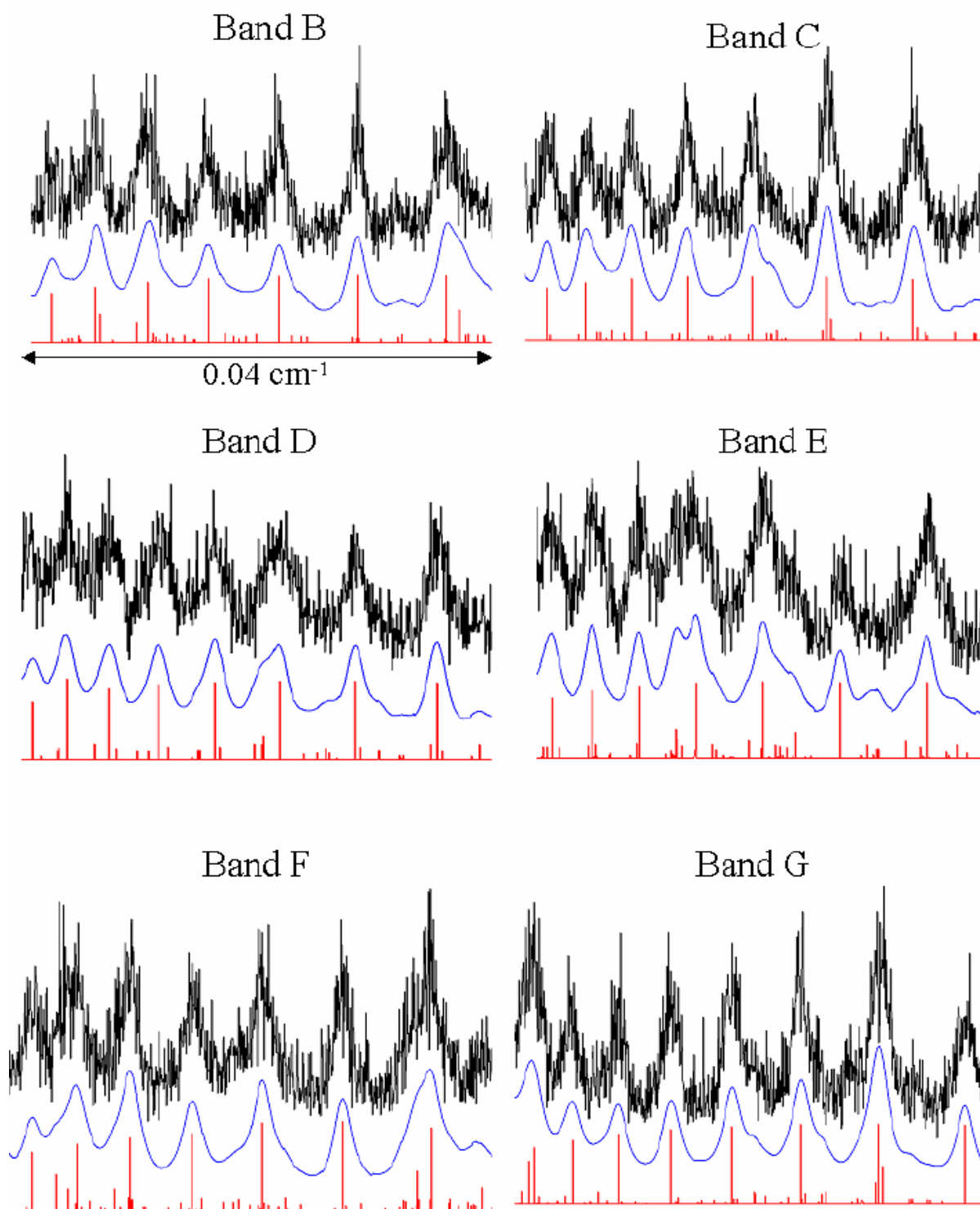
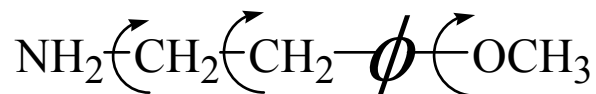


Figure 4-3. Comparisons of similar portions of the R-branch in Bands B through G, at full experimental demonstrating the unique character of each spectrum. The top trace is the experimental spectrum. Two computer simulations, with and without a deconvoluted lineshape, are shown below.

4.5. Discussion.

Before beginning the assignment process, a brief review of the conformational landscape of MPEA is in order. MPEA has three relevant degrees of freedom, shown schematically below;

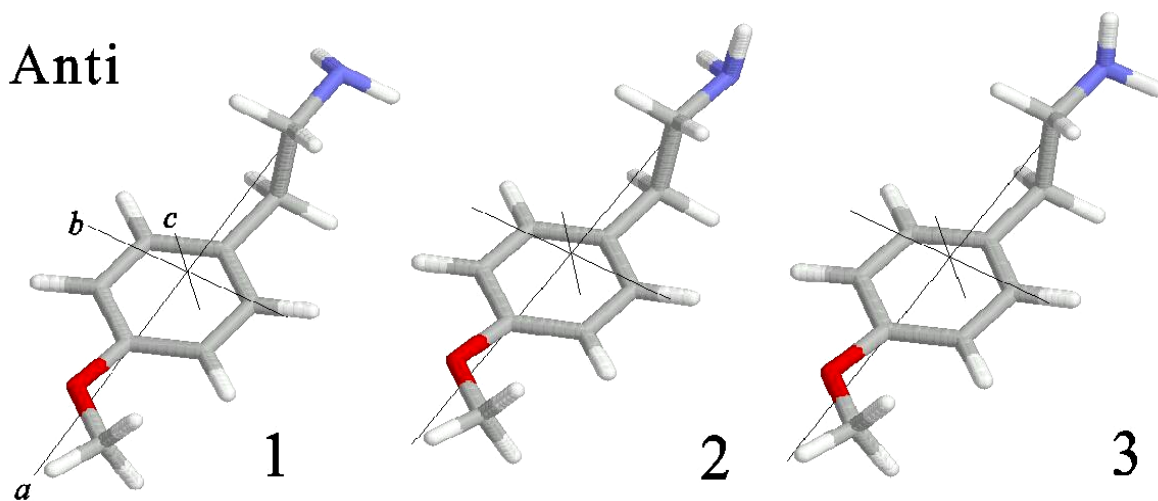


a three-fold rotation about the N-C_β bond, a three-fold rotation about the C_β – C_α bond, and a two-fold rotation about the φ – OCH₃ bond. (Other degrees of freedom are ignored.) Rotation about the C_β – C_α bond distinguishes *anti* from *gauche* structures, and rotation about the φ – OCH₃ bond divides the *gauche* structures into two classes, *trans* and *cis*. *Anti*, *gauche-trans* and *gauche-cis* classes each have three members, corresponding to the three possible orientations of the N–C_β bond. Thus, nine conformers of MPEA are expected, in all. These are illustrated in Figure 4-4. Also shown there are the approximate locations of the inertial axes of each structure.

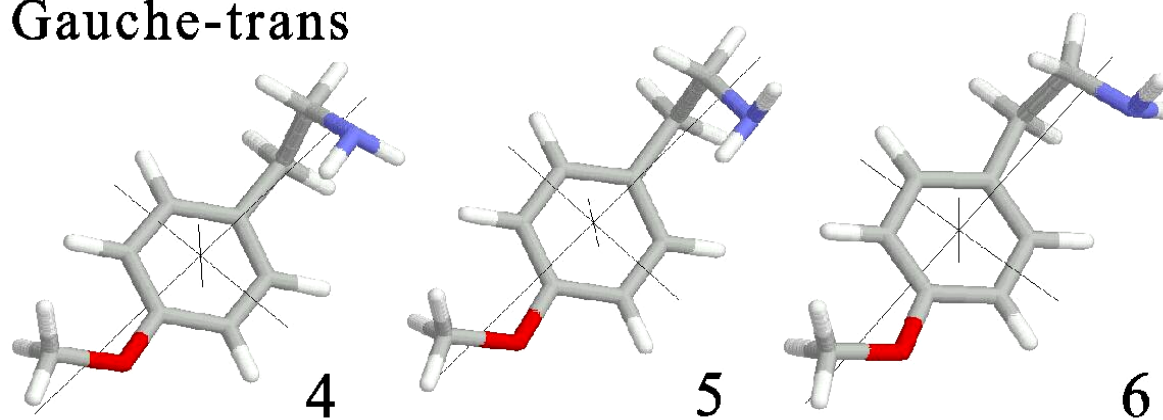
The different possible structures of MPEA can be distinguished, in large measure, by differences in their rotational constants. Examining the data in Table 4-1, we see that the carriers of all bands in Figure 4-1 have relatively large (negative) inertial defects. Therefore, the structures responsible for the electronic transitions of MPEA are all nonplanar owing to the extended ethylamine chain. (Anisole, by contrast, has an inertial defect of $\Delta I = -3.41 \text{ amu \AA}^2$).¹² But the degree of nonplanarity of each structure is different. The conformers responsible for Bands B, F, and G all have smaller $|\Delta I|$'s than those responsible for Bands A, C, D, and E. The

MPEA

Anti



Gauche-trans



Gauche-cis

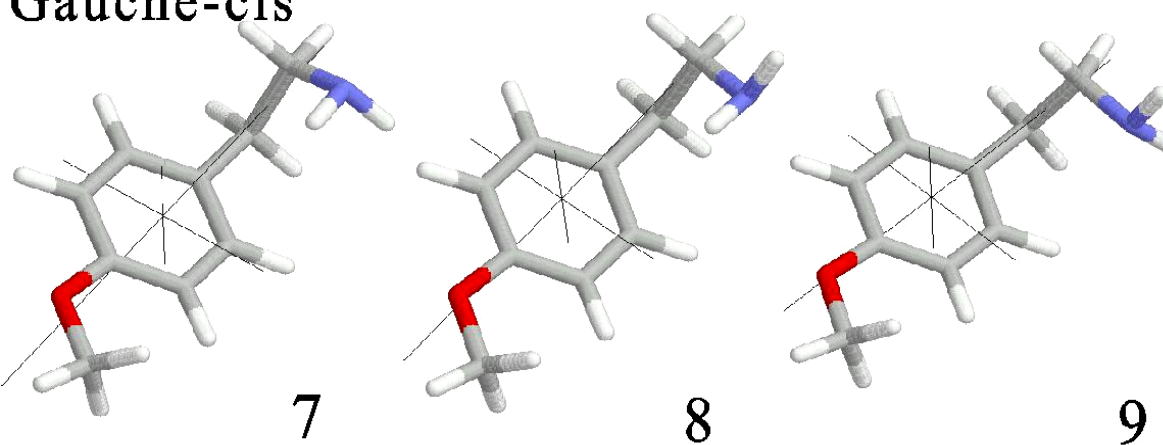


Figure 4-4. Nine unique conformations of MPEA, based on *ab initio* calculations at the MP2/6-31G** level.

conformers responsible for Bands B, F, and G also have significantly larger A rotational constants. Since rotational constants are inversely proportional to moments of inertia, this means that the conformers responsible for Bands B, F, and G are *anti* conformers. The masses of the heavy atoms in the ethylamine chains of the *anti* conformers are relatively close to the a axis. The *gauche* conformers, those responsible for Bands A, C, D, and E, are folded conformers with more mass displaced from the a inertial axis.

Distinguishing the conformers within the three different classes of structures is a more challenging task, owing to the subtle mass displacements involved. Therefore, *ab initio* calculations were performed on ground state MPEA using the Gaussian suite of programs¹³ to provide some guidance on this issue. Table 4-2 lists the results obtained at the MP2 level with a 6-31G** basis set. As predicted, the three *anti* conformers (1-3) have significantly larger A values than the six *gauche* conformers (4-9). The calculated A values of the *anti* structures (3583.9, 3627.6, and 3634.2 MHz) are different from the observed values (3624.4, 3662.4, and 3670.8 MHz) by as much as 1%. But the differences in the theoretical and experimental values are nearly the same (43.7 and 6.6 MHz vs. 38.0 and 8.4 MHz, respectively) unambiguously assigned to conformers 1, 2, and 3, respectively.

Table 4-2. Calculated (MP2/6-31G**) rotational constants and relative energies of nine conformers of MPEA in their ground (S_0) electronic states.

Structure	1	2	3	4	5	6	7	8	9
A(MHz)	3583.9	3627.6	3634.2	2795.4	2853.6	3020.4	2702.4	2723.8	2704.9
B(MHz)	459.9	460.3	460.1	541.8	544.5	529.5	552.3	556.9	550.9
C(MHz)	430.5	430.8	430.8	512.2	510.4	483.2	510.9	511.2	488.4
ΔE (cm ⁻¹)	351	489	498	54	34	678	38	0	675

Conformers 1, 2, and 3 differ only in the orientation of their NH₂ groups with respect to the *ac* inertial plane. The two N-H bonds are displaced on either side of this plane in conformer 1, giving it a larger moment of inertia about *a*, and a smaller *A* rotational constant. One N-H bond lies essentially in this plane in conformers 2 and 3, giving them smaller moments of inertia about *a*, and larger *A* rotational constants. The *A* rotational constant of conformer 3 is slightly larger (8.4 MHz) than that of conformer 2 because the displacement of its “perpendicular” N-H bond from the *ac* plane is slightly less than the corresponding displacement in conformer 2.

Assignment of Bands A, C, D, and E to specific structures in the *gauche* classes is made more challenging by the “off-axis” –OCH₃ and –CH₂CH₂NH₂ groups, which tilt the inertial axes (and change the rotational constants) in non-intuitive ways. Still, a careful examination of the inertial parameters in Tables 4-1 and 4-2 shows that Bands A and D belong to structures 4 and 5, respectively, two of the possible *gauche-trans* conformers. These have slightly higher *A* values than the *gauche-cis* structures. The reason for this behavior is apparent from Figure 4-4. Bands C and E belong to structures 7 and 8, respectively. The difference between the observed and calculated rotational constants is in all cases less than 2%. But, again, the differences in these constants are reproduced rather accurately by theory at the MP2 level.

Different criteria may be used to provide independent confirming assignments of Bands A, C, D, and E. For example, as shown in Figure 4-4, structures 4 and 5, and 7 and 8, differ in the orientation of the NH₂ group with respect to the *bc* plane. The conformers responsible for Bands A and C have slightly smaller *B* rotational constants than the conformers responsible for Bands D and E. Examining the structures in Figure 4-4, we see that these differences (2.8 and

5.1 MHz, respectively) can safely be attributed to differences in the displacements of the N-H hydrogens from this plane and mirror the calculated differences (2.7 MHz and 4.6 MHz).

Similarly, the ΔA ($A'-A''$) values of the different classes of structures are significantly different. All are negative as a consequence of the ring expansion produced by $\pi\pi^*$ excitation. But *anti* structures have $\Delta A = -202$, -217 , and -170 MHz; *gauche-trans* structures have $\Delta A = -115$ and -108 MHz; and *gauche-cis* structures have $\Delta A = -87$ and -92 MHz. The large differences in these values can be traced to a non-uniformity in the expansion of the benzene ring. As originally discussed by Cvitas, *et al.*¹⁴, and elaborated further in many other places¹⁵, *p*-substituted benzenes are typically “quinoidal” in their S_1 states, with shorter parallel C–C bonds than perpendicular ones. This is the source of the large (and negative) ΔA in the MPEA conformers. In *anti* structures, the *ac* plane is mostly parallel and perpendicular to these bonds, giving rise to the largest observed change. But the *ac* plane in the *gauche* conformers is significantly tilted with respect to these bonds, reducing the magnitude of the observed ΔA . The smaller, but significantly different ΔB and ΔC values can be rationalized in the same way.

Recall, finally, that the S_1 - S_0 transition moment (TM) orientations are significantly different among the seven bands. Bands B, F, and G are principally *b*-type bands, a fact that is directly traceable to their *anti* structures 1, 2, and 3. The attached substituents do not significantly break the C_2 -axis perpendicular to the benzene ring, blocking the mixing pathways previously associated with “off-axis” substituents.¹⁶ The small amounts of *a*- and *c*-type character in their high resolution spectra (*cf.* Table 4-1) can be traced to the inertial contributions of the $-\text{OCH}_3$ and $-\text{CH}_2\text{CH}_2\text{NH}_2$ groups.

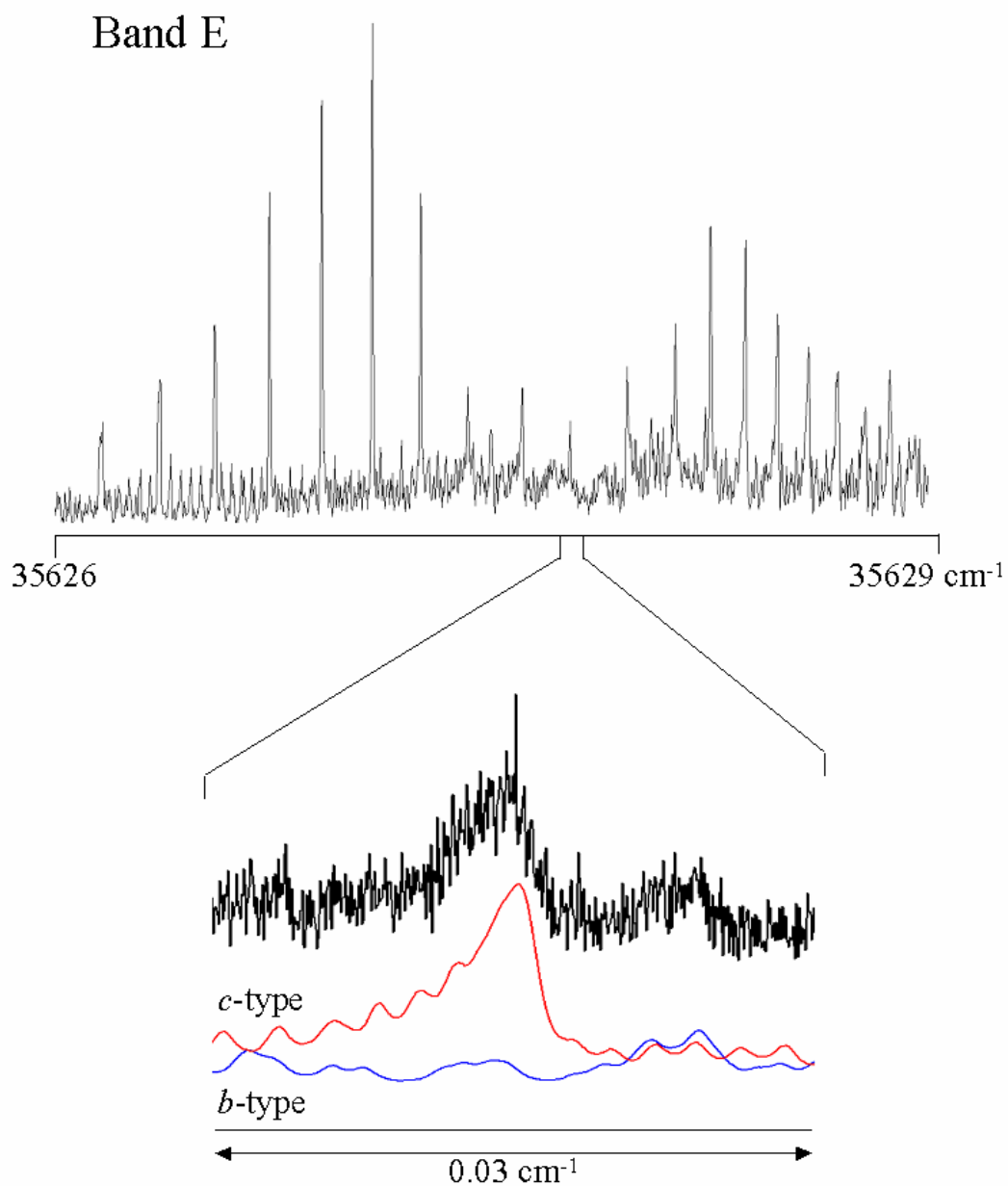


Figure 4-5. Rotationally resolved fluorescence excitation spectrum of Band E recorded in a molecular beam. The bottom panel shows a section of the Q-branch at full resolution, and its deconvolution into *b* and *c*-type transitions.

The *gauche-trans* and *gauche-cis* structures exhibit larger tilts of their S₁-S₀ TM orientations. An example is shown in Figure 4-5. In addition to the strong P- and R-branches, the spectrum of Band E shows significant *c*-type character. This is especially apparent in the central Q-branch ($\Delta J=0$) region, where the *c*-type transitions are most prominent. Careful computer simulations show that the hybrid band character in this case is $a:b:c = 4:79:17$, very different from that of Band B. Notably, a similar band character is detected in the spectrum of Band C, whereas Bands A and D exhibit an intermediate character. These differences are also principally inertial in origin. Independent CIS calculations¹³ show that there are no large “electronic” contributions to the TM orientations in these off-axis structures, probably owing to the presence of the methoxy group, which appears to “lock” the electronic structure of the benzene ring into place.¹⁷ Thus, the observed TM orientations in the high resolution spectra of MPEA also may be used to unambiguously assign specific bands to specific conformers of the isolated molecule.

Table 4-3 compares the attributions made in this work with those previously made in the literature.¹⁻³ All authors agree on the assignment of Bands F and G to *anti* structures. But there is substantial disagreement in the remaining assignments. As noted before³, this can be traced to the previously unappreciated importance of ring-tail interactions. Thus, for example, Martinez, *et al.*¹ and Unamuno, *et al.*², while recognizing that a uniquely oriented amino group would produce an extra set of *gauche* conformers, failed to anticipate that this group would, in some orientations, strongly interact with the ring, and that these interactions would produce “non-intuitive” shifts in the spectra.. Therefore, Bands B, F, and G can be A simple example will suffice to illustrate this point. Castaño and co-workers^{2,4}, and earlier Martinez, *et al.*¹, assumed

that pairs of *gauche* conformers which differ only in the orientation of the methoxy group would have their band origins split by a constant amount. Examining the data presented here, we see that this is not the case. Bands A and C, assigned to the conformer pairs 4 and 7, are separated by 55 cm⁻¹, whereas Bands D and E, assigned to the conformer pairs 5 and 8, are separated by only 29 cm⁻¹. Therefore, assignments based on this criterion are incorrect.

Table 4-3. Assignments of specific bands in the electronic spectrum of MPEA to specific conformers (see Figs. 4-1 and 4-4).

Band	Ref [1]	Ref [2]	Ref [3]	This work
A	<i>g</i>	8(<i>gc</i>)	4(<i>gt</i>)	4(<i>gt</i>)
B	<i>g</i>	5(<i>gt</i>)	1(<i>a</i>)	1(<i>a</i>)
C	<i>g</i>	7(<i>gc</i>)	7(<i>gc</i>)	7(<i>gc</i>)
D	<i>g</i>	4(<i>gt</i>)	5(<i>gt</i>)	5(<i>gt</i>)
E	<i>a</i>	1(<i>a</i>)	8(<i>gc</i>)	8(<i>gc</i>)
F	- ^a	2(<i>a</i>)	2(<i>a</i>)	2(<i>a</i>)
G	- ^a	3(<i>a</i>)	3(<i>a</i>)	3(<i>a</i>)

^a Not assigned

The data presented here provide some rationalization for the failure of this criterion. Bands D and E are the strongest bands in the spectrum. The carriers of these bands (structures 5 and 8) both have N–H bonds pointing towards the ring. In contrast, structures 6 and 9, which have so far not been observed in the spectrum, have no N–H bonds pointing towards the ring (*cf.* Fig. 4-4). From these observations, we conclude that the N-H... π interaction is highly stabilizing, in both electronic states. But we now recall that the ring π -electron distribution is asymmetric, owing to the attached –OCH₃ group. The oxygen lone pair electrons will interact

differently with both sides of the ring. Thus, the energy of interaction of a given N–H bond with one side of the ring is likely to be different from the other, resulting in an asymmetry in their respective band positions, as observed. Presumably, the same effect occurs in tyramine, since the oxygen atom of its OH group has asymmetrically displaced lone pair electrons.

4.6. Conclusions.

Seven $S_1 \leftarrow S_0$ electronic origin bands of *p*-methoxyphenethylamine have been isolated in molecular beam and examined with high resolution fluorescence excitation techniques. Each spectrum is unique at 70 MHz resolution and has been fully assigned, yielding rotational constants of the carrier of each band in both of its electronic states. Comparisons of these constants to each other, and with the predictions of theory lead to unambiguous assignments of the seven bands to seven different conformers of the isolated molecule.

4.7. Acknowledgments.

We thank Tri V. Nguyen for helpful discussions. This work has been supported by NSF (INT-9722029 and CHE-9987048) to whom we are grateful.

4.8. References.

- 1 S. J. Martinez III, J. C. Alfano and D. H. Levy, *J. Mol. Spectrosc.*, 1993, **158**, 82.
- 2 I. Unamuno, J. A. Fernandez, A. Longarte and F. Castaño, *J. Phys. Chem.*, 2000, **104A**, 4364.
- 3 E. G. Robertson, J. P. Simons and M. Mons, *J. Phys. Chem.*, 2001, **105A**, 9990.
- 4 J. A. Fernandez, I. Unamuno and F. Castaño, *J. Phys. Chem.*, 2001, **105A**, 9993.
- 5 P. D. Godfrey, L. D. Hatherley and R. D. Brown, *J. Am. Chem. Soc.*, 1995, **117**, 8204.
- 6 S. Sun and E. R. Bernstein, *J. Am. Chem. Soc.*, 1996, **118**, 5086.
- 7 J. A. Dickinson, M. R. Hockridge, R. J. Kroemer, E. G. Robertson, J. P. Simons, J. McCombie and M. Walker, *J. Am. Chem. Soc.*, 1998, **120**, 2622.
- 8 B. Alberts, D. Bray, J. Lewis, M. Raff, K. Roberts and J. D. Watson, *Molecular Biology of the Cell*, 3rd Ed., Garland Publishing, New York, 1994.
- 9 W. A. Majewski, J. F. Pfanstiel, D. F. Plusquellic, D. W. Pratt, in *Laser Techniques in Chemistry*, edited by A. B. Myers and T. Rizzo, J. Wiley & Sons, New York, 1995, pp. 101-148.
- 10 J. A. Fernandez, I. Unamuno, A. Longarte and F. Castaño, *J. Phys. Chem.*, 2001, **105A**, 961.
- 11 D. F. Plusquellic, to be published.
- 12 J. W. Ribblett, Ph.D Thesis, University of Pittsburgh, 1999.
- 13 Gaussian 98 (Revision A.9), M. J. Frisch, G. W. Trucks, H. B. Schlegel, G. E. Scuseria, M. A. Robb, J. R. Cheeseman, V. G. Zakrzewski, J. A. Montgomery, R. E. Stratmann, J. C. Burant, S. Dapprich, J. M. Millam, A. D. Daniels, K. N. Kudin, M. C. Strain, O. Farkas, J. Tomasi, V. Barone, M. Cossi, R. Cammi, B. Mennucci, C. Pomelli, C. Adamo, S. Clifford, J. Ochterski, G. A. Petersson, P. Y. Ayala, Q. Cui, K. Morokuma, D. K. Malick, A. D. Rabuck, K. Raghavachari, J. B. Foresman, J. Cioslowski, J. V. Ortiz, A. G.

- Baboul, B. B. Stefanov, G. Liu, A. Liashenko, P. Piskorz, I. Komaromi, R. Gomperts, R. L. Martin, D. J. Fox, T. Keith, M. A. Al-Laham, C. Y. Peng, A. Nanayakkara, M. Challacombe, P. M. W. Gill, B. G. Johnson, W. Chen, M. W. Wong, J. L. Andres, C. Gonzalez, M. Head-Gordon, E. S. Replogle and J. A. Pople, Gaussian, Inc., Pittsburgh PA, 1998.
- 14 T. Cvitas, J. M. Hollas and G. H. Kirby, *Mol. Phys.*, 1970, **19**, 305.
- 15 See, for example, D. R. Borst and D. W. Pratt, *J. Chem. Phys.*, 2000, **113**, 3658.
- 16 J. W. Ribblett, D. R. Borst and D. W. Pratt, *J. Chem. Phys.*, 1999, **111**, 8454.
- 17 P. A. Hepworth, J. McCombie, J. P. Simons, J. F. Pfanstiel, J. W. Ribblett and D. W. Pratt, *Chem. Phys. Lett.*, 1996, **249**, 34.

5. Rotationally Resolved Electronic Spectroscopy of Tryptophol in the Gas Phase.

John T. Yi and David W. Pratt

Department of Chemistry, University of Pittsburgh
Pittsburgh, PA 15260 USA

5.1. Abstract.

High resolution S_1 - S_0 fluorescence excitation spectra of tryptophol have been observed in the collision-free environment of a supersonic beam. Each origin band has been assigned to a unique conformer based on its observed rotational constants. Unlike its close relative tryptamine, which exhibits seven distinguishable conformers under similar conditions, tryptophol exhibits only four (GPy-in, GPh-in, and two *anti* structures). Possible reasons for this difference in behavior are discussed.

Phys. Chem. Chem. Phys., submitted

5.2. Introduction.

Many tryptophan analogs have been studied in a gas phase environment in recent years. Using a large variety of spectroscopic techniques, this work has shed much light on the structural and dynamical properties of isolated amino acids, peptides and proteins, properties that are believed to be relevant to their behavior in the condensed phase. A representative example is tryptamine (TRA), an ethylamine substituted indole. Seven different conformers of TRA have been identified in a series of experiments performed by Levy¹⁻⁴, Felker⁵⁻⁸, Zwier⁹ and co-workers. These include *gauche*-pyrrole (GPy) conformers, in which the amine group points towards the pyrrole ring, *gauche*-phenyl (GPh) conformers, in which the amine group points towards the phenyl ring, and *anti* conformers, in which the amine group points away from both of the rings. Most recently, Nguyen *et al.*¹⁰ have discovered tunneling splittings in the high resolution electronic spectra of two of the *anti* conformers which reveal a pathway on the energy landscape that connects them.

Tryptophol (TRH), the ethyl alcohol substituted analog of TRA, has not yet been studied in such detail. Sulkes and co-workers^{11,12} recorded the vibrationally resolved S₁-S₀ fluorescence excitation spectrum of TRH in the gas phase. They observed that the number of electronic origins was reduced to three when the amine group was replaced by a hydroxy group in the side chain. They also made complexes of TRH with several different solvent molecules and performed extensive molecular mechanics calculations, but they were unable to assign the different origins in the S₁-S₀ spectrum to different conformers of TRH.

In this work, we have used high resolution electronic spectroscopy techniques to assign the different electronic origin bands previously observed by Sulkes and co-workers to specific conformers of the gas phase molecule. Previously, this technique was successfully applied to a

number of conformationally complex molecules including TRA, and the single-ring analog *p*-methoxyphenethylamine¹³ (MPEA) that also has an ethylamine side chain. We also report the discovery of a fourth conformer of TRH, and offer an interesting explanation for why the number of stable minima on its energy landscape is sharply reduced, compared to TRA and MPEA.

5.3. Experimental.

Tryptophol (TRH) was purchased from Aldrich and used without further purification. In the vibrationally resolved experiment, the sample was seeded into ~ 50 psi of He gas and expanded into a vacuum chamber (10^{-5} torr) through a 1 mm diameter orifice pulse valve (General Valve Series 9) operating at 10 Hz. One centimeter downstream of the valve, the sample was excited with the second harmonic of a Quanta Ray Nd³⁺: YAG (Model DCR-1A) pumped dye laser (Model PDL-1). The dye laser (Rhodamine 590) output was frequency doubled with an external KDP crystal providing a spectral resolution of 0.6 cm^{-1} in the ultraviolet (UV). From the point of intersection between the nozzle and laser, the molecules were excited and the fluorescence was collected with a photomultiplier tube (PMT). Finally, the collected data were processed by a boxcar integrator (Stanford Research Systems) and recorded with a DATAQ data acquisition system.

Rotationally resolved electronic experiments on TRH were performed using the CW laser spectrometer described elsewhere.¹⁴ Briefly, the sample was seeded into Ar or He gas, expanded through a 240 μm quartz nozzle, and probed 15 cm downstream of the nozzle by an Ar⁺ pumped CW tunable dye laser. The CW laser was operated with Rhodamine 590 dye; 100-200 μW of UV radiation was obtained by intracavity frequency doubling the fundamental of the dye using a

BBO 580 crystal. The fluorescence excitation spectrum, the iodine absorption spectrum, the relative frequency markers, and the laser output power were simultaneously collected and processed by the jba95 data acquisition system. Absolute transition frequencies were calibrated by comparing them with the I₂ absorption spectrum and relative frequency markers were obtained from a stabilized etalon with a free spectral range of 299.7520 ± 0.0005 MHz.

5.4. Results.

Figure 5-1 shows the vibrationally resolved S₁←S₀ fluorescence excitation spectrum of tryptophol. The most intense feature located at ~ 34965 cm⁻¹ is assigned as Band A. Bands B and C are red shifted by 70 and 45 cm⁻¹ with respect to Band A. All three of these bands have been assigned as electronic origins.¹² The band labeled A', 37 cm⁻¹ to the blue of Band A, has been previously identified as a higher vibronic of Band A on the basis of dispersed fluorescence experiments.¹² The band with an asterisk at 35015 cm⁻¹ has been assigned as a water complex band.

Figure 5-2 shows the rotationally resolved S₁-S₀ fluorescence excitation spectrum of Band A of TRH. The spectrum spans about 2.8 cm⁻¹ and exhibits well-defined P, R, and Q branches indicating that it is dominated by *a*-type transitions. The procedure used to fit such a spectrum has been described previously.¹⁵ Briefly, calculated rotational constants of both the ground and excited electronic states of TRH and *a*-type selection rules were used to simulate an initial spectrum. Then, single transitions were selected from the simulation and assignments were made corresponding to the experimental spectrum. A refined simulation was obtained by modifying the initial parameters to fit the calculated frequencies to the observed ones, using a least-squares procedure. The final fit of Band A utilized 190 transitions and rigid rotor

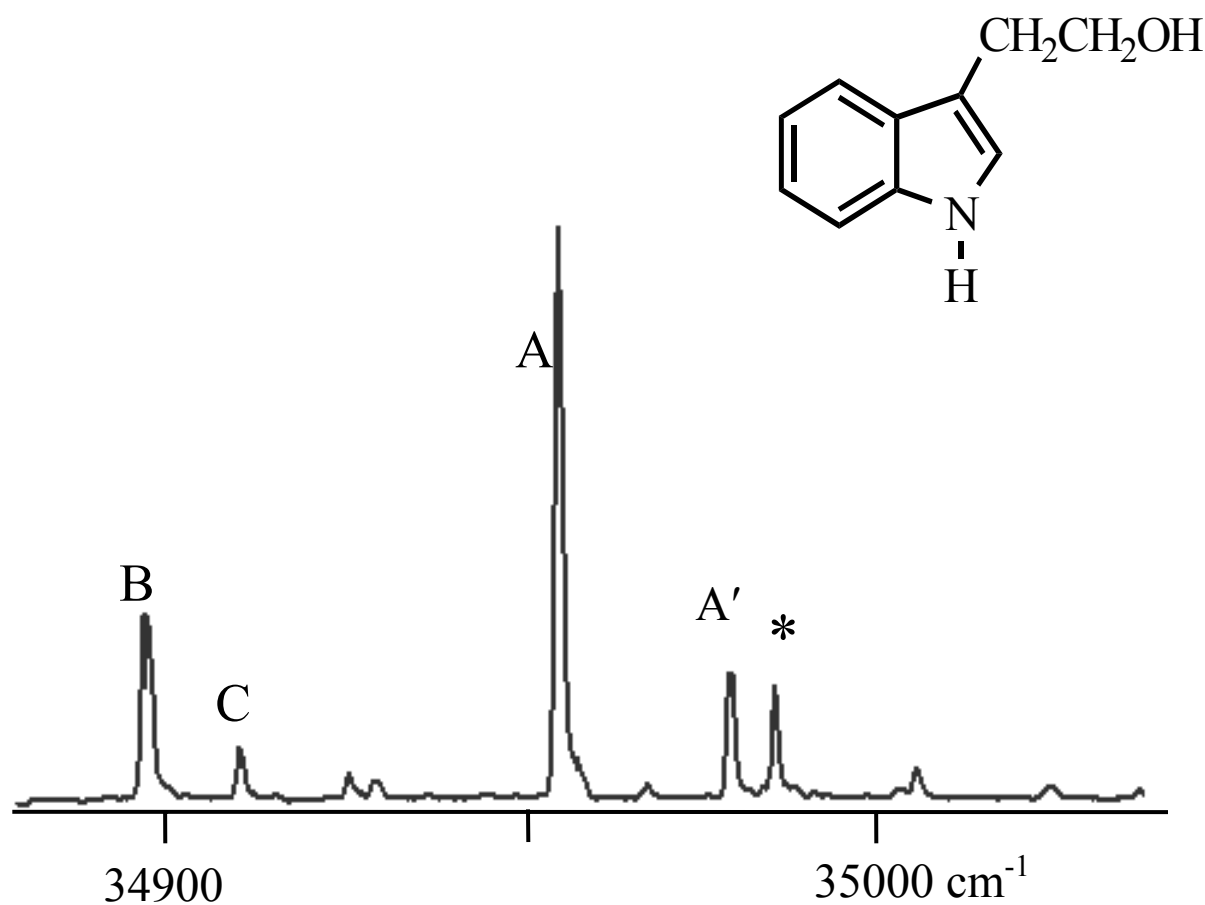


Figure 5-1. Vibrationally resolved S_1 - S_0 fluorescence excitation spectrum of tryptophol.

Hamiltonians for both electronic states and resulted in an observed minus calculated (OMC) standard deviation of less than 2.3 MHz.

The bottom panel in Fig. 5-2 illustrates the quality of this fit. The top trace is a portion of the experimental spectrum taken from the R branch. The bottom two traces are simulations with and without a lineshape function. The spectrum has minor contributions from *b*- and *c*-type transitions and exhibits a hybrid band ratio *a/b/c* of 92/4/4. The relative intensities of the lines in the spectrum could be fit to a rotational temperature of 4 ± 2 K. Finally, a Gaussian linewidth of 18 MHz and a Lorentzian linewidth of 22 ± 3 MHz were used in a Voigt profile to fit the shapes

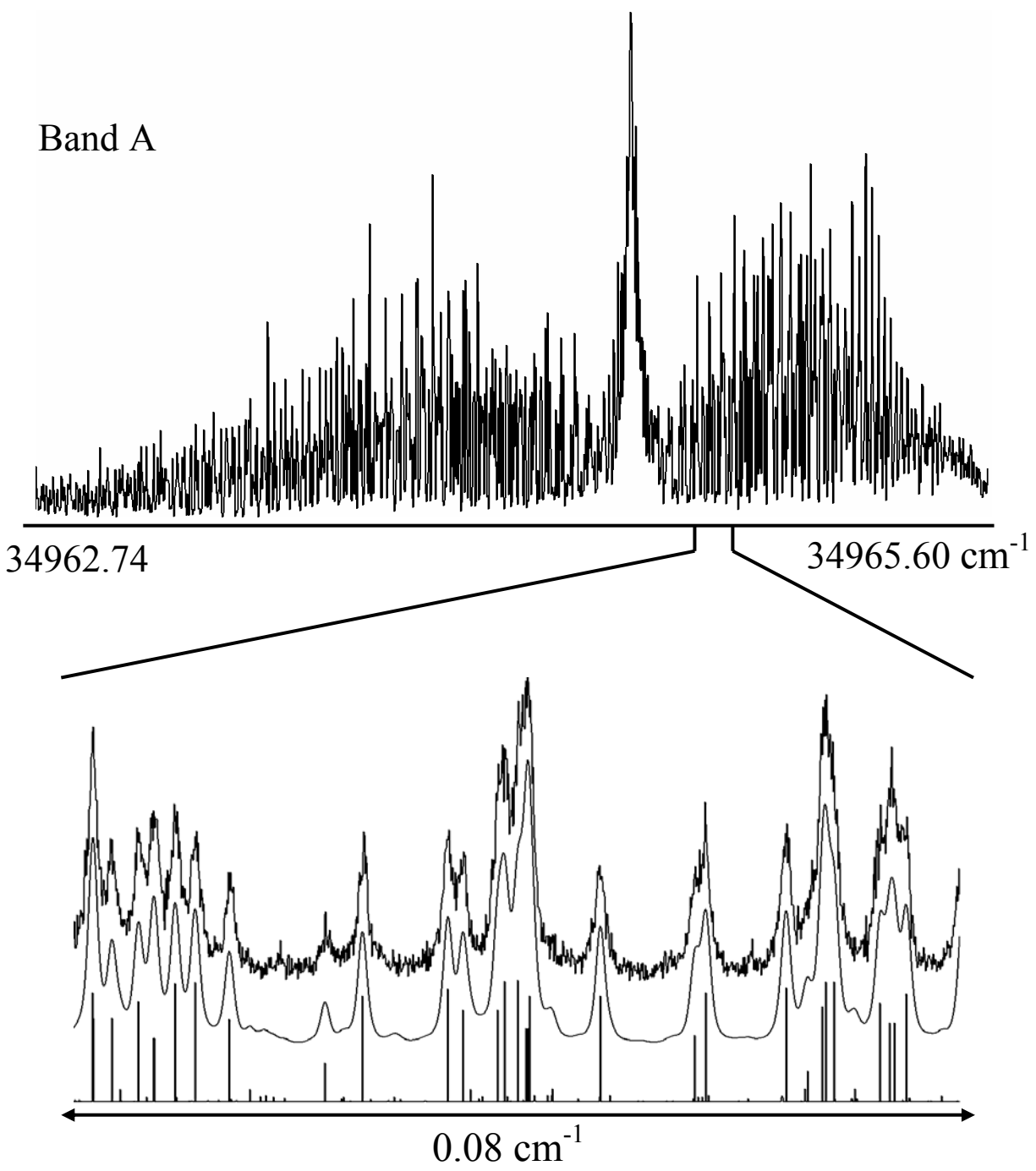


Figure 5-2. Rotationally resolved S_1 - S_0 fluorescence excitation spectrum of tryptophol Band A. In the bottom panel, the top trace is a portion of the experimental spectrum and the succeeding traces are simulated spectra with and without a convoluted lineshape function.

of individual rovibronic lines. The corresponding fluorescence lifetime is ~ 7 ns. Each individual line has a full width at half maximum linewidth (FWHM) of 31 ± 3 MHz.

The same procedure was used to fit Bands B and C in the spectrum of TRH, see Figs. 5-3 and 5-4. Each band shows unique features. Individual lines have FWHM values of 35 ± 4 (Band B) and 25 ± 3 MHz (Band C). The Gaussian widths of these lines are the same, 18 MHz. However, the corresponding Lorentzian linewidths are different, 28 ± 3 MHz for Band B and 18 ± 3 MHz for Band C, corresponding to lifetimes of 6 and 9 ns, respectively.

A new feature appeared in the spectrum of TRH when the high resolution experiment was repeated using helium as the carrier gas, rather than argon. This is shown in Fig. 5-5. Band C exhibits a second, weaker band whose origin is displaced by ~ 16.5 GHz to the blue of the main band, when the experiment was carried out under these conditions. The two bands are shown in the bottom panel of Fig. 5-5, as Fig. 5-5a (the simulated spectrum of Band C_{red}, the stronger band) and 5-5b (the simulated spectrum of Band C_{blue}, the weaker band). Both bands are clearly required to fit the observed spectrum.

Initially, we thought that these two bands were sub-bands belonging to a single conformer that was undergoing a large amplitude motion like internal rotation, especially since the intensity ratio is similar to that expected for such a motion ($\sim 1:2$). However, we now believe that these two bands belong to two distinct conformers of TRH, with very similar energies and rotational constants. Primarily, this is because only the stronger of the two bands can be observed in argon expansions.

Table 5-1 lists the parameters that were derived from the least-squares fits of all four bands that were observed at high resolution.

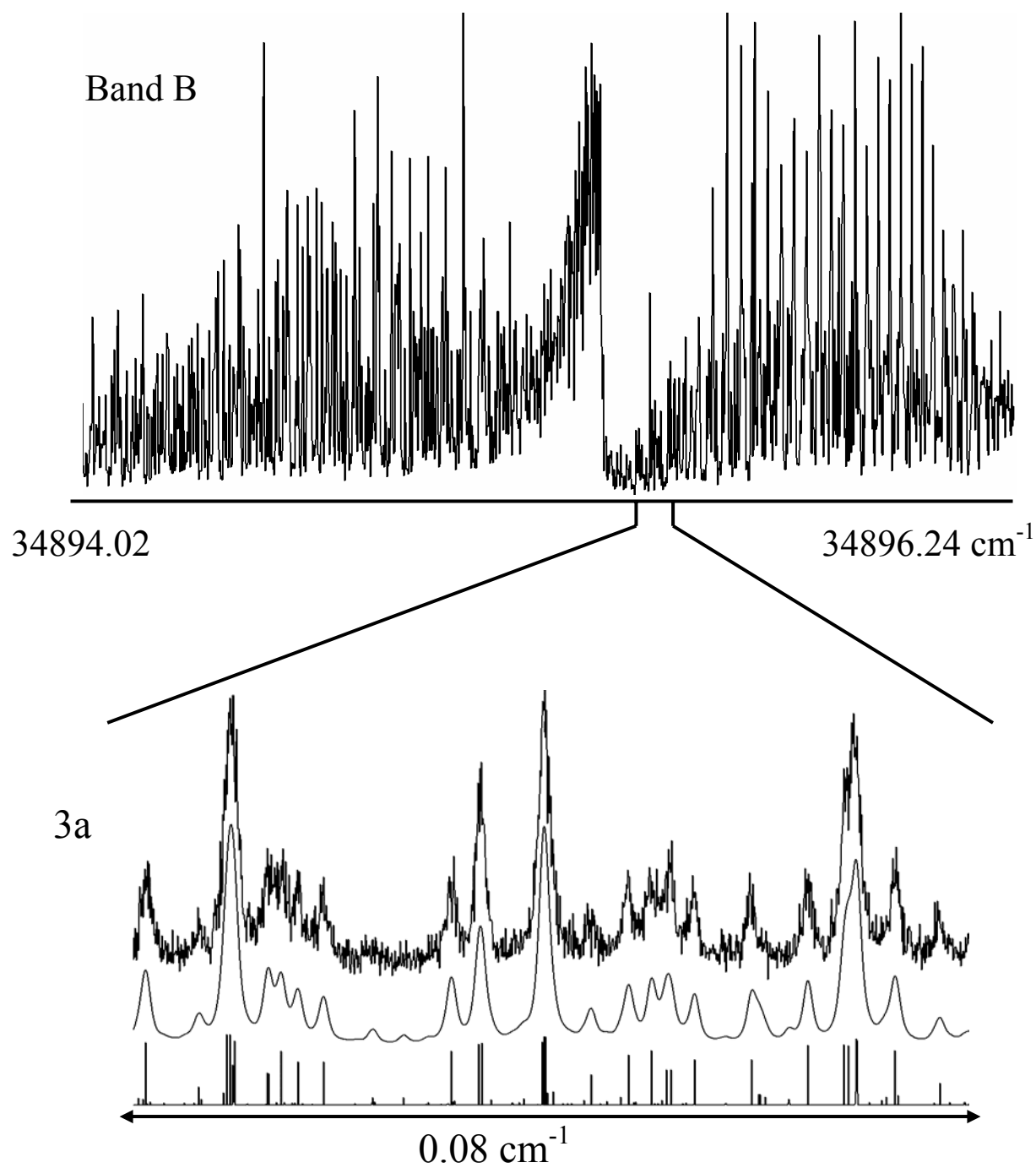


Figure 5-3. Rotationally resolved S_1 - S_0 fluorescence excitation spectrum of tryptophol Band B. In the bottom panel, the top trace is a portion of the experimental spectrum and the succeeding traces are simulated spectra with and without a convoluted lineshape function.

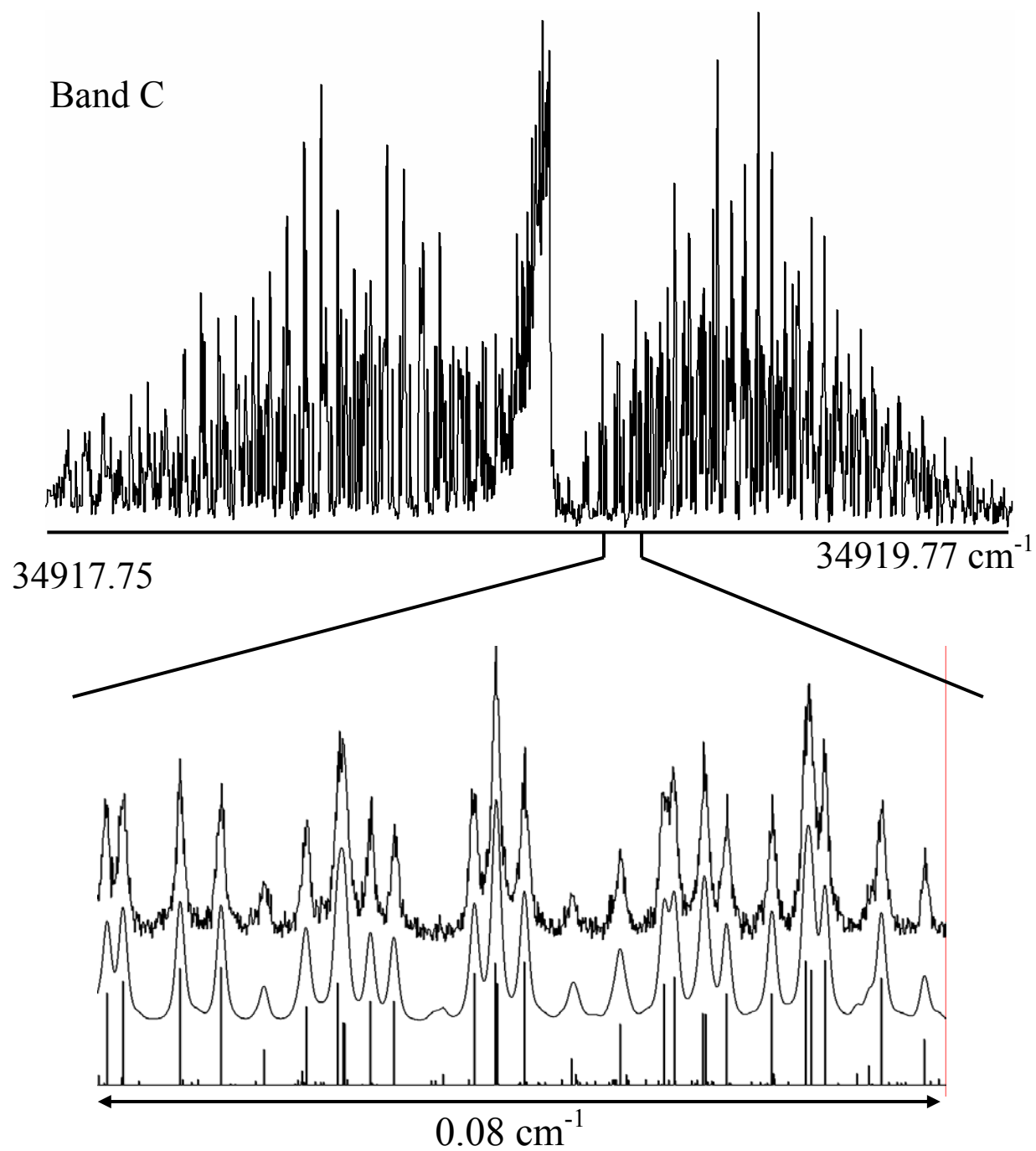


Figure 5-4. Rotationally resolved S_1 - S_0 fluorescence excitation spectrum of tryptophol Band C obtained in an argon carrier gas. In the bottom panel, the top trace is a portion of the experimental spectrum and the succeeding traces are simulated spectra with and without a convoluted lineshape function.

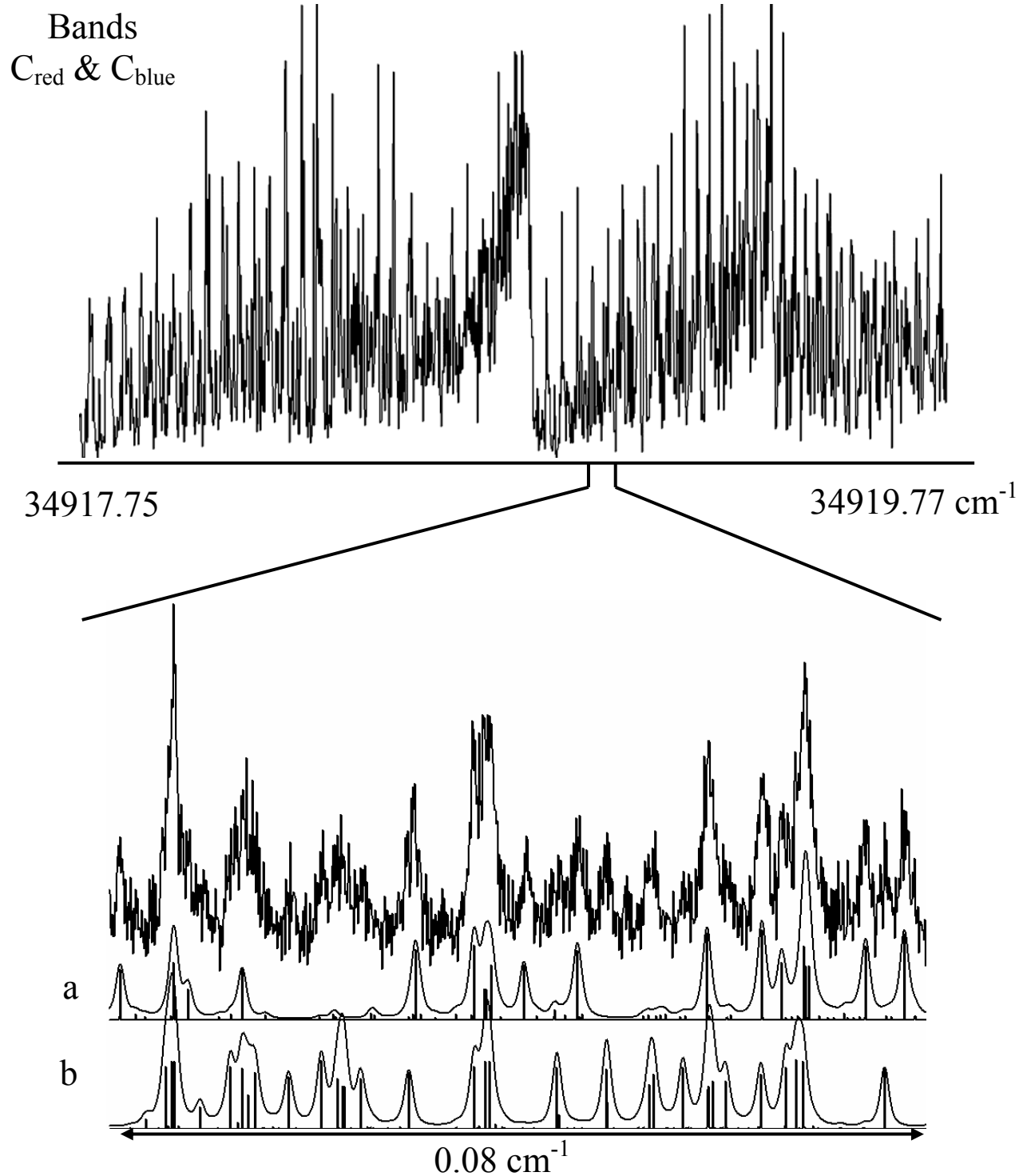


Figure 5-5. Rotationally resolved S_1 - S_0 fluorescence spectrum of tryptophol Band C obtained in a helium carrier gas. The bottom panel shows a portion of the experimental spectrum and two simulated spectra, the Band C spectrum (a) and the additional simulated spectrum (b), shifted by $+0.55 \text{ cm}^{-1}$, that is required to fit all of the intensity in the observed spectrum.

Table 5-1. Inertial parameters of four conformers of tryptophol in their ground and excited electronic states.

Parameter	Band A	Band B	Band C _{red}	Band C _{blue}
A(MHz)	1750.0 (0.8)	1587.4 (0.7)	1778.7 (0.7)	1775.3 (6.0)
B(MHz)	678.1	763.6	612.3	609.1 (3.0)
C(MHz)	549.5	563.6	474.6	473.5 (1.0)
$\Delta I(\text{amu } \text{Å}^2)$	-114.5	-83.5	-44.7	-42.7
$\Delta A(\text{MHz})$	12.2 (0.8)	-15.0 (0.7)	-14.6 (0.7)	-14.2 (6.0)
$\Delta B(\text{MHz})$	-14.9	-9.3	-5.1	-5.3 (3.0)
$\Delta C(\text{MHz})$	-10.2	-7.7	-3.5	-3.4 (1.0)
$\Delta I(\text{amu } \text{Å}^2)$	-111.8	-82.4	-46.1	-44.1
Band origin (cm^{-1})	34964.5	34895.3	34918.8	34919.4
% <i>a/b/c</i> (± 3)	92/4/4	84/9/7	90/5/5	90/5/5
OMC (MHz)	2.3	3.2	2.0	5.0

Errors in the rotational constants are ± 0.1 MHz except where indicated.

5.5. Discussion.

We begin with a classification of the possible structures of TRH, using a model that is similar to that for tryptamines.⁹ Three families of structures may be distinguished; GPy (*gauche*-pyrrole), GPh (*gauche*-phenyl) and *anti*; these are shown in Fig. 5-6. The terms GPy, *anti*, and GPh refer to the positions of the ethylhydroxy side chain with respect to the indole ring. Additionally, the OH hydrogen can take up three different orientations with respect to their ring; in, up, and out. Here, our conformational designations differ from those used for TRA, in which in, up, and out refer to the three different orientations of the lone pair of electrons nitrogen atom

single with respect to the indole ring. The oxygen atom in TRH has two lone pairs of electrons making a distinction based on them no longer unique.

Next, we performed *ab initio* calculations on the nine different conformers of TRH at the MP2/6-31G** level¹⁶ to determine their rotational constants, inertial defects, and relative energies, in the ground state. Table 5-2 lists the results obtained. GPy-in and GPh-in are predicted to be the most stable structures with GPh-in lying 93 cm⁻¹ higher in energy than GPy-in. Both structures have the hydroxyl hydrogen atom pointing towards the indole ring. Analogous structures with one of the two amino hydrogen atoms pointing towards the indole ring were also found to lie at relatively low energy in TRA; the analogous structure GPy-out is the global minimum. Attractive π -hydrogen bonding interactions are clearly important in both systems.

Table 5-2. Calculated rotational constants, inertial defects, and relative energies of seven conformers of TRH in their ground electronic states at the MP2/ 6-31G** level.^a

Parameter	GPy-up	GPy-in	GPh-up	GPh-in	<i>anti</i> -up	<i>anti</i> -ph	<i>anti</i> -py
A(MHz)	2320.6	1782.7	1569.5	1575.5	1779.1	1778.5	1765.4
B(MHz)	579.6	676.5	776.8	784.4	613.9	610.0	615.0
C(MHz)	473.1	550.7	552.5	568.0	476.4	474.8	476.5
$\Delta I(\text{amu } \text{Å}^2)$	-21.4	-112.8	-57.9	-75.4	-46.5	-48.3	-47.3
$\Delta E(\text{cm}^{-1})$	520	0	621	9.3	275	333	342

^a Stable minima could not be found for two remaining conformers, GPy-out and GPh-out.

While similar in this respect, TRH and TRA are importantly different in another. There are only two stable members of the GPy and GPh families in TRH whereas there are three in TRA. All calculations that were started at or near the structure GPy-out and GPh-out minima converged on the GPy-up and GPh-up structures. Apparently, there are no stable GPy- or GPh-

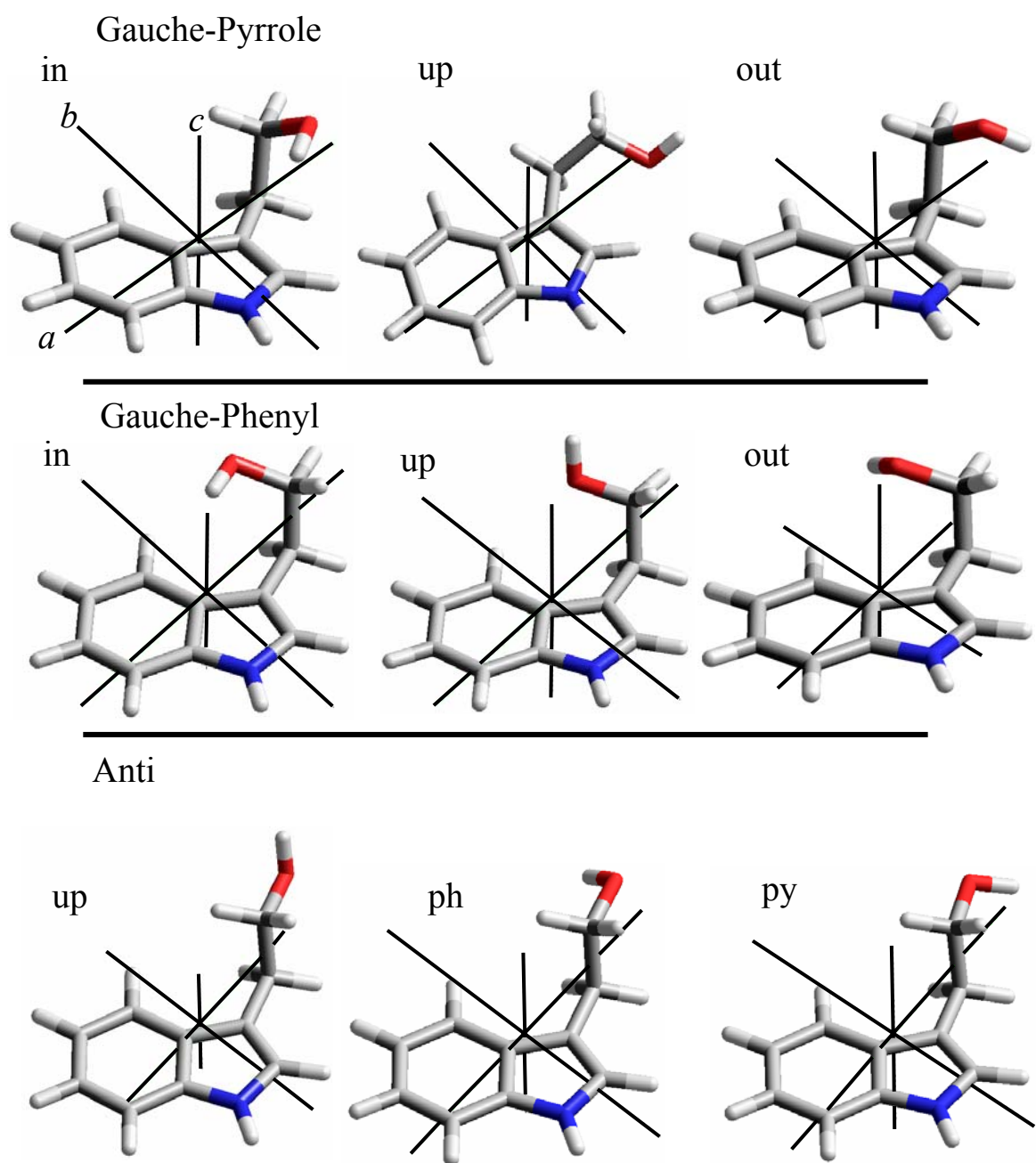


Figure 5-6. The nine conformers of TRH as calculated at the MP2/6-31G** level. See text for a description of the nomenclature used.

out structures. In contrast, the analogous presumed in TRA (GPy- and GPh-in) were found to have stable minima in *ab initio* calculation, though their energies are relatively high. We speculate that in TRH, the two oxygen lone pairs are found in two essentially degenerate linear combinations with each other, and that only one of these is stabilized by interaction with the indole ring, in the *gauche* structures. In agreement with this suggestion, both “up” and geometries “out” are found in the *anti* conformers, since neither oxygen lone pair interacts with the ring. Thus explained is a reduction of the number of stable conformations of TRH from nine to seven. A further reduction to five energetically accessible conformations is a consequence of the much higher relative energies of GPy- and GPh-up, calculated to lie at least 500 cm^{-1} above the GPy-in global minimum. There are no O–H--- π interactions in the *gauche* “up” conformers of TRH.

Finally, we assign the observed origin bands in the S_1 - S_0 electronic spectrum of TRH to four of these structures. The first criterion we use is their relative energy Bands A and B are the strongest bands in the spectrum and they must be assigned to the more stable structures. Of these, GPy-in and GPh-in are the most likely candidates. Then, we can distinguish these by their inertial parameters. The rotational constant of the species responsible for Band A are nearly the same as those calculated for the GPy-in conformer, in the ground state. Similarly, the rotational constants of the species responsible for Band B are nearly the same as those calculated for the GPh-in conformer, in the ground state. The predicted A rotational constant of GPy-in and the predicted B constants of GPh-in are substantially different from experiment ($\sim 2\%$); the rest of the predicted values are in excellent agreement with experiment. Additionally, the two species have very different inertial constants, including inertial defects. Therefore, we confidently

assign Band A as the band origin of GPy-in, and Band B as the band origin of GPh-in. Experiment and theory agree that the π -hydrogen bonding interaction involving the –OH hydrogen atom plays the dominant role in determining the global minimum on the energy landscape of TRH.

Similar conclusions have been reached for other -OH containing biomolecules, including 2-phenethylalcohol¹⁷ and 4-hydroxyphenethylalcohol¹⁸ (p-tyrosol). Both molecules have ethyl alcohol “tails”, and the most stable structure in each case is a folded, *gauche* structure with the –OH hydrogen atom pointing into the aromatic ring. However, in these cases the *gauche* band is red shifted relative to the other, weaker bands. On the other hand, the low resolution spectrum of 2-indanol¹⁹ is virtually identical to that of TRH. In this case, the large blue shift of the π -hydrogen bonded, -OH “in” conformer relative to the other conformers is clearly associated with a weakening of this bond on excitation. Interestingly, the Gpy-in conformer of TRH is unique in having an *A* rotational constant that is larger in the S_1 state than in the S_0 state. Our *ab initio* calculation suggests that the –OH hydrogen atom is very close to the *a*-axis in the S_0 state. Hence, it is possible that a weakening of the π -hydrogen band in the S_1 state could lead to a decrease in the displacement of the –OH group from the *a*-axis, which would explain the increase in *A*.

Some mysteries remain. Chief among these is the correct assignment of Bands C_{red} and C_{blue} . A comparison of the measured rotational constants and especially the inertial defects of these two bands with the predicted values show clearly that both bands belong to *anti*-structures. The fact that C_{red} is somewhat more intense than C_{blue} also suggests that the former belongs to *anti-up*, since this conformer is predicted to have the lower energy. And, finally, it is possible

that Band C_{blue} belongs to the same kind of “linear combination” state as was found in the GPy and GPh families, there in fact being only two members of the *anti* family, rather than the three that are predicted theoretically. Further experiments and more refined calculations will be necessary to clarify these issues.

5.6. Summary and Conclusions.

Four unique conformers; GPy-in, GPh-in, and two *anti* structures have been observed in the S₁-S₀ fluorescence excitation spectra of tryptophol, the –OH analog of tryptamine. The GPy-in species is the global minimum; it is significantly stabilized by a π -hydrogen bond involving the –OH group and the π electrons of the pyrrole ring. The corresponding GPh-in structure lies at $\sim 100\text{ cm}^{-1}$ higher energy. The significantly larger number of stable conformers in tryptamine (seven rather than four) may be attributed to the fact that its terminal –NH₂ group has two hydrogen atoms that may hydrogen bond with the aromatic rings.

5.7. Acknowledgments.

This work has been supported by NSF (CHE-0315584) to whom we are grateful.

5.8. References.

1. Y. D Park, T. R. Rizzo, L. A. Peteanu and D. H. Levy, *J. Chem. Phys.* **84** (1986) 6539.
2. L. A. Phillips and D. H. Levy, *J. Chem. Phys.*, **85** (1986) 1327.
3. L. A. Phillips and D. H. Levy, *J. Chem. Phys.* **89** (1988) 85.
4. Y. R. Wu, and D. H. Levy, *J. Chem. Phys.*, **91** (1989) 5278.
5. L. L. Connell, T. C. Corcoran, P. W Joireman and P. M. Felker, *Chem. Phys. Lett.* **166** (1990) 510.
6. L. L. Connell, T. C. Corcoran, P. W Joireman and P. M. Felker, *J. Phys. Chem.* **94** (1990) 1229.
7. P. M. Felker, *J. Phys. Chem.*, **96** (1992) 7844.
8. P. M. Felker, *Chem. Rev.* **94** (1996) 1784.
9. J. R. Carney and T. S. Zwier, *J. Phys. Chem. A* **104** (2000) 8677.
10. T. V. Nguyen, T. M. Korter and D. W. Pratt, *Mol. Phys.* **103** (2005) 1603.
11. J. Sipior and M. Sulkes, *J. Chem. Phys.* **98** (1993) 9389.
12. J. Sipior and M. Sulkes, *J. Chem. Phys.* **88** 1988 6146.
13. J. T. Yi, E. G. Robertson and D. W. Pratt, *Phys. Chem. Chem. Phys.* **4** (2002) 5244.
14. W. A. Majewski, J. F. Pfanstiel, D. F. Plusquellic and D. W. Pratt, *Laser Techniques in Chemistry*. T. R. Rizzo, A. B. Myers, Eds. J. Wiley & Sons, New York, 1995. p. 101.
15. D. W. Pratt, *Annu. Rev. Phys. Chem.* **49** (1998) 481.
16. M. J. Frisch, G. W. Trucks, H. B. Schlegel, G. E. Scuseria, M. A. Robb, J. R. Cheeseman, V. G. Zakrzewski, J. A. Montgomery, Jr., R. E. Stratmann, J. C. Burant, S. Dapprich, J. M. Millam, A. D. Daniels, K. N. Kudin, M. C. Strain, O. Farkas, J. Tomasi, V. Barone, M. Cossi, R. Cammi, B. Mennucci, C. Pomelli, C. Adamo, S. Clifford, J. Ochterski, G. A. Petersson, P. Y. Ayala, Q. Cui, K. Morokuma, D. K. Malick, A. D. Rabuck, K. Raghavachari, J. B. Foresman, J. Cioslowski, J. V. Ortiz, A. G. Baboul, B. B. Stefanov, G. Liu, A. Liashenko, P. Piskorz, I. Komaromi, R. Gomperts, R. L. Martin, D. J. Fox, T. Keith, M. A. Al-Laham, C. Y. Peng, A. Nanayakkara, M. Challacombe, P. M. W. Gill, B. Johnson, W. Chen, M. W. Wong, J. L. Andres, C. Gonzalez, M. Head-Gordon, E. S. Replogle and J. A. Pople, Gaussian, Inc., Gaussian 98, Revision A.9, Pittsburgh PA, 1998.

17. J. A. Dickinson, M. R. Hockridge, R. T. Kroemer, E. G. Robertson, J. P. Simons, J. McCombie, and M. Walker, *J. Am. Chem.* **120** (1998) 2622.
18. M. R. Hockridge, S. M. Knight, E. G. Robertson, J. P. Simons, J. McCombie and M. Walker, *Phys. Chem. Chem. Phys.* **1** (1999) 407.
19. A. Das, K. K. Mahato, S. S. Panja and T. Chakraborty, *J. Chem. Phys.* **119** (2003) 2523.

6. Rotationally Resolved Electronic Spectra of Fluorene, Carbazole and Dibenzofuran: Evidence for Herzberg-Teller Vibrational Coupling with the S_2 Electronic State.

John T. Yi, Leonardo Alvarez-Valtierra and David W. Pratt

Department of Chemistry, University of Pittsburgh
Pittsburgh, PA 15260 USA

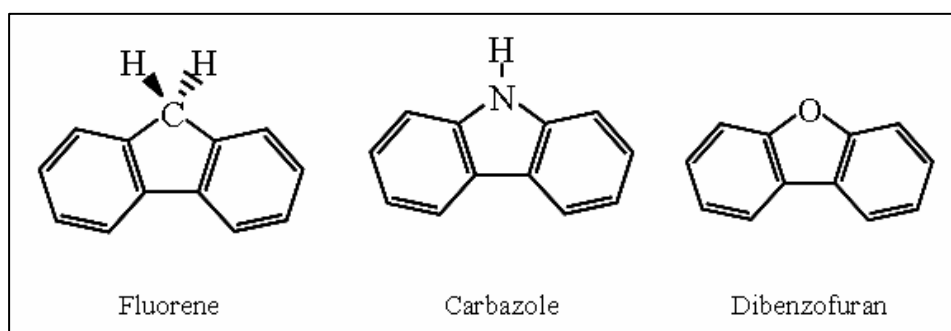
6.1. Abstract.

Rotationally resolved fluorescence excitation spectra of the S_1 - S_0 origin bands and higher vibrational bands of fluorene (FLU), carbazole (CAR), and dibenzofuran (DBF) have been observed and assigned. Analyses of these data shows that replacement of the CH_2 group in FLU with an NH group in CAR and an O atom in DBF produces only localized changes in structure, in the ground state. But the three molecules exhibit different changes in geometry when they are excited by light. The S_1 states of the three molecules also are electronically very different. The S_1 - S_0 transition moments of CAR and DBF are parallel to the C_2 symmetry axis whereas the corresponding transition moment in FLU is perpendicular to this axis. Herzberg-Teller coupling involving the S_2 state also has been observed in the spectra of CAR and DBF. Possible reasons for these behaviors are discussed.

J. Chem. Phys., submitted

6.2. Introduction .

Fluorene (FLU), carbazole (CAR) and dibenzofuran (DBF) constitute an interesting family of molecules in which the CH₂ group in the 9-position of FLU is replaced by an NH group in CAR and an oxygen atom in DBF; see below.



Even though these groups are isoelectronic, the resulting molecules exhibit different characteristics upon absorption of light. Bree and Zwarich¹⁻³ discovered in studies of low temperature crystals that their S₁-S₀ electronic transitions are differently polarized. The S₁-S₀ electronic origins in CAR and DBF are polarized along the short *b*-axis, whereas the corresponding transition in FLU is polarized along the long *a*-axis. Later, all three molecules were studied by many authors in the gas phase⁴ and in supersonic jets; FLU by Jortner and co-workers,^{5,6} Meerts, *et al.*,⁷ and Knee and co-workers;⁸ CAR by Phillips and co-workers,⁹ and CAR and DBF by Chakraborty and Lim,¹⁰ and more recently by Baba, *et al.*¹¹ Photoexcited van der Waals dimers of these and many other molecules exhibit excimer formation on short time

scales, a phenomenon that sensitively depends on the mutual orientation of their transition moments in both the gas phase and the condensed phase.

Here described are rotationally resolved S_1 - S_0 fluorescence excitation spectra of the origin bands and some higher energy vibronic bands of all three molecules in the gas phase. (Analogous experiments were attempted on the sulfur analog, dibenzothiophene, but these were unsuccessful.) We find that the origin bands of CAR and DBF are both perpendicular bands, while that of FLU is a parallel band, as in the condensed phase. We also find that some of the higher energy vibronic bands in CAR and DBF are parallel bands, evidencing vibronic coupling with the higher lying S_2 electronic state. Possible reasons for these behaviors are discussed.

6.3. Experimental.

FLU, CAR, and DFB were each purchased from Aldrich and used without further purification. Low resolution experiments were performed by seeding the sample into 30 psi of Ar gas, expanding it into a vacuum through a 1 mm diameter orifice pulsed valve, and exciting it with the second harmonic of a Quanta Ray Nd^{3+} : YAG (Model DCR-1A) pumped dye laser (Model PDL-1). High resolution experiments were performed using the CW laser spectrometer, described elsewhere.¹² Briefly, the sample was seeded into Ar gas, expanded through a 240 μ m quartz nozzle, and probed 15 cm downstream of the nozzle by an Ar^+ pumped CW tunable dye laser. The pulsed and CW lasers operated with Rhodamine 590 and DCM dyes; in the CW case, ~ 200 μ W of UV radiation was obtained by intracavity frequency doubling using BBO 580 and LiO_3 640 crystals. The fluorescence excitation spectra, the iodine absorption spectrum, the relative frequency markers, and the laser output power were simultaneously collected and processed by an in-house data acquisition system; the high resolution data were analyzed using

jb95.¹³ Transition frequencies were calibrated by comparison with the I₂ absorption spectrum and frequency markers were obtained from a stabilized etalon with a free spectral range of 299.7520 ± 0.0005 MHz.

6.4. Results.

Figure 6-1 shows the first ~ 300 cm⁻¹ in the vibrationally resolved fluorescence excitation spectra of FLU, CAR, and DBF in a supersonic jet. Surprisingly, the 0₀⁰ bands of FLU and DBF appear at similar frequencies, but that of CAR is shifted ~ 3000 cm⁻¹ to the red. Not shown in full detail are the higher vibronic bands in each spectrum; FLU has bands at 0₀⁰ + 204, + 394, and + 598 cm⁻¹; CAR has bands at 0₀⁰ + 209 and + 511 cm⁻¹, and DBF has bands at 0₀⁰ + 209 and + 443 cm⁻¹. The latter band is much stronger than the 0₀⁰ band in DBF. Also, all three molecules exhibit bands that have previously been assigned to weakly bound argon complexes.⁵⁻⁷

Figures 6-2, 6-3, and 6-4 show the rotationally resolved S₁ ← S₀ fluorescence excitation spectra of the 0₀⁰ bands of FLU, CAR, and DBF, respectively. Each spectrum spans approximately 2.5 cm⁻¹. As previously reported,⁶ the 0₀⁰ band of FLU is a pure *a*-type spectrum, indicating that its S₁-S₀ transition moment (TM) is parallel to the *a*-inertial axis. In contrast, the corresponding bands of CAR and DBF are pure *b*-type spectra, though this might not be readily apparent at first glance. All three bands were fit utilizing rigid-rotor Hamiltonians for both states, using previously described fitting strategies.¹² Examples of these fits are also shown in Figs. 6-2, 6-3 and 6-4; the standard deviations of these fits are ~ 2.0 MHz for all three molecules.

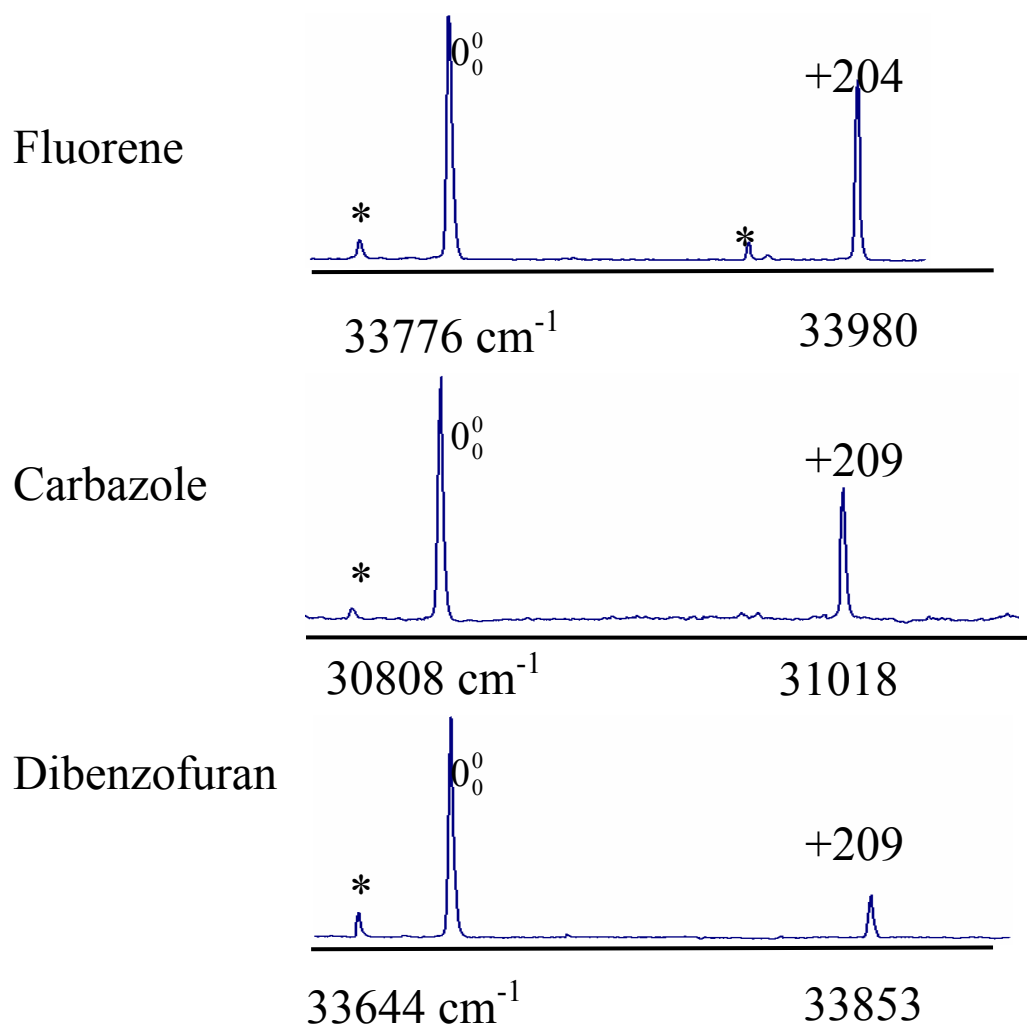


Figure 6-1. Fluorescence excitation spectra of the $S_1 \leftarrow S_0$ electric transitions of fluorene, carbazole and dibenzofuran in a supersonic jet. The origins are indicated as 0_0^0 and the first vibronic bands of each molecule are also shown. Bands marked with asterisks are due to argon complexes.

lists the rotational constants that were derived from these fits. The A'' value obtained for FLU (2174.3 MHz) is slightly different from that previously measured by Meerts, *et al.* (2183.2 MHz).⁶ We estimate ~ 15 MHz Lorentzian contributions to the Voigt lineshape profiles of single lines in all three spectra. The corresponding lifetime of 10 ns agrees reasonably well with the measured fluorescence lifetimes of 15.6 ns for FLU, 29.4 ns for CAR, and 14.8 ns for DBF.¹⁴

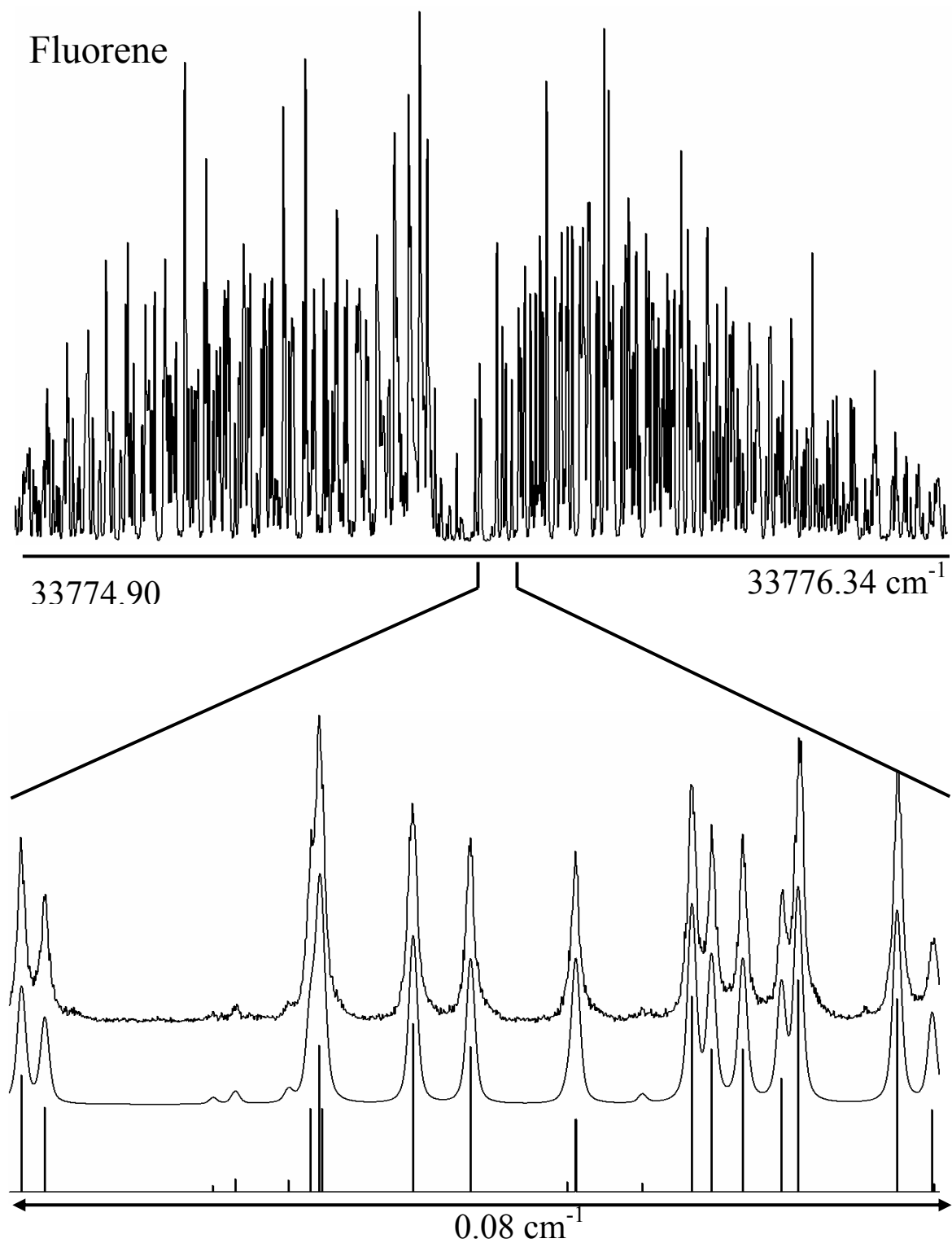


Figure 6-2. Rotationally resolved fluorescence excitation spectrum of the electronic origin in the $S_1 \leftarrow S_0$ transition of fluorene (top). A portion of the experimental spectrum at full resolution and the corresponding simulated spectrum with and without a convoluted line-shape function are also shown (bottom).

Carbazole

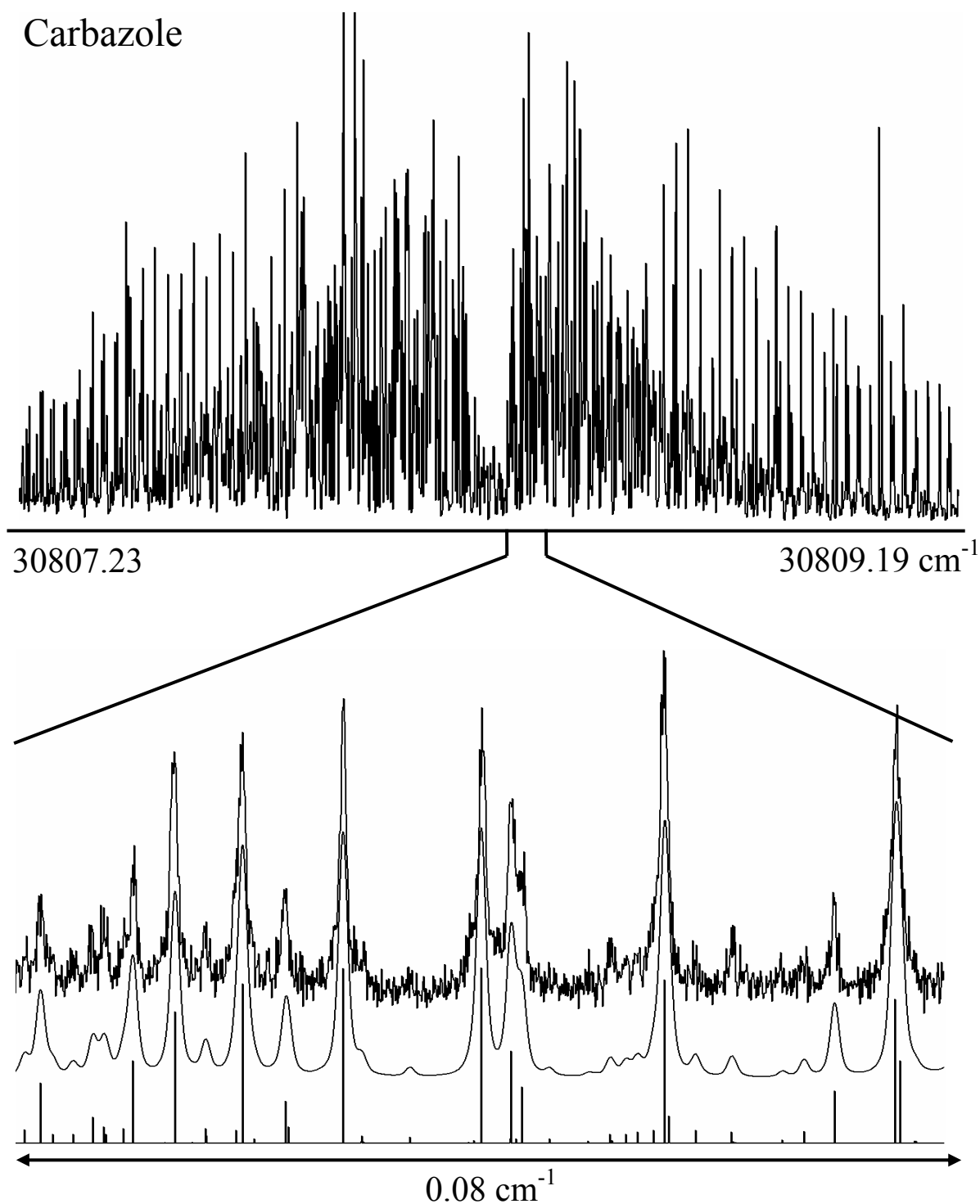


Figure 6-3. Rotationally resolved fluorescence excitation spectrum of the electronic origin in the $S_1 \leftarrow S_0$ transition of carbazole (top). A portion of the experimental spectrum at full resolution and the corresponding simulated spectrum with and without a convoluted line-shape function are also shown (bottom).

Dibenzofuran

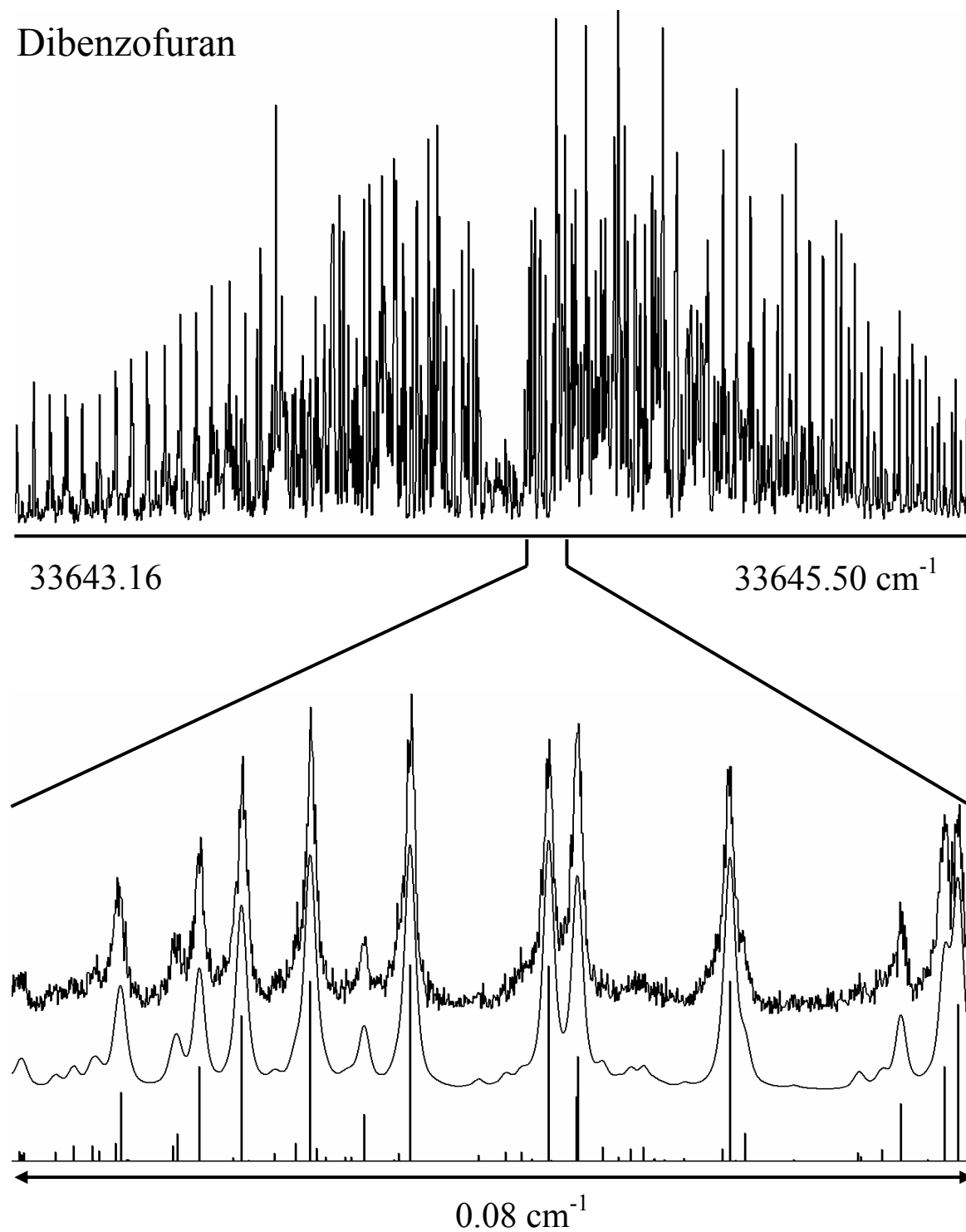


Figure 6-4. Rotationally resolved fluorescence excitation spectrum of the electronic origin in the $S_1 \leftarrow S_0$ transition of dibenzofuran (top). A portion of the experimental spectrum at full resolution and the corresponding simulated spectrum with and without a convoluted line-shape function are also shown (bottom).

Table 6-1. Inertial parameters of the zero-point vibrational levels of the S_0 and S_1 electronic states of fluorene carbazole and dibenzofuran.

	Fluorene ^a	Carbazole ^b	Dibenzofuran ^c
S_0			
A"(MHz)	2174.3 (3.2)	2253.2 (0.2)	2278.2 (0.1)
B"(MHz)	586.6 (0.1)	594.2 (0.2)	601.1 (0.1)
C"(MHz)	463.5 (0.1)	470.4 (0.2)	475.8 (0.1)
S_1-S_0			
ΔA (MHz)	-73.4 (3.2)	-2.6 (0.2)	-21.3 (0.1)
ΔB (MHz)	6.7 (0.1)	-7.9 (0.2)	-6.7 (0.1)
ΔC (MHz)	0.8 (0.1)	-5.1 (0.2)	-5.1 (0.1)
band-type	<i>a</i>	<i>b</i>	<i>b</i>
Band origin (cm^{-1})	33775.55	30808.13	33644.36
OMC (MHz)	2.20	2.08	1.99
Temp (K)	2.8	2.5	2.3

a. MP2/6-31G** values: $A''= 2177.67$, $B''= 586.56$, and $C''= 463.41$ MHz.

b. MP2/6-31G** values: $A''= 2253.98$, $B''= 593.99$, and $C''= 470.10$ MHz.

c. MP2/6-31G** values: $A''= 2273.18$, $B''= 600.63$, and $C''= 475.10$ MHz

Figure 6-5 shows the rotationally resolved fluorescence excitation spectra of four higher vibrational bands of the three molecules; FLU + 204, FLU + 394, CAR + 209, and DBF + 209. The spectra of FLU are both *a*-type spectra whereas those of CAR and DBF are *b*-type, just like their respective origin bands. Analyses of these spectra proceeded as before with one exception; the FLU + 204 spectrum could not be fit using rigid-rotor Hamiltonians for both electronic states. High J' value lines are shifted by as much as 100 MHz with respect to their predicted positions, leading to large standard deviations. Attempts to fit this band with the distortable rotor

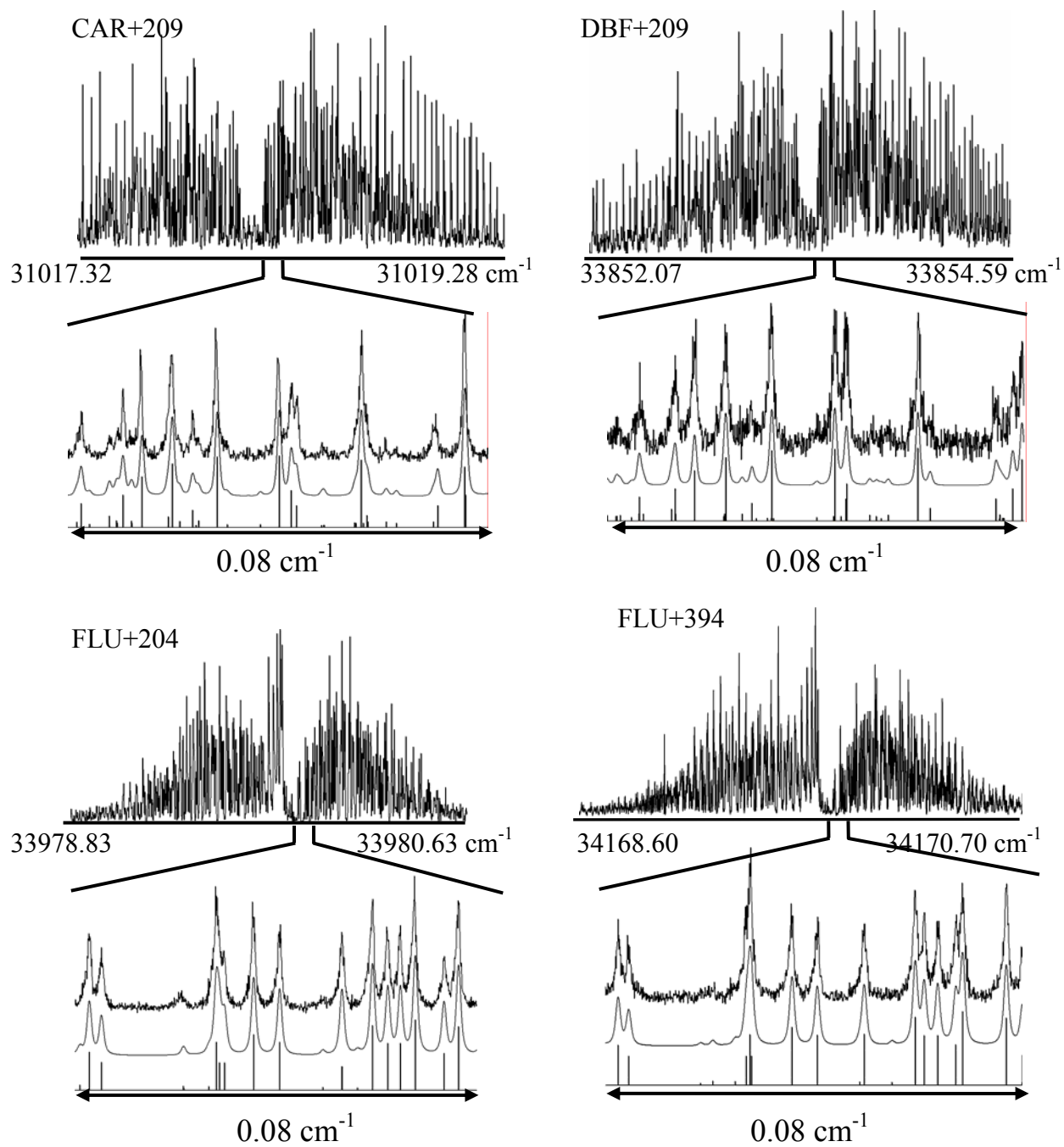


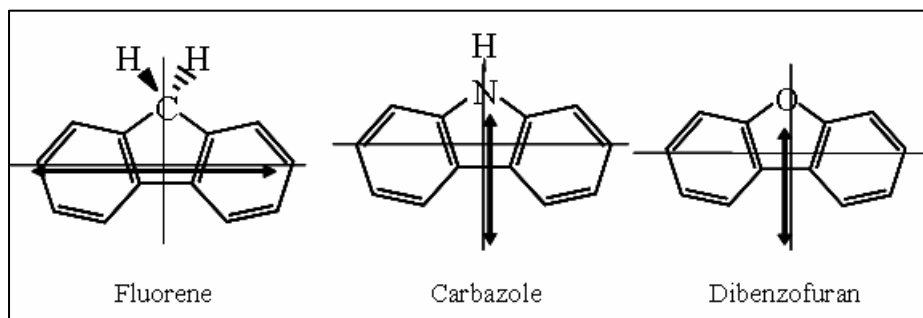
Figure 6-5. Rotationally resolved fluorescence excitation $S_1 \leftarrow S_0$ spectra of the a_1 -symmetry vibronic bands of FLU, CAR and DBF in a molecular beam. For every single spectrum, a portion at full experimental resolution is also shown, together with the corresponding fits. Note that every spectrum is unique.

Hamiltonian of Watson¹⁵ have generated better results, but still some high J' rovibronic lines remain shifted. No such perturbations were observed in the higher energy FLU + 394 band.

Figure 6-6 shows the rotationally resolved fluorescence excitation spectra of two additional higher vibronic bands, CAR + 511 and DBF + 443. Surprisingly, neither of these bands has the same band type as the respective origin bands; CAR + 511 and DBF + 443 are both pure a -type bands. No b - or c - type transitions were found in either spectrum. Both bands could be fit with rigid-rotor Hamiltonians, with standard deviations of 3.8 and 1.9 MHz, respectively. Table 6-2 lists the inertial parameters of the six examined vibronic bands of FLU, CAR, and DBF.

6.5. Discussion.

Electronic state mixing and/or re-ordering is at the heart of chemistry. The ability of one substance to be transformed into another depends on where its electrons are, and on how easily a given electron distribution can be modified by its interactions with the electron distributions of other substances. We find that FLU has a long-axis polarized S_1 - S_0 electronic transition but that two closely related derivatives, CAR and DBF, have short-axis polarized S_1 - S_0 transitions, in agreement with previous condensed phase results.¹⁻³



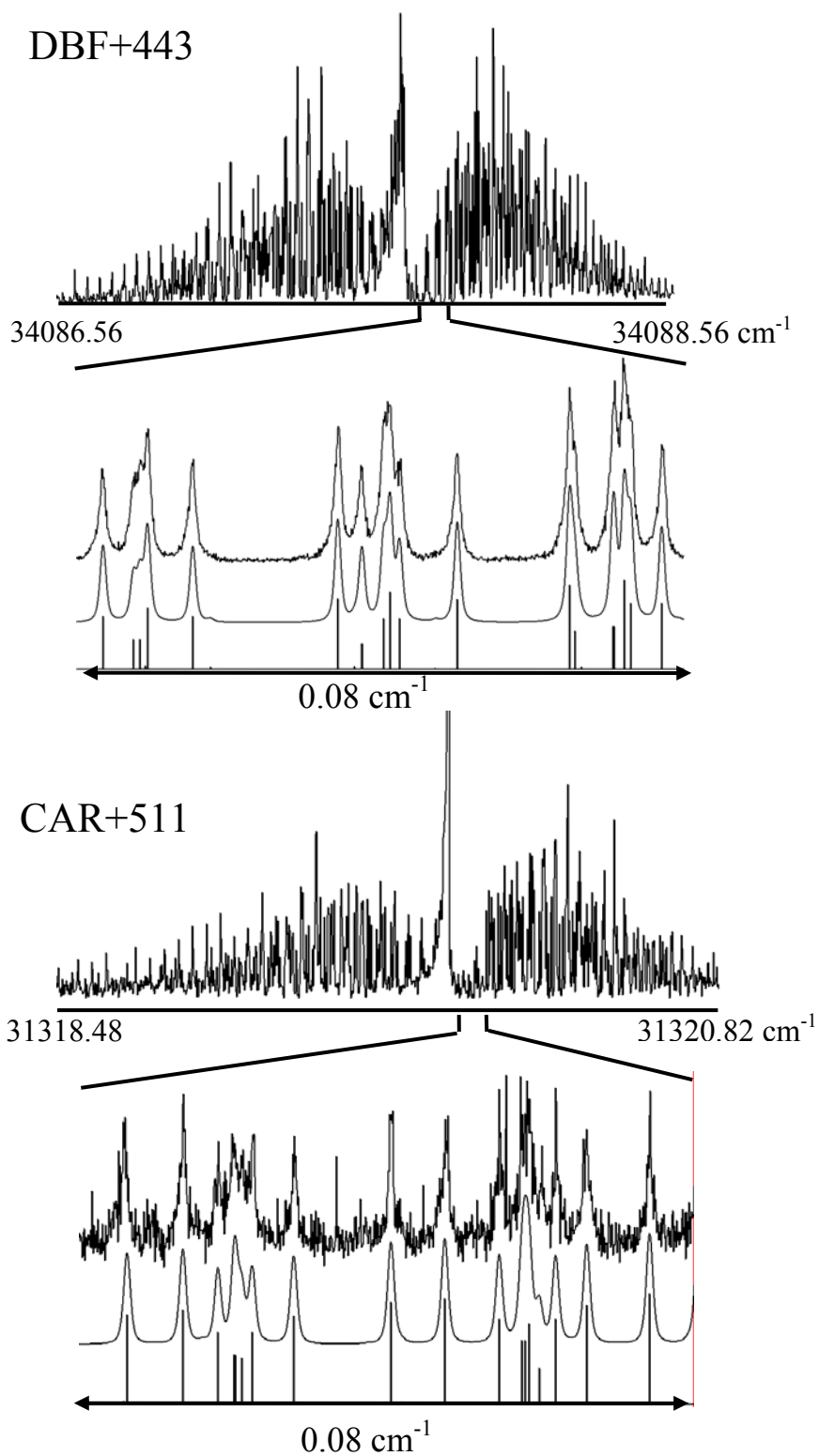


Figure 6-6. Rotationally resolved fluorescence excitation $S_1 \leftarrow S_0$ spectra of the b_2 -symmetry vibronic bands of CAR and DBF in a molecular beam. For each spectrum, a portion at full experimental resolution is also shown, together with their respective simulations.

Table 6-2. Inertial parameters of some higher S_1 vibrational bands of fluorene, carbazole and dibenzofuran.

	FLU+204	FLU+394	CAR+209	CAR+511	DBF+209	DBF+443
S_0						
A''(MHz)	2195.7 (50)	2174.3 (0.1)	2253.2 (0.2)	2250.8 (8.6)	2277.7 (0.5)	2276.7 (2.1)
B''(MHz)	586.9 (0.1)	586.6 (0.1)	594.1 (0.1)	589.4 (5.0)	601.2 (0.1)	601.1 (0.1)
C''(MHz)	463.4 (0.1)	463.5 (0.1)	470.4 (0.1)	466.0 (4.0)	475.8 (0.1)	475.8 (0.1)
S_1-S_0						
ΔA (MHz)	-58.9 (50)	-73.2 (0.1)	1.4 (0.1)	-1.4 (8.6)	-17.2 (0.5)	-26.9 (2.1)
ΔB (MHz)	6.7 (0.1)	6.6 (0.1)	-7.6 (0.1)	-7.6 (5.0)	-6.3 (0.1)	-5.8 (0.1)
ΔC (MHz)	0.8 (0.1)	0.6 (0.1)	-5.1 (0.1)	-5.0 (4.0)	-5.1 (0.1)	-4.7 (0.1)
band-type	<i>a</i>	<i>a</i>	<i>b</i>	<i>a</i>	<i>b</i>	<i>a</i>
Band origin (cm^{-1})	33979.80	34169.75	31018.12	31319.70	33853.38	34087.69
OMC (MHz)		1.54	3.46	3.84	1.75	1.91
Temp (K)		3	3	3	3.3	2.6

The S_1 state of the isolated FLU molecule is an 1L_a state whereas the S_1 states of isolated CAR and DBF molecules are 1L_b states. This means that replacing the CH_2 group in the central five-member ring with an NH group or an O atom modifies the distributions of electrons in the attached six-numbered rings, and leads to the expectation that the photochemical behavior of the S_1 states of CAR and DBF might be very different from that of FLU.

Ab initio calculations (MP2 for the S_0 states with a 6-31G** basis set, and CIS for the S_1 states with a 6-31G basis set)¹⁶ have been performed to explore the reasons for these behaviors. The calculated rotational constants of all three molecules in their ground states are in excellent agreement with the experimental values (*cf.* Table 6-1). The ground state values A'', B'', and C'' show the expected increases across the series FLU, CAR, and DBF owing to replacement of the

CH₂ group by the NH group and the O atom closer to the center-of-mass. (Also, the C-X bond length decreases with X=C, N, and O.) Generally, the excited state A', B', and C' values are less than their ground state counterparts, owing to small ring expansions that are typical of $\pi\pi^*$ states. But the values of ΔA , ΔB , and ΔC ($\Delta A = A' - A''$, *etc.*) in CAR and DBF are qualitatively different from those in FLU. Apparently, all three molecules are essentially planar in both electronic states. FLU has an inertial defect of - 3.689 amu \AA^2 in its ground state (Table 6-3), a value that is consistent with two out-of-plane C-H bonds. The inertial defects of CAR and DBF are nearly the same. - 0.348 amu \AA^2 and - 0.353 amu \AA^2 respectively; the N-H hydrogen in CAR must lie in the plane. None of these values change substantially when the molecules absorb light.

Table 6-3. Inertial defects (in amu \AA^2) of fluorene, carbazole and dibenzofuran in their S_0 and S_1 states.

Band		S_0		S_1	
Fluorene	0_0^0	-3.689	(0.430)	-3.896	(0.450)
	+394			-3.705	(0.100)
Carbazole	0_0^0	-0.348	(0.190)	-0.287	(0.190)
	+209			0.267	(0.090)
	+511			2.896	(29.0)
Dibenzofuran	0_0^0	-0.353	(0.090)	-0.335	(0.100)
	+209			0.620	(0.140)
	+443			-0.811	(0.295)

Figure 6-7 shows a sketch of the relevant MO's of the energy optimized structures that were derived from these calculations. According to CIS, the principal one-electron excitation that contributes to the S_1 state is the HOMO-LUMO transition ($\sim 65\%$); three other excitations each contribute about 10%. The oscillating charge distribution that is associated with the HOMO-LUMO transition is oriented along the a -axis, as shown below. Thus, CIS agrees with experiment in predicting a long-axis polarized S_1 - S_0 transition. However, it is equally evident that CIS fails to predict the polarizations of the corresponding transitions in CAR and DBF. The relevant orbitals (especially the HOMO and LUMO, see Fig. 6-7) and the principal excitation that contributes to the S_1 state in these two molecules are virtually the same as for FLU. Thus, theory predicts long-axis polarized 0_0^0 bands in CAR and DBF as well, in clear disagreement with experiment. Their S_1 states are L_a states.

Since the NH group in CAR and the O atom in DBF both lie in-plane, both molecules have out-of-plane lone pairs of electrons, unlike FLU. Thus, we speculate that these electrons play a significant role in the observed electronic state reordering in these molecules. Both Bree, *et al.*¹⁻³ and Pinkham and Wait⁴ have made similar arguments, noting that the difference in the shifts of the absorption and fluorescence spectra of CAR and DBF relative to FLU could be explained by differences in the magnitudes of their S_1 - S_0 (permanent) electric dipole moments. A similar effect has been observed in 1-aminonaphthalene (1-AN).¹⁷ 1AN exhibits a largely b -type origin band in its fully resolved electronic spectrum, whereas other 1-substituted naphthalenes exhibit largely a -type bands. Conjugation of the nitrogen lone pair electrons with the ring was offered as an explanation for this behavior. The conjugation leads to a twisting of the NH_2 group on S_1 excitation, perhaps suggesting the existence of a conical intersection along

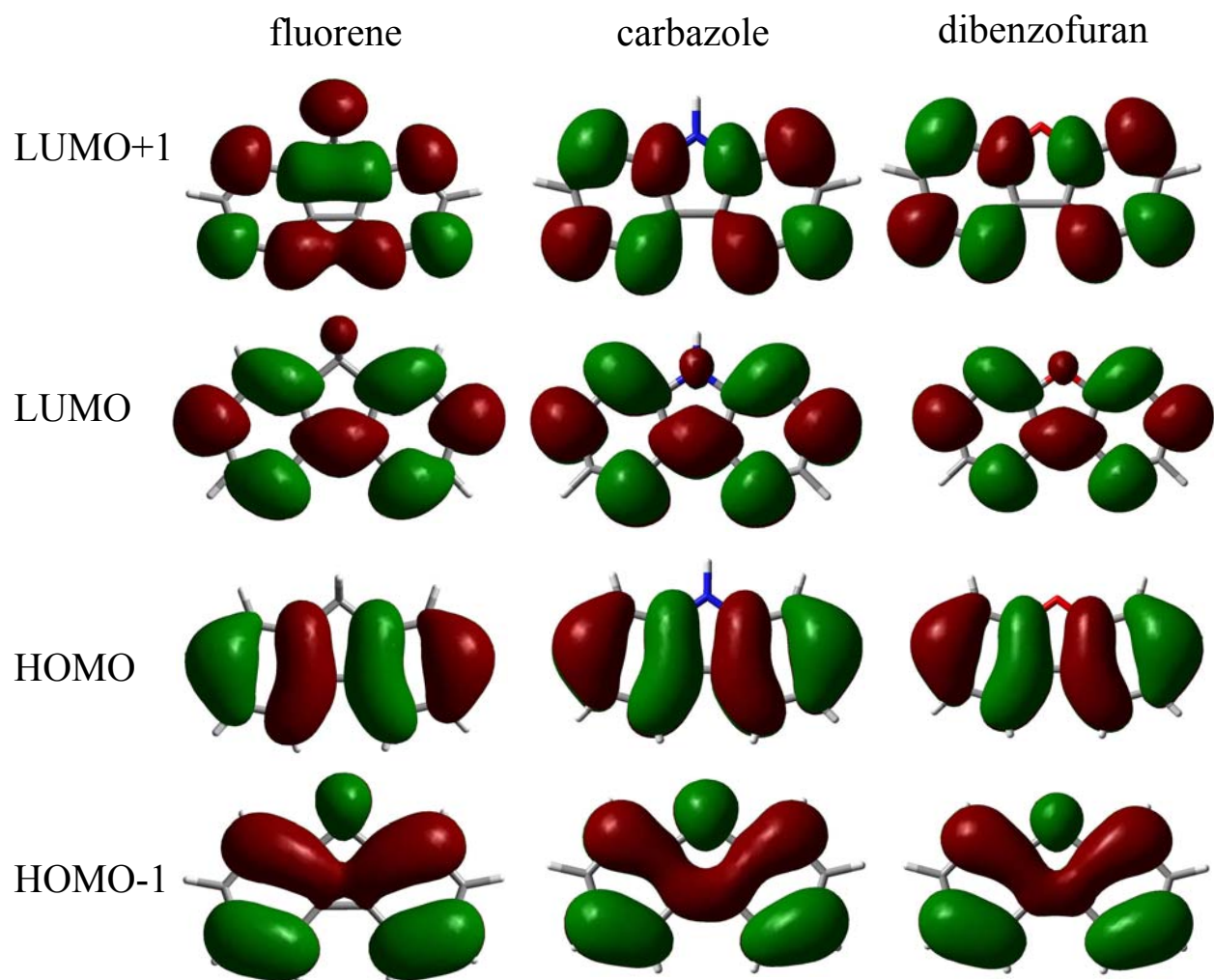


Figure 6-7. MP2 / 6-31G** molecular orbitals of fluorene, cabazole and dibenzofuran.

their coordinate. Thus, significantly higher level calculations may be necessary to capture these behaviors in CAR and DBF. (CIS calculations based on DFT wavefunctions give the same result as *ab initio* ones.)

Assignment of the S_1 states of CAR and DBF as 1L_b states and the S_1 state of FLU as a 1L_a state helps explain the differences in the ΔA values of the three species. The electron density in L_a states is primarily localized at atoms whereas the electron density in L_b states is primarily localized at the centers of bonds.⁸ Thus, FLU should have a relatively large negative value of ΔA , and relatively small values of ΔB and ΔC , owing to a ring expansion that preferentially lengthens the molecule in direction perpendicular to the a internal axis. This is what is observed; $\Delta A = -73.4$, $\Delta B = 6.7$ and $\Delta C = 0.8$ MHz. On the other hand, CAR and DBF are qualitatively different. CAR has $\Delta A = -2.6$, $\Delta B = -7.9$ and $\Delta C = -5.0$ MHz. The three nearly equal values suggest that the resulting displacements now make nearly equal projections along both a and b . DBF has $\Delta A = -21.3$, $\Delta B = -6.7$ and $\Delta C = -5.1$ MHz, a slight difference in ΔA . The degree of conjugation between the double bonds and the lone pair electrons of the substituent atom must be different.

A relevant observation is that the 0_0^0 band of CAR is red shifted with respect to the corresponding band in FLU by ~ 3000 cm^{-1} . Similarly, the 0_0^0 band of 1AN is red shifted with respect to the corresponding band in naphthalene by ~ 2000 cm^{-1} .¹⁷ This is the expected result if the affected electrons are significantly delocalized over the whole molecule. The 0_0^0 band of DBF is red shifted by only 132 cm^{-1} . But the S_1 - S_0 origin band of dibenzothiophene, a related

member of the family, is again shifted by $\sim 2600 \text{ cm}^{-1}$ to the red, and is also a *b*-type band (in the condensed phase).¹⁹

Higher vibronic bands that appear in the S_1 - S_0 excitation spectra of FLU, CAR, and DBF show additional interesting properties. The TM orientations of the four bands shown in Fig. 6-5 (FLU + 204, FLU +394, CAR +209, and DBF + 209) are the same as their respective origins whereas the TM orientations of the two bands shown in Fig. 6-6 (CAR + 511 and DBF + 443) are different from their respective origins. Similar effects have been observed in the condensed phase.¹⁻³ A logical explanation, then, is that the two bands in question terminate in non-totally symmetric vibrational bands of the S_1 state, and that these molecules are active in Herzberg-Teller (HT) coupling²⁰ to the S_2 state.

In HT coupling, if rovibronic wavefunctions are considered as first approximation as a product of electronic, vibrational, and rotational wavefunctions, and higher order effects are neglected, then the transition dipole moment for an electronic transition between an upper and a lower vibronic state may be written as:

$$\begin{aligned} \langle \psi'_e \psi'_v \psi'_r | \mu_Z | \psi''_e \psi''_v \psi''_r \rangle = & \left\{ \sum_g \mu_g^0(e', e'') \langle \psi'_e | \psi''_e \rangle + \sum_s \left[\partial \mu_g(e', e'') / \partial Q_s \right]_0 \langle \psi'_v | Q_s | \psi''_v \rangle \right. \\ & \left. + \sum_a \left[\partial \mu_g(e', e'') / \partial Q_a \right]_0 \langle \psi'_v | Q_a | \psi''_v \rangle \right\} \langle \psi'_r | \lambda_{Zg} | \psi''_r \rangle \quad (1) \end{aligned}$$

Here, μ_Z is the component of the electric dipole moment operator along the space-fixed axis Z, the μ_g are its projections along the inertial axes g ($=a, b, c$), with direction cosines λ_{Zg} , and the $[\mu_g(e', e'') / \partial Q]_0$ are the transition moment derivatives with respect to nuclear motions (s representing symmetric ones and a representing antisymmetric ones), evaluated at the equilibrium nuclear configuration. For symmetry-allowed electronic transitions the first two

terms on the right of Eq. (1) are nonzero. But for symmetry-forbidden transitions, only the last term in Eq. (1) is nonzero, and the transitions are said to be “vibrationally induced”.²⁰ In that event, the polarization of the bands will depend upon the symmetry of the inducing coordinate Q_a , and that of the electronic state to which it is coupled.

That this interpretation is likely the correct one is supported by the results of our *ab initio* calculations. These calculations show that S_1 FLU has an a_1 symmetric in-plane bending mode at 207 cm^{-1} , and an a_1 symmetric breathing mode at 403 cm^{-1} . Given their frequencies, and symmetries, the two observed bands at FLU + 204 and FLU + 394 may be assigned to these normal modes. The upper state rotational constants and inertial defects (Table 6-3) are consistent with these assignments. Similarly, the two observed bands at CAR + 209 and DBF + 209 may also be assigned to the a_1 symmetric in-plane bending mode, since their calculated S_1 frequencies (207 cm^{-1}), are in excellent agreement with the experiment. But the CAR + 511 and DBF + 443 vibronic bands must involve non-totally symmetric modes, since their polarizations are different. CAR has an S_1 , b_2 symmetry, in-plane skeletal distortion mode at 504 cm^{-1} , and DBF has an S_1 , b_2 symmetry, in-plane skeletal distortion mode at 498 cm^{-1} . These are likely candidates as inducing modes in HT coupling; their symmetries make possible a mixing of the zero-order S_1 states of CAR and DBF with S_2 states, which are expected to possess higher oscillator strengths. Thus explained are the observed b -axis polarizations of the corresponding vibronic bands. More sophisticated calculations will be required to determine whether or not motion along these coordinates leads to other types of dynamical behavior.

6.6. Summary.

Several unusual properties of the S_0 and S_1 electronic states of fluorene (FLU), carbazole (CAR) and dibenzofuran (DBF) are revealed by fluorescence excitation experiments on the isolated molecules in a molecular beam. These properties include differences in their rotational constants, in the orientations of their electronic transition moments, and in the polarizations of higher vibronic bands in their fully resolved spectra. Comparisons of the results for the three molecules with the predictions of theory suggest that the S_1 state of FLU is an 1L_a state, that the S_1 states of CAR and DBF are 1L_b states, and that couplings between these states of the Herzberg-Teller type are promoted by displacements along certain non-totally symmetric vibrational coordinates.

6.7. Acknowledgments.

This work has been supported by NSF (CHE-0315584) to whom we are grateful.

6.8. References.

1. A. Bree and R. Zwarich, *J. Chem. Phys.* **49** (1968) 3355.
2. A. Bree and R. Zwarich, *J. Chem. Phys.* **51** (1969) 903.
3. A. Bree, V. V. B. Vilkos and R. Zwarich, *J. Mol. Spectrosc.* **48** (1973) 135.
4. C. A. Pinkham and S. C. Wait Jr., *J. Mol. Spectrosc.* **27** (1968) 326.
5. A. Amirav, U. Even and J. Jortner, *Chem. Phys.* **67** (1982) 1.
6. S. Leutwyler, U. Even, and J. Jortner, *Chem. Phys. Lett.* **86** (1982) 439.
7. W. L. Meerts, W. A. Majewski and W. M. van Herpen, *Can. J. Phys.* **62** (1984) 1293.
8. X. Zhang, J. D. Pitts, R. Nadarajah, and J. L. Knee, *J. Chem. Phys.* **107** (1997) 8239.
9. A. R. Auty, A. C. Jones and D. Phillips, *Chem. Phys. Lett.* **112** (1984) 529.
10. T. Chakraborty and E. C. Lim, *Chem. Phys. Lett.* **207** (1993) 99.
11. M. Baba, A. Doi, Y. Tatamitani, M. Yamawaki, S. Kasahira, and H. Kato, 60th International Symposium on Molecular Spectroscopy, Columbus, OH, June, 2005.
12. W. A. Majewski, J. F. Pfanstiel, D. F. Plusquellic and D. W. Pratt, *Laser Techniques in Chemistry*. T. R. Rizzo, A. B. Myers, Eds., J. Wiley & Sons, New York, 1995, p. 101
13. D. F. Plusquellic, jb95 Spectral fitting program, NIST, Gaithersburg, MD, <http://physics.nist.gov/jb95>
14. A. R. Auty, A. C. Jones and D. Phillips, *J. Chem. Soc. Faraday Trans. 2* **82** (1986) 1219.
15. J.K.G. Watson, in *Vibrational Spectra and Structure*, J.R. Durig, Ed., Elsevier, Amsterdam, 1977, Vol.1, p.6.
16. M. J. Frisch, G. W. Trucks, H. B. Schlegel, G. E. Scuseria, M. A. Robb, J. R. Cheeseman, V. G. Zakrzewski, J. A. Montgomery, Jr., R. E. Stratmann, J. C. Burant, S. Dapprich, J. M. Millam, A. D. Daniels, K. N. Kudin, M. C. Strain, O. Farkas, J. Tomasi, V. Barone, M. Cossi, R. Cammi, B. Mennucci, C. Pomelli, C. Adamo, S. Clifford, J. Ochterski, G. A. Petersson, P. Y. Ayala, Q. Cui, K. Morokuma, D. K. Malick, A. D. Rabuck, K. Raghavachari, J. B. Foresman, J. Cioslowski, J. V. Ortiz, A. G. Baboul, B. B. Stefanov, G. Liu, A. Liashenko, P. Piskorz, I. Komaromi, R. Gomperts, R. L. Martin, D. J. Fox, T. Keith, M. A. Al-Laham, C. Y. Peng, A. Nanayakkara, M. Challacombe, P. M. W. Gill, B.

- Johnson, W. Chen, M. W. Wong, J. L. Andres, C. Gonzalez, M. Head-Gordon, E. S. Replogle and J. A. Pople, Gaussian, Inc., Gaussian 98, Revision A.9, Pittsburgh PA, 1998.
17. G. Berden, W. L. Meerts, D. F. Plusquellic, I. Fujita and D. W. Pratt, *J. Chem. Phys.* **104** (1996) 3935.
 18. W. S. Struve, *Fundamentals of Molecular Spectroscopy*, John Wiley & Sons, New York, 1989.
 19. A. Bree and R. Zwarich, *Spectrochim. Acta.* **27A** (1971) 621.
 20. G. Herzberg and E. Teller, *Z. Phys. Chem.* **21** (1933) 410.

Appendix A. Work in Progress.

I. Conformational isomers

1) *o*-Methoxyphenol (*o*-MP) and *m*-Dimethoxybenzene (*m*-DMB)

Low-resolution

o-MP

o-MP + H₂O

m-DMB

m-DMB + H₂O

m-DMB + D₂O

High-resolution

o-MP

Bands A, B, and C

m-DMB

Bands A, B, and C

Completed spectral analysis

Rotational parameters

Ab initio calculations

Collaborating with Jessica Thomas.

2) 5-Methoxytryptamine

Low resolution

Frequency assignment of bands

3) Melatonin

Low resolution

High resolution

Bands A and B

Spectral analysis of melatonin

Contour fit of Band B

Ab initio calculations

II. Transition moments

1) 5-Methoxyindole (5-MOI), 1,2,3,4-Tetrahydro-2-carboline (THCL) and 1,2,3,4-Tetrahydrocarbazole (THCZ)

- Low resolution
- High resolution
- Completed spectral analysis
- Rotational parameters
- Ab initio calculations

“The transition moments of indole analogs: Evidence for 1L_b states”
John T. Yi, Leonardo Alvarez-Valtierra and David W. Pratt.

2) Oxindole (1L_a)

- Low resolution
- Oxindole
- Oxindole + H₂O
- High resolution
- Origin Band
- Completed spectral analysis
- Rotational parameters
- Ab initio calculations

III. Three aromatic rings

1) Dibenzothiophene

- Low resolution

2) 2,5-Diphenyl-1,3,4-oxdiazole

- High resolution
- Origin band
- Origin band +Ar
- Spectral analysis
- Contour fit
- Ab initio calculations

3) 2,5-Diphenyl-furan

- High resolution
- Origin band
- Spectral analysis
- Contour fit
- Ab initio calculations

4) Triptycene

High resolution

Rotational contour spectra and I_2 frequency of bands

IV. Ar complexes

1) Fluorene

High resolution

0_0^0 + Ar (L. Meerts)

+204 + Ar

+394 + Ar

Spectral analysis

Contour fit

Ab initio calculations

2) Dibenzofuran

High resolution

0_0^0 + Ar

+444 + Ar

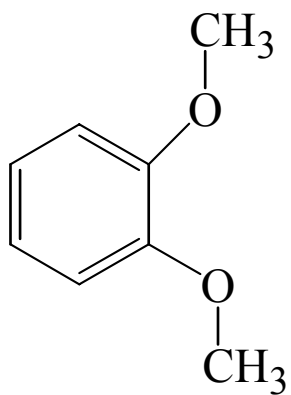
Spectral analysis

Contour fit

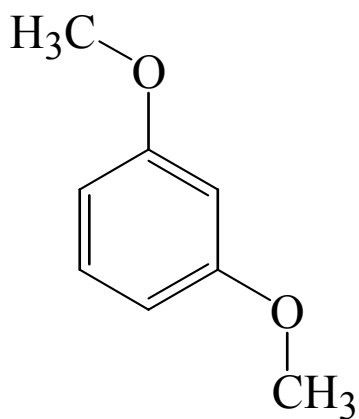
Ab initio calculations

“Rotationally resolved electronic spectra of fluorene and dibenzofuran argon complexes.”
Leonardo Alvarez-Valtierra, John T. Yi and David W. Pratt.

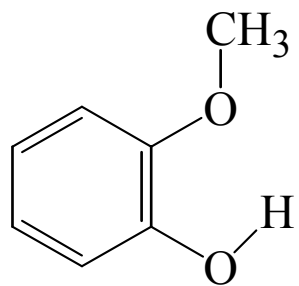
Appendix B. Molecules Studied.



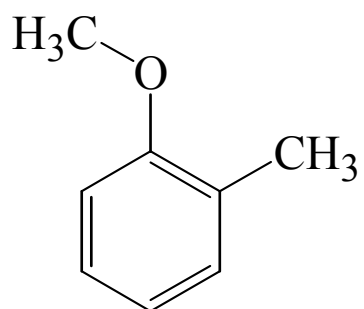
1,2-Dimethoxybenene



1,3-Dimethoxybenene

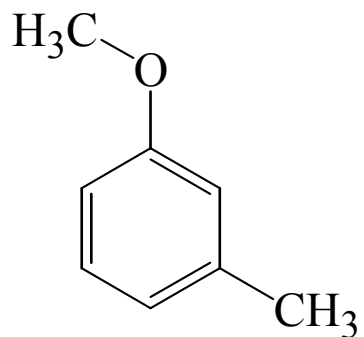


2-Methoxyphenol



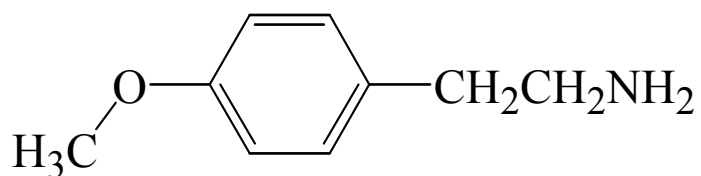
(L. Alvarez-Valtierra)

2-Methylanisole

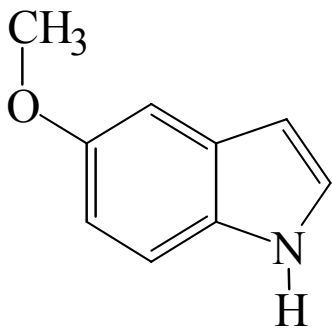


(L. Alvarez-Valtierra)

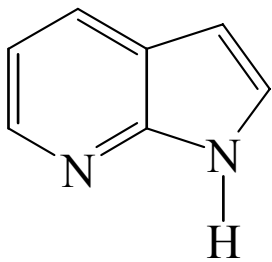
3-Methylanisole



4-Methoxyphenethylamine

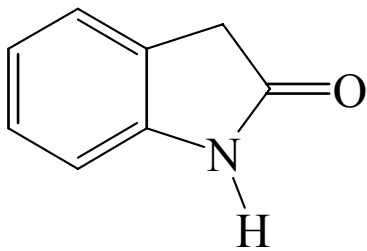


5-Methoxyindole

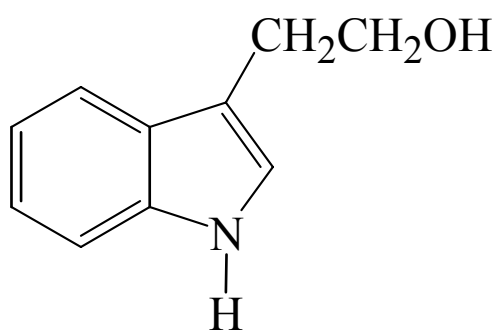


(C. Kang)

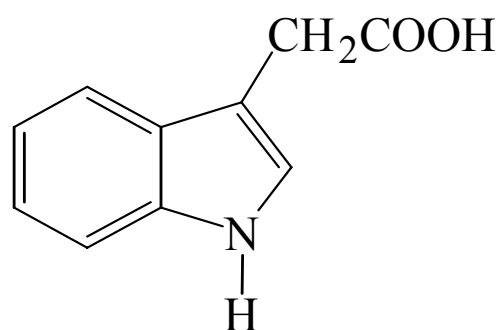
7-Azaindole



Oxindole

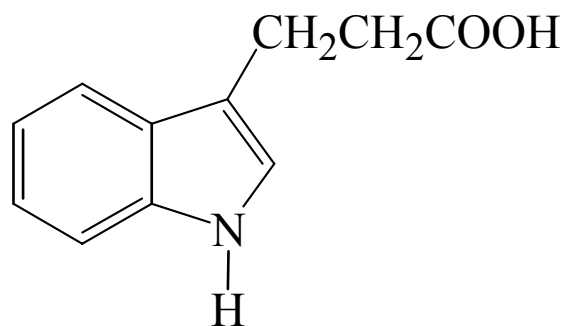


Tryptophol



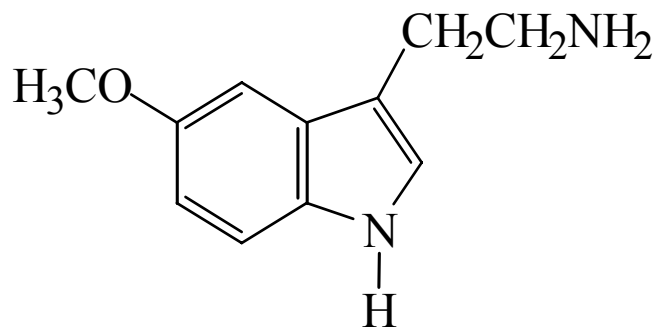
(T. Nguyen)

3-Indoleacetic acid

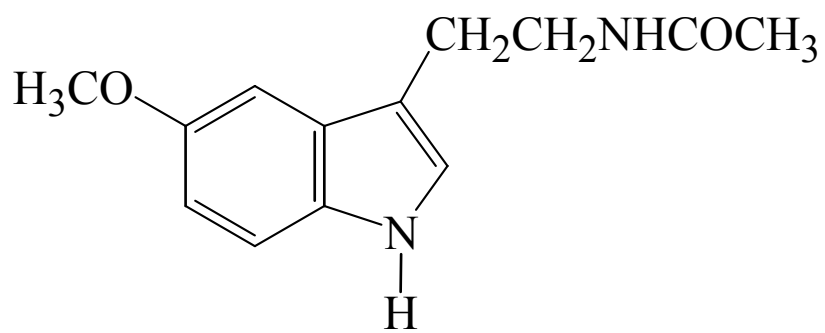


(T. Nguyen)

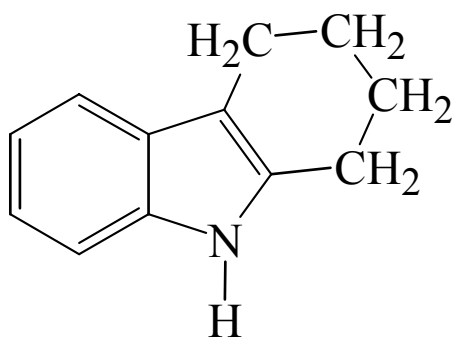
3-Indolepropionic acid



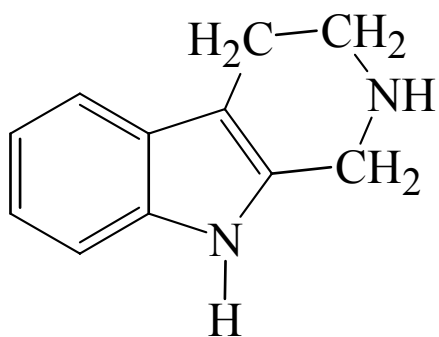
5-Methoxytryptamine



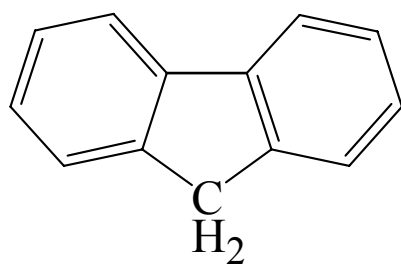
N-Acetyl-5-methoxytryptamine
(Melatonin)



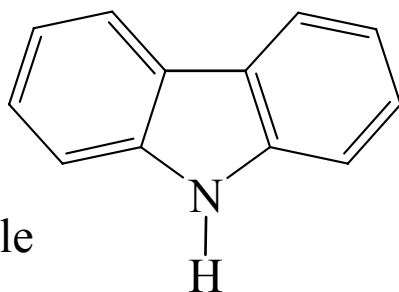
1,2,3,4-Tetrahydrocarbazole



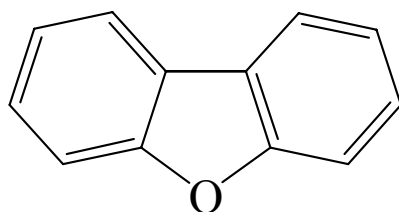
1,2,3,4-Tetrahydro-2-carboline



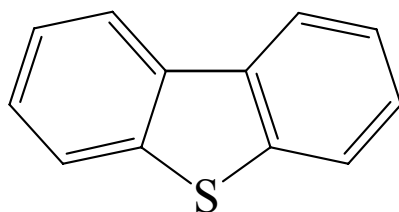
Fluorene



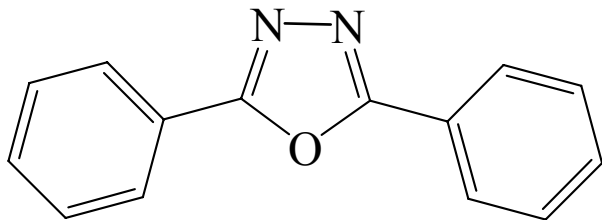
Carbazole



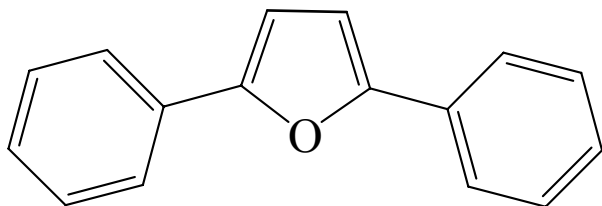
Dibenzofuran



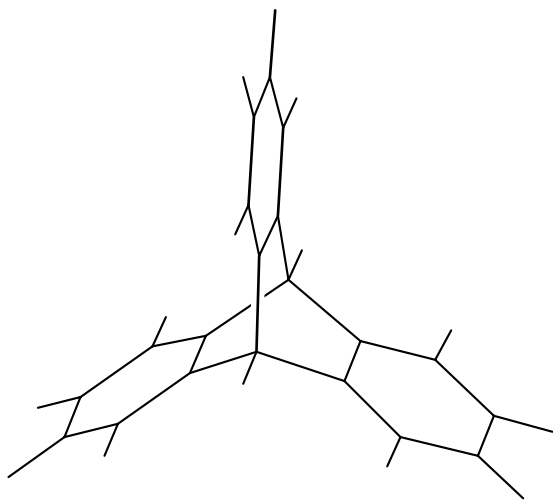
Dibenzothiophene



2,5-Diphenyl-1,3,4-oxdiazole



2,5-Diphenyl-furan



Triptycene